Title
ON THE NUCLEAR STRUCTURE AND STABILITY OF HEAVY AND SUPERHEAVY ELEMENTS

Authors
Nilsson, Sven Gosta
Tsang, Chin Fu
Sobiczewski, Adam
et al.

Publication Date
1969-01-13

Submitted to Nuclear Physics

UCRL-18692
Preprint

ey. 2

ON THE NUCLEAR STRUCTURE AND STABILITY OF HEAVY AND SUPERHEAVY ELEMENTS

Sven Gösta Nilsson, Chin Fu Tsang, Adam Sobiczewski, Zdzislaw Szymanski, Slawomir Wycech, Christer Gustafson, Inger-Lena Lamm, Peter Möller and Björn Nilsson

January 1969

AEC Contract No. W-7405-eng-48

LAWRENCE RADIATION LABORATORY
UNIVERSITY of CALIFORNIA BERKELEY

ey. 2

UCRL-18692

DISCLAIMER

ON THE NUCLEAR STRUCTURE AND STABILITY OF HEAVY AND SUPERHEAVY ELEMENTS*

Sven Gösta Nilsson† and Chin Fu Tsang

Lawrence Radiation Laboratory, University of California
Berkeley, California

Adam Sobiczewski, Zdzislaw Szymanski and Slawomir Wycech

Institute for Nuclear Research and University of Warsaw
Warsaw, Poland

Christer Gustafson, Inger-Lena Lamm, Peter Möller and Björn Nilsson

Department of Mathematical Physics, Lund Institute of Technology
Lund, Sweden

January 13, 1969

* Work supported by the U.S. Atomic Energy Commission, the Swedish Council of Atomic Research and the Polish Atomic Energy Commission.

† Present address: The Department of Mathematical Physics, Lund Institute of Technology, Lund, Sweden.

ABSTRACT

Nuclear potential energy surfaces as a function of deformations are calculated on the basis of a modified oscillator model. In particular, quadrupole (P_2) and hexadecapole (P_4) deformations are considered. The average behavior of the surface is normalized to that of a liquid drop through the employment of a generalized Strutinski prescription. In this way a synthesis of the single particle model and the liquid drop model is obtained.

Lowest minima in the potential energy surfaces give the ground state masses and distortions. These results compare extremely well with experimental data. Spontaneous fission half lives are obtained. The inertial parameters associated with fission barrier penetration are derived empirically as well as by a microscopic model. Shape (fission) isomeric states are also found. Their N and Z dependence in the present model are discussed and results tabulated.

The calculations are extended to the predicted superheavy region around Z = 114 and N = 184. The total overall stability with respect to alpha and beta decay, and spontaneous fission is found to be most favorable in the vicinity of Z = 110 and N = 184. Detailed diagrams and tables are exhibited.

ON THE NUCLEAR STRUCTURE AND STABILITY OF HEAVY AND SUPERHEAVY ELEMENTS

OUTLINE

0. Introduction

1. One-body Potential

   1.1. Deformed Oscillator Potential

   1.2. Condition of Volume Conservation

   1.3. Oscillator Frequency and Proton and Neutron Matter Radii

   1.4. Results for Single Particle Energies

2. The Pairing Force

   2.1. Isospin Dependence of Pairing

   2.2. Surface Dependence of Pairing

3. Coulomb Energy

4. Ground State Distortions

5. Generalized Strutinski Prescription and Normalization to the Liquid Drop Model

6. Nuclear Masses

7. Potential Energy Surfaces

   7.1. The Structure of Spontaneous Fission Barriers of Heavy and Superheavy Nuclei

   7.2. Shape (Fission) Isomers

   7.3. The Octupole Degree of Freedom

8. Barrier Penetration and Microscopic Theory of the Fission Process

9. Nuclear Stabilities

   9.1. Spontaneous Fission Half Lives

9.2. Island of Stability in the Superheavy Region

9.3. Surviving Superheavy Elements

10. Possible Experimental Production of Superheavy Nuclei

10.1. Heavy Ion Reactions

10.2. Neutron Capture Reactions

INTRODUCTION

It was found a long time ago[1,2,3] that simple equilibrium calculations based on the deformable shell model[4] were able to reproduce the experimental quadrupole moments in the "rare earth" and "actinide" regions. In the Mottelson-Nilsson calculations[1] single particle energies are simply added as a function of the quadrupole distortions, and the shape corresponding to the minimum energy was found. The calculations neglected the effects of Coulomb and pairing interactions, which are, however, considered by Bés and Szymanski[2], Szymanski[5], and also by Sobiczewski[6]. On the whole, the results of ref.[1] are reproduced, indicating that Coulomb and pairing forces at the equilibrium point counteract each other. In these latter calculations the positions of the low- and high-lying shells are rather critical in contrast to the calculations first mentioned where the combinations of entering orbitals were restricted. Our present aim is to extend and generalize this treatment to describe larger and more general distortions that are associated with the fission process.

In the present work the Bés and Szymanski method is further developed by

1) The employment of an improved form of nuclear field.
2) The inclusion of the hexadecapole (P_4) degree of freedom.
3) An evaluation of the Coulomb interaction without resort to expansion.
4) The use of a surface dependent pairing force.

As in earlier calculations the constancy of nuclear central density is provided by the condition of conservation of volume enclosed by equipotential surfaces.

Although this method appears adequate to treat equilibrium distortions, it fails to give the absolute value of the total binding energy and to describe the energy surface at very large distortions. A renormalization of the energy surface is achieved by the application of a method first introduced by Strutinski[7]. By this method the total energy is renormalized so that its smooth overall trend reproduces the deformation behavior of a liquid drop[8,9,10]. The parameters of the liquid-drop model that enter are not adjusted in the present calculations, but are taken equal to the latest parameters of Myers and Swiatecki[11].

In this way we have obtained ground-state shapes in P_2 and P_4 deformations which are within a few percent of the experimental values. Nuclear masses are also obtained as minimum point energies. These are found to agree well with experimental results.

The potential energy surfaces present secondary minima for large prolate distortions. This effect was pointed out by Strutinski[7] and may also be found in our calculations reported at the Lysekil Conference[12]. They are associated experimentally with the occurrence of fission (shape) isomers and (n,f) resonances. The phenomenon is particularly prominent for nuclei in the vicinity of $A \approx 240$.

To obtain the spontaneous-fission half lives we have employed the WKB approximation for barrier penetration. The inertia parameter associated with the barrier penetration has been estimated both

empirically from the spontaneous fission half lives of the actinides and also by means of a microscopic theory developed in analogy with the time dependent treatment of vibrations.

Half lives of alpha decay and spontaneous fission as well as stability against beta decay are calculated for the actinide elements and for the region of superheavy nuclei around $Z \approx 114$ and $N \approx 184$, which are predicted to be relatively stable by the present quantitative calculations as well as by earlier studies. A discussion is given for the possible production of these superheavy nuclei and the possible candidates for survival in earthly matter and in primary cosmic radiation.

Most of the results given here have also been presented by one of the authors (SGN) in ref. [13].

1. ONE-BODY POTENTIAL

Our calculations are based on a modified harmonic oscillator potential with a given dependence of co-ordinates describing deformations[12]. The oscillator frequencies and strengths of couplings of angular momenta are assumed to have a slow variation with the mass number.

Such a phenomenological model may appear unreliable as we try to extrapolate to very heavy nuclei far beyond presently known regions. Indeed a Hartree-Fock calculation based on detailed knowledge of nuclear forces may be more attractive. However the large number of matrix elements associated with interactions among the great number of particles involved makes such a calculation impractical with presently available computers.

The most realistic one-body central potential at present is considered to be the Woods-Saxon shape with constant surface diffuseness. We are currently studying such a potential for deformed nuclei. It has been found that the deformed harmonic oscillator potential with a few correction terms can do as well as the Woods-Saxon potential to reproduce the empirical level order and the angular-momentum composition of the single-particle state obtained from an empirical analysis of (d,p) and (p,d) reactions. We have therefore, as a first step, assumed the same deformed harmonic-oscillator potential to be applicable also for considerably larger distortions than those of the nuclei studied in the above reactions.

1.1 DEFORMED OSCILLATOR POTENTIAL

The deformed oscillator potential in the shape of a spheroid may be written as

$$V_{osc} = \frac{M}{2}[\omega_\perp^2(x^2 + y^2) + \omega_z^2 z^2] \quad .$$

If we introduce the deformation parameter ε [4]:

$$\omega_z = \omega_0(\varepsilon)\ (1 - \tfrac{2}{3}\varepsilon)$$

$$\omega_\perp = \omega_0(\varepsilon)\ (1 + \tfrac{1}{3}\varepsilon)$$

we obtain a quadrupole part of the potential proportional to

$$\varepsilon(1 - \tfrac{1}{6}\varepsilon)\ r^2 P_2(\cos\theta)$$

up to second order in ε. As in ref. [4] we use stretched co-ordinates (ξ, η, ζ) $\xi = \sqrt{(M\omega_\perp/\hbar)}\, x)$ etc. By doing this, one can transform away coupling terms of $r^2 P_2(\cos\theta)$ between shells N and $N \pm 2$. We then get, to first order in ε,

$$V_{osc} = \tfrac{1}{2}\hbar\omega_0\left(\rho^2 - \tfrac{2}{3}\varepsilon\rho^2 P_2(\cos\theta_t)\right)$$

where θ_t is angle in the stretched co-ordinates and

$$\rho^2 = \xi^2 + \eta^2 + \zeta^2 \quad .$$

We introduce deformations of higher multipoles† at this stage (compare ref. [12]) by adding terms proportional to

$$\varepsilon_4 \rho^2 P_4(\cos\theta'), \quad \varepsilon_6 \rho^2 P_6(\cos\theta') \quad \text{and} \quad \varepsilon_3 \rho^2 P_3(\cos\theta') \ .$$

The main reason for applying the higher multipole terms in these forms with the ρ^2 factor is that they enable us to write down the condition for volume conservation very simply (see below).

The oscillator potential shapes with P_2 and P_4 given by

$$V_{osc} = \frac{1}{2}\hbar\omega_0(\varepsilon, \varepsilon_4)\rho^2(1 - \frac{2}{3}\varepsilon P_2 + 2\varepsilon_4 P_4)$$

are illustrated in Fig. 1 on an ε, ε_4 plane.

Fig 1.

The spin-orbit term is an essential feature of the shell model. Since the only three available vectors of nucleon motion are its spin $\underset{\sim}{s}$, velocity $\underset{\sim}{v}$, and gradient of the potential at its position, $\underset{\sim}{\nabla}V$, the simplest invariant term one may construct is[3] $\underset{\sim}{s} \cdot (\underset{\sim}{p} \times \underset{\sim}{\nabla}V)$. With this we get a spin-orbit potential:

$$V_{so} \propto \left(\frac{\omega_z}{\omega_\perp}\right)^{1/3} (\underset{\sim}{\ell}_T \cdot \underset{\sim}{s}) + \left\{\left(\frac{\omega_\perp}{\omega_z}\right)^{2/3} - \left(\frac{\omega_z}{\omega_\perp}\right)^{1/3}\right\} \ell_3 s_3$$

$$\approx \underset{\sim}{\ell}_T \cdot \underset{\sim}{s} \quad \text{for small deformations}$$

where $\underset{\sim}{\ell}_T$ is defined in terms of the doubly-stretched co-ordinates

$$\underset{\sim}{e} = \sqrt{\left(\frac{M\omega_0}{\hbar}\right)} \frac{\omega_\perp}{\omega_0} \ x \quad \text{etc.} \quad \text{which transform the harmonic oscillator}$$

ellipsoid into a sphere. Presently we approximate this term by $\underset{\sim}{\ell}_t \cdot \underset{\sim}{s}$ where $\underset{\sim}{\ell}_t$ is defined in the stretched co-ordinates (ξ, η, ζ):

$$V_{so} \propto \underset{\sim}{\ell}_t \cdot \underset{\sim}{s} \quad .$$

It is well known that one cannot fit the level spectra of deformed nuclei by the oscillator potential with a spin-orbit term only. One needs a correction term that truncates the potential more and more with increasing A. It is natural to consider an expansion of the radial dependence of the potential, in which the $\underset{\sim}{\ell}^2$ or r^2 harmonic (oscillator) term is the lowest-order term. The next term (anharmonic) one should consider is then the $\underset{\sim}{\ell}^4$ term, whose matrix elements within one oscillator shell are actually the same as those of $(-\frac{1}{2}\underset{\sim}{\ell}^2)$ apart from additive constants. An alternative approach would be to look at V_{osc} as the lowest-order term of an expansion and to add a term proportional to V_{osc}^2. However, we choose the former approach and write down the correction as

$$V_{corr} \propto \underset{\sim}{\ell}^4 - (\underset{\sim}{\ell}^4)_N$$

where the second term is the average of the correction within a shell N.

We may summarize by writing down the single-particle Hamiltonian as[12]

$$H_{sp} = \frac{1}{2}\hbar\,\underset{\sim}{\omega}_0(\underset{\sim}{\varepsilon},\underset{\sim}{\epsilon}_4)\left[-\Delta_{\underset{\sim}{\rho}} + \frac{2}{3}\underset{\sim}{\varepsilon}\frac{1}{2}\left(2\,\frac{\partial^2}{\partial\underset{\sim}{\zeta}^2} - \frac{\partial^2}{\partial\underset{\sim}{\xi}^2} - \frac{\partial^2}{\partial\underset{\sim}{\eta}^2}\right)\right.$$

$$\left. + \underset{\sim}{\rho}^2 - \frac{2}{3}\underset{\sim}{\varepsilon}\,\underset{\sim}{\rho}^2 P_2(\cos\underset{\sim}{\theta}_t) + 2\,\epsilon_4\,\underset{\sim}{\rho}^2 P_4(\cos\underset{\sim}{\theta}_t)\right]$$

$$- 2\underset{\sim}{\kappa}\hbar\,\overset{\circ}{\underset{\sim}{\omega}}_0(\underset{\sim}{\ell}_t\cdot\underset{\sim}{s} - \underset{\sim}{\mu}(\underset{\sim}{\rho}^4 - \langle\underset{\sim}{\rho}^4\rangle_N)) \quad ,$$

where the first two terms in the square bracket give the kinetic energy and $\underset{\sim}{\kappa}$ and $\underset{\sim}{\mu}$ are adjustable coupling parameters. We define $\overset{\circ}{\underset{\sim}{\omega}}_0$ by $\overset{\circ}{\underset{\sim}{\omega}}_0{}^3 = \underset{\sim}{\omega}_\perp{}^2\,\underset{\sim}{\omega}_z$, which enters from volume conservation (see below) and is a function of mass number only. The above Hamiltonian includes only P_2 and P_4 co-ordinates. P_3 and P_6 deformations can be included similarly. Only terms of $\underset{\sim}{\rho}^4$ within one N-shell are presently considered.

1.2. CONDITION OF VOLUME CONSERVATION

It is well known that nuclear density is approximately constant except near the nuclear surface for any deformations. In other words, the nuclear volume remains the same when the nucleus is deformed: Due to the short-range nature of nuclear two-body interactions, the nuclear potential field should also have about the same volume in space independent of deformation. One way to formulate this condition mathematically is to require that the volume enclosed by a given equipotential surface is conserved.

For the spheroid harmonic oscillator potential, the condition corresponds to

$$\underset{\sim}{\omega}_z \, \underset{\sim}{\omega}_\perp^2 = \text{constant} = \underset{\sim}{\overset{o}{\omega}}_0^3 \, .$$

The condition applies to all equipotential surfaces at the same time. When terms involving $\underset{\sim}{\epsilon}_3 P_3$, $\underset{\sim}{\epsilon}_4 P_4$, and $\underset{\sim}{\epsilon}_6 P_6$ are involved, we get volume conservation as a scaling of $\underset{\sim}{\omega}_0$:

$$\frac{\underset{\sim}{\omega}_0^3}{\underset{\sim}{\overset{o}{\omega}}_0^3} = \frac{1}{(1 + \frac{1}{3}\underset{\sim}{\epsilon})(1 - \frac{2}{3}\underset{\sim}{\epsilon})^{\frac{1}{2}}} \int_{-1}^{1} \frac{\frac{1}{2}\, d(\cos \underset{\sim}{\theta})}{(1 - \frac{2}{3}\underset{\sim}{\epsilon} P_2 + 2\underset{\sim}{\epsilon}_3 P_3 + 2\underset{\sim}{\epsilon}_4 P_4 + 2\underset{\sim}{\epsilon}_6 P_6)^{3/2}} \, .$$

It should be emphasized here that this condition holds for all equipotential surfaces at one time. The relative simplicity of this expression is one reason for taking $\underset{\sim}{\epsilon}_4 \underset{\sim}{\rho}^2 P_4$, $\underset{\sim}{\epsilon}_3 \underset{\sim}{\rho}^2 P_3$, and $\underset{\sim}{\epsilon}_6 \underset{\sim}{\rho}^2 P_6$ in these forms. Added terms that can be written as powers of V_{osc} can conveniently be included in a volume conservation condition on $\underset{\sim}{\omega}_0(\underset{\sim}{\epsilon}, \underset{\sim}{\epsilon}_4, \cdots)$, but only for one equipotential surface at a time.

However, it is not simple to impose volume conservation on $\underset{\sim}{\rho}^4$ and $\underset{\sim}{\ell}_t \cdot \underset{\sim}{s}$ terms in the potential. As the effect of these terms is to bring down levels from other shells, it is not expected that they have negligible effect on volume conservation condition. To correct for this roughly we subtract from the potential the average value of these terms for each shell while retaining the volume conservation condition given above. As $\langle \underset{\sim}{\ell}_t \cdot \underset{\sim}{s} \rangle$ for each shell vanishes but not $\langle \underset{\sim}{\rho}^4 \rangle$, we have introduced in the last section potentials

$V_{so} \propto \underset{\sim}{\ell}_t \cdot \underset{\sim}{s}$ and also $V_{corr} \propto \underset{\sim}{\rho}^4 - \langle \underset{\sim}{\rho}^4 \rangle_N$.

We have noted before that within one N-shell the matrix elements of $\underset{\sim}{\rho}^4 - (\underset{\sim}{\rho}^4)_N$ are identical (within an additive constant) to those of $-\frac{1}{2}(\underset{\sim}{\ell}^2 - (\underset{\sim}{\ell}^2)_N)$. Actually the addition of $\underset{\sim}{\rho}^4$ makes the well narrower and hence tends to push the shells apart beyond the oscillator spacing $\hbar\underset{\sim}{\omega}_0$. A subtraction of $(\underset{\sim}{\rho}^4)_N$ restores the width of the potential for each shell but still causes the potential walls to rise faster locally. On the other hand, the addition of $-\underset{\sim}{\ell}_t^2$ lowers the effective oscillator shell spacing below $\hbar\underset{\sim}{\omega}_0$, while $(-\underset{\sim}{\ell}_t^2 + (\underset{\sim}{\ell}_t^2)_N)$ restores the spacing to $\hbar\underset{\sim}{\omega}_0$. This is possible only with the introduction of the peculiarity that each shell be given its own potential shape. In spite of this artifice, orthogonality is still preseved as long as one entire matrix is diagonalized.

1.3. OSCILLATOR FREQUENCY AND PROTON AND NEUTRON MATTER RADII

The oscillator parameter $\overset{o}{\underset{\sim}{\omega}}_0$ is usually determined from the condition that the nuclear radius be reproduced. The commonly employed value of $\hbar\overset{o}{\underset{\sim}{\omega}}_0 = 41\ A^{-1/3}$MeV leads, for a spherical shape, to a value of the root-mean-square radius of proton matter 5-10% less than that of neutron matter. Obviously one is not restricted to employing the same value of $\hbar\overset{o}{\underset{\sim}{\omega}}_0$ for neutrons and protons. One may let the different neutron and proton potentials and the Coulomb repulsion among the protons be reflected in the use of $\overset{o}{\underset{\sim}{\omega}}_n \neq \overset{o}{\underset{\sim}{\omega}}_p$. Indeed one can ensure approximately equal neutron and proton root-mean-square radii by choosing

$$\underset{\sim}{\omega}_n = \underset{\sim}{\omega}_0\left(1 + \frac{1}{3}\frac{N - Z}{A}\right)$$

$$\underset{\sim}{\omega}_p = \underset{\sim}{\omega}_0\left(1 - \frac{1}{3}\frac{N - Z}{A}\right) .$$

This corresponds to an isospin vector term

$$\frac{1}{2} M \underset{\sim}{\omega}_0^2 r^2 \frac{4}{3}\frac{N - Z}{A} \cdot t_3$$

whose average value is approximately

$$20 \frac{N - Z}{A} \cdot t_3 \text{ MeV} .$$

There are presently empirical indications that the nuclear surface is neutron rich. But at this time one is not sure whether one wants as much excess in the neutron radius as corresponds to $\underset{\sim}{\omega}_n = \underset{\sim}{\omega}_p$; or whether one should require $\langle r^2 \rangle_n = \langle r^2 \rangle_p$ and a larger neutron surface diffuseness; or whether an intermediate situation is more desirable. Calculations carried out with alternative assumptions exhibit only small relative differences for ground state masses, shapes, and fission barrier heights.

1.4. RESULTS FOR SINGLE PARTICLE ENERGIES

There are two shell parameters $\underset{\sim}{\kappa}$ and $\underset{\sim}{\mu}$ in the single particle Hamiltonian $\underset{\sim}{H}_{sp}$. These are optimized to reproduce the experimental level schemes for the rare-earth nuclei ($\underset{\sim}{A} \approx 165$) and the actinides ($\underset{\sim}{A} \approx 242$).

In Figs. 2-5 of ref.[12] we exhibit the energy eigenvalues as functions of ϵ, for ϵ_3, ϵ_4, ϵ_6, equal to zero, for the two important regions of deformed nuclei. These diagrams are roughly adequate for $165 < A < 175$ and $245 < A < 260$. As hexadecapole distortions are important at the beginning and the end of the rare earth and also the beginning end end of the actinide regions, we exhibit diagrams (Figs. 2a-d) valid for nuclei with $150 < A < 165$, $175 < A < 190$, $225 < A < 235$, $250 < A < 260$, where $\epsilon_4 = -0.04$, 0.04, -0.04, and 0.04, respectively. Some improvement of the level schemes is noticeable particularly for rare-earth neutron levels.

For the other regions, we assume that κ and μ vary linearly with the mass number A. We have used the following linear relations (see Table 1)

$$\left.\begin{aligned} \mu_n &= 0.624 - 1.234\,\frac{A}{1000} \\ \kappa_n &= 0.0641 - 0.0026\,\frac{A}{1000} \end{aligned}\right\} \text{Neutrons}$$

$$\left.\begin{aligned} \mu_p &= 0.493 + 0.649\,\frac{A}{1000} \\ \kappa_p &= 0.0766 - 0.0779\,\frac{A}{1000} \end{aligned}\right\} \text{Protons}$$

As a check the spectrum obtained by interpolation for κ and μ to $A = 208$ is plotted in Figs. (3a,b). The agreement with the single-hole levels of ^{207}Tl and ^{207}Pb is encouraging. On the other hand, the spectra of ^{209}Bi and ^{209}Pb are less well reproduced. The

levels in the latter cases start at a binding energy of only 3-4 MeV, and the insufficiency of the oscillator well is therefore expected to become increasingly important with excitation energy in the ^{209}Bi and ^{209}Pb spectra.

For the $A \approx 300$ region, as did other authors[17,18,19,20] we find proton number 114 to be a fairly good magic number[12]. For the neutrons, there does not appear anything clearly "magic" for the shell parameters appropriate to the actinide region. As the parameters κ and μ are extrapolated into the $A \approx 300$ region (see Fig. 3a,b), the $N = 164$ subshell disappears entirely while the shell closing at $N = 184$ may be said to approach magicness (as does also $N = 196$).

For comparison we have included in the same figures the level schemes obtained by Rost according to similar extrapolation rules outlined in ref. [21]. Although in the details there are considerable differences, there is an overall agreement in the prediction of low level density for spherical shapes for $A = 114 - 126$ and for $N = 178 - 184$. As detailed calculations bear out, this situation is favorable to the establishment of a spherical ground state and hence a large barrier against fission.

2. THE PAIRING FORCE

Of relatively minor importance for the equilibrium distortion is the pairing force once the coupling scheme is established for deformed nuclei. However, we require the binding energy for the ground state and the transition region to be good to 1 part in 3000 for our purpose of studying nuclear stability. Then the pairing effect is decisive.

The pairing force, originally introduced by Bohr, Mottelson, and Pines[22], was basically thought of as being a simplified representation of δ-force interaction, but further limited to act only between pairs of time reversed states, which have the largest orbital overlap. The single-particle energy sum is replaced by the expression

$$E = \sum_{\nu} e_{\nu} 2v_{\nu}^2 - G\Big(\sum_{\nu} u_{\nu} v_{\nu}\Big)^2 - G \sum_{\nu} v_{\nu}^4 + G \sum_{\nu}{}' 1$$

where e_{ν} are the single-particle energies and u_{ν} and v_{ν} the usual pairing factors. The sums are taken separately over neutrons and protons with pairing matrix elements G_n and G_p, respectively. The last term, with summation $\sum'$ over occupied energy levels, represents the subtraction of the diagonal pairing energy† so that only the strict correlation energy remains.

The overall A dependence of G is assumed to be proportional to A^{-1}. This corresponds to the fact that in lieu of any other correlations, the overlap integral should be inversely proportional to the volume. In the simplified version of pairing energy one employs

one single average pairing matrix element as given above and a corresponding choice of the cut-off energy above and below the Fermi level. To some extent a greater cut-off energy can be compensated by a smaller matrix element within a given region of A. However, in addition one has to account for the empirical result that the odd-even mass difference, which in the simple pairing theory is equal to Δ, half the pairing gap, depends on A as follows:

$$\Delta = \frac{12}{\sqrt{A}} \text{ MeV} \quad .$$

The magnitude of Δ and its A dependence will set some limits on the freedom of choice (see below).

2.1. ISOSPIN DEPENDENCE OF PAIRING

The pairing effect has its main contribution from ^{1}S-interaction, which depends critically on the collision energies. The collision energies may be found from the depths of the neutron and proton potential wells which, in turn, depend not only on A but also on Z. Thus, the pairing matrix element is isospin dependent.

In the limit N = Z, the collision velocities are to the lowest order similarly distributed for both neutrons and protons. It is therefore reasonable to assume an expansion in N - Z:

Multiplication sign

$$G \cdot A = g_0 \pm g_1 \frac{N - Z}{A}$$

where the plus sign holds for protons and the minus sign holds for neutrons. In other words, we have replaced the usual paramters G_n

and G_p by g_0 and g_1 defined above. Actually even in the $N = Z$ case, though similar orbitals are filled, the protons are affected by the Coulomb field. One might allow for this by giving different g_0 and g_1 values to neutrons and protons. This would also account for some higher-order terms in $(N-Z)/A$ in the expansion. However, we assume at the moment the same set of g_0 and g_1 for neutrons and protons, without introducing any additional parameters.

It was found that we could reproduce reasonably well the empirical odd-even mass differences and their $A^{-\frac{1}{2}}$ dependence for constant g_0 and g_1 from $A \approx 150$ to $A \approx 250$ by including $\sqrt{(15\,Z)}$ or $\sqrt{(15\,N)}$ states above and below the proton or neutron Fermi level.† These somewhat arbitrary cut-offs correspond roughly to the inclusion of three proton or neutron oscillator shells.

With these prescriptions we find $g_0 = 19.2$ MeV and $g_1 = 7.4$ MeV by fitting Δ to odd even mass differences in the rare earth and actinide nuclei. Figures 4a,b show the fit achieved in the rare earth region.

Fig 4a,b

2.2. SURFACE DEPENDENCE OF PAIRING

To reproduce the indicated energy gap at the fission saddle point[23] of about 2 MeV for ^{240}Pu and of about 3-4 MeV at the fission saddle point for ^{210}Po one must, as Stepien and Szymanski did[24], assume an increase of G with distortion. Such an assumption receives support from the energy gap calculation based on the "slab model" by Kennedy, Wilets, and Henley[25]. We have in separate

calculations assumed G to be constant with deformation and to be proportional to the surface area, respectively. The latter assumption appears to account better for fission half-lives as well as for the apparently large energy gap at the fission saddle point.

Setting G directly proportional to S corresponds to the simplified assumption that the contribution to the pairing from the inner regions of the nucleus is negligible and that the surface region is entirely responsible for the pairing. The assumption that pairing is largely a surface phenomenon is based on the fact that, at the large collision velocities encountered in the center of the nucleus, the ^1S phase shift becomes very small and ultimately changes sign. The slab model calculations[25] bear out that Δ is proportional to $S^{3/2}$ while the simple assumption of $G \approx S$ leads to $\Delta \approx S^3$ as borne out by Fig. 5. The surface dependence of G suggested by the slab model thus appears to fall half-way between the two assumptions of G = const. and $G \approx S$.

That the assumption of $G \approx S$ implies $\Delta \approx S^3$, can be seen from the following simple arguments. For the case of doubly degenerate evenly spaced levels distributed between $-C/2$ and $C/2$ with a level distance of ρ^{-1} one obtains the approximate relation

$$\Delta = C\, e^{-\frac{1}{G\rho}} .$$

Considering a small deviation in G from a "normal" value G_0

$$G = G_0 + \delta G ,$$

one obtains

$$\frac{\delta\Delta}{\Delta_0} = \frac{1}{G_0\rho} \frac{\delta G}{G_0} .$$

Provided δS is small and $\frac{\delta G}{G} \approx \frac{\delta S}{S}$ we thus obtain

$$\Delta \sim S^{\frac{1}{G_0\rho}}$$

For the empirically realistic case of $G\rho \approx \frac{1}{3}$ we obtain $\Delta \sim S^3$.

The effect of the inclusion of pairing relative to a simple summation of single-particle energies is exhibited in Fig. 6 for the case of ^{254}Fm. While the pairing energy is about 14 MeV for $\epsilon = 0$, it is reduced to about 1 MeV at the equilibrium distortion and thereafter exhibiting strong fluctuations. The variation in Δ_n and Δ_p with ϵ for ^{254}Fm may be studied in Fig. 7.

Fig 6

Fig 7

3. COULOMB ENERGY

The Coulomb energy may be written as

$$E_c = \sum_{i>j}\sum \int \underset{\sim}{\Psi}^*(\underset{\sim}{r}_1 \cdots \underset{\sim}{r}_Z) \frac{e^2}{|\underset{\sim}{r}_i - \underset{\sim}{r}_j|} \underset{\sim}{\Psi}(\underset{\sim}{r}_1 \cdots \underset{\sim}{r}_Z)\, d\underset{\sim}{\tau}_1 \cdots d\underset{\sim}{\tau}_Z \quad ,$$

where, if correlations are neglected, $\underset{\sim}{\Psi}$ is the Slater determinant of single-particle states. If we further neglect antisymmetrization and replace $\underset{\sim}{\Psi}$ by a simple product of single-particle wavefunctions, we get

$$E_c = \sum_{i>j}\sum \iint \underset{\sim}{\rho}_i(\underset{\sim}{r}_i)\, \underset{\sim}{\rho}_j(\underset{\sim}{r}_j) \frac{e^2}{|\underset{\sim}{r}_i - \underset{\sim}{r}_j|}\, d\underset{\sim}{\tau}_i d\underset{\sim}{\tau}_j \quad ,$$

where the single-particle density $\underset{\sim}{\rho}_i$ is defined as

$$\underset{\sim}{\rho}_i = \underset{\sim}{\Psi}_i^* \underset{\sim}{\Psi}_i \quad .$$

The Coulomb energy can then be evaluated with the single-particle wavefunction calculated in Section 1†. Presently we have been content with the simplification of assuming $\underset{\sim}{\rho} = \underset{\sim}{\rho}_i$ to be a homogeneous charge distribution with constant density inside a sharp surface enclosing a volume equal to $\frac{4\pi}{3} \underset{\sim}{R}_c^3$, where $\underset{\sim}{R}_c$ is the effective radius, so defined that the total charge is enclosed if the charge density is constant everywhere $\underset{\sim}{\rho}(\underset{\sim}{r} \leq \underset{\sim}{R}_c) = \underset{\sim}{\rho}(0)$. The surface may be described by $\underset{\sim}{r}(\underset{\sim}{\theta})$, which is a function of deformation.

In principle this is a six-dimensional integral. It can however be reduced[26] to a two-dimensional integral in terms of elliptic functions. This two-dimensional integral is then evaluated numerically for axially symmetric but otherwise arbitrary shape.

We have introduced corrections for surface diffuseness and exchange energy, which are of the order of a few percent. The expression used may be written as

$$E_c = \frac{3}{5}\frac{Z^2e^2}{R_c}\left[g(\xi, \epsilon_4, \ldots) - \frac{\pi^2}{2}\frac{5}{3}\left(\frac{a}{R_c}\right)^2 - \frac{0.7636}{Z^{2/3}}\right] ,$$

where the first term is obtained by the integration described above. $g(\xi, \epsilon_4 \cdots)$ assumes the value of one for a simple sphere. The second term is the diffuseness correction as derived by Myers and Swiatecki[11] with a denoting the diffuseness depth (taken to be 0.546 fm). To lowest order in a/R_c, the correction has no shape dependence. If we had used, instead of R_c, the half density radius $R_{\frac{1}{2}}$, the diffuseness correction would be $-\frac{3}{5}\frac{Z^2e^2}{R_{\frac{1}{2}}}\frac{\pi^2}{2}\frac{7}{3}\left(\frac{a}{R_{\frac{1}{2}}}\right)^2$ for a sphere but would have a shape dependence on deformation. Finally the third term corrects for the extra correlation of the protons implied by the requirement of antisymmetry of nuclear wavefunctions. From the derivation of this term by Bethe and Bacher[9], one may verify that it represents a volume energy and is thus independent of nuclear shape. Since the exchange term is the result of short-range correlations, the correction to this term resulting from the finite size of the nucleus is proportional to the

nuclear surface area and is smaller by $A^{1/3}$ than the leading term given above. This surface correction to the exchange correction has not been included.

4. GROUND STATE DISTORTIONS

For each nucleus, the potential energy as a function of deformation is obtained by adding the Coulomb energy to the sum of single-particle and pairing energies. Ground state distortions in ϵ, ϵ_4, and ϵ_6 correspond to the position of the lowest minimum in the potential energy surface in these deformation co-ordinates.

Experimental quantities do not usually relate directly to any one of these co-ordinates. Thus the quadrupole moment receives a large contribution from the interference of ϵ and ϵ_4 deformations. It can be more accurately calculated directly from the nucleonic wavefunctions. When nuclear quadrupole moments so calculated are compared with measurements of cross-sections for Coulomb excitation of deformed nuclei, good agreement of the general trend with Z and A is found, but the absolute values from the theory are generally 5-10% too small[27]. We do not exhibit any comparison as earlier results in the field are essentially reproduced[1,2,5].

In the case of ϵ_4 and ϵ_6 deformations, more direct comparison is presently possible. A detailed optical-potential analysis of inelastic alpha scattering data on the rare earth nuclei has recently been carried out by Hendrie et al[28]. They assume nuclear equipotential surfaces to be given by†

$$R_{\frac{1}{2}} = \overset{\circ}{R}_{\frac{1}{2}}(1 + \beta_2 Y_{20} + \beta_4 Y_{40} + \beta_6 Y_{60}) .$$

The differential cross-sections involving populations of rotational bands of even-even deformed nuclei up to 6^+ (and in some cases 8^+) are fitted by a combination of β_2, β_4, and β_6.

From Fig. 8, the agreement between theoretical and empirical β_4 values appears remarkable. It has been pointed out[29,30] that β_4 deformation is already present in the zeroth order distortion by the prescribed filling of levels in the deformed well. Thus the first few spheroid orbitals outside the closed shell have a large positive contribution to β_4. The same is true for the last filled orbitals. On the other hand, the orbitals near the middle of a shell have a large negative contribution to β_4. Thus β_4 is expected to grow from zero for closed shells up to a maximum value at about $\frac{1}{4}$ through the shell; then decrease to a negative minimum $\frac{3}{4}$ through the shell; until at the closing of the shell β_4 increases to zero. Actually, just the inclusion of the couplings within each N-shell, reduces the distortions somewhat relative to those obtained by keeping only the diagonal contributions as in ref.[31]. It is found that polarization (coupling between shells N and N ± 2) enhances the effect by a factor of 2 or 3. Coulomb interaction generally favours positive β_4 for small deformations. However pairing has a smearing trend and therefore tends to counteract the effects of polarization and Coulomb interaction. For this reason earlier calculations[31,32] that neglected pairing, polarization, and Coulomb repulsion still gave rather similar results to those of the present calculations. (see Figs. 10a and 10b).

The parameter β_6 is less accurately determined. It appears, however, safe to say that in general and over the whole region studied, $152 \leq A \leq 178$, numerically small and negative β_6 values are present (see Fig. 11 for comparison with theory).

In Figs. 12a and 12b we exhibit theoretical deformation parameters ϵ and ϵ_4 associated with nuclei in the rare earth and actinide regions. These diagrams should be consulted before using the single-particle energy diagrams in order to choose the diagrams corresponding to the appropriate deformations.

5. GENERALIZED STRUTINSKI PRESCRIPTION AND NORMALIZATION TO THE LIQUID DROP MODEL

To study the behavior of a nucleus at large deformations we have calculated the total potential energy surface for the range of ϵ between -0.5 and 0.95 and ϵ_4 between -0.08 and 0.16. The co-ordinates ϵ_3 and ϵ_6 have been set equal to zero. Smaller ranges of ϵ and ϵ_4 are studied for some nuclei whose physically interesting features appear to be in a smaller region. It is found that (Fig. 13) the behavior of the energy surface is unsatisfactory for large ϵ.

The conservation of the volume enclosed by equipotential surfaces is only roughly adequate, first because the saturation condition is reached only in the more central parts of the nucleus, not in the surface area. Also matter and potential shapes agree only at equilibrium points. The situation is made worse by the fact that our volume conservation condition does not include the entire nuclear potential. In particular, it does not include the term ρ^4 or $\underset{\sim}{\ell}^2$. Although the $\underset{\sim}{\ell}^2$ term has some properties of a surface energy at small distortions, it is inadequate at large distortions and large A-values[29], for which cases, it favors shapes with smaller $|\underset{\sim}{\ell}|$ contrary to the surface energy effect. Hence some smooth corrections to the geometry of the potential energy surfaces are not unexpected.

One may note that the magnitude of the correction may be large, as the restoring energy introduced by the volume conservation condition is of large magnitude, being roughly proportional to $\frac{1}{9}\varepsilon^2$ times the total nuclear energy, which is of order of 1000 MeV for $\varepsilon = 0.9$. On the other hand, the topological character of the surface should be correct as the empirical level order is reproduced.

It is also found that the absolute value of the potential-energy surface does not behave correctly, in particular not, as a function of mass number A. Thus it is necessary to make a smooth renormalization of the potential-energy surface not only with respect to distortions but also with respect to A. The absolute magnitude of the potential-energy surface at its minimum gives the mass of the nucleus.

The basic idea, advocated by Myers and Swiatecki[11], Strutinski[7] and others is the following. The average behavior of nuclear binding energies or masses as a function of distortion and mass number and charge number is well reproduced by the liquid drop mass formula which consists of a volume term proportional to A and a surface term proportional to $A^{2/3}$ as well as symmetry and Coulomb energies. The success of the liquid-drop model as applied to fission theory, where large distortions are involved, and for the calculation of nuclear masses, where large numbers of masses are considered, seems to indicate that, if shell effects are averaged out by some means, the

potential energy surface as a function of deformation and mass number can be well accounted for by this model. The idea is then that if we take away the average trend from the single particle and pairing calculations and replace it by the liquid drop formula, we will get a much improved energy surface where the local structure is given by the shell model calculations and the smooth trends are given by the liquid drop formula:

$$\text{Potential Energy } (\underline{N},\ \underline{Z},\ \text{distortions})$$

$$= E_{LD} + E_{Shell}(N) + E_{Pair}(N) + E_{Shell}(Z) + E_{Pair}(Z) \quad ,$$

$$E_{Shell} + E_{Pair}$$

$$= \sum_{\underline{\nu}} e_{\underline{\nu}}\, 2\, V_{\underline{\nu}}^{2} - \frac{\Delta^2}{G} - G\Big(\sum_{\underline{\nu}} V_{\underline{\nu}}^{4} - \sum_{\nu}{}' 1\Big) - E(\underline{g}) - \langle E_{Pair} \rangle \quad ,$$

where $\underline{E}(\underline{g})$ is the smooth average trend of the total single particle energies with variations of deformation and $\underline{A}$ (the meaning of $\underline{g}$ will be clear later); $\langle E_{\underline{pair}} \rangle$ is the average of pairing energy at the ground state distortions and $\underline{E}_{LD}$ is the liquid drop energy. Let us discuss these terms separately.

The pairing energy is averaged at the ground state distortions. The systematic growth in pairing energy with deformation due to the assumption that the pairing strength is proportional to nuclear surface

area is not subtracted out. This is a feature associated solely with large distortions and is assumed not to be built into the liquid drop mass formula which is derived for spherical and moderately deformed nuclei.

One may estimate the small quantity $\langle E_{pair} \rangle$ from the following approximate relations

$$E_{pair} \approx -\left(\frac{1}{2} \rho_n \Delta_n^2 + \frac{1}{2} \rho_p \Delta_p^2 \right) .$$

We have chosen G_n and G_p such that (see above)

$$\langle \Delta_n \rangle \approx \langle \Delta_p \rangle \approx \frac{12}{\sqrt{A}} \text{ MeV} .$$

The level densities can be estimated for the simple oscillator model as

$$\rho_n \approx \rho_p \approx \frac{1}{2} \left(\frac{3}{2} \right)^{2/3} \frac{A^{2/3}}{\hbar\omega_0} \text{ (MeV}^{-1}) .$$

In this way one obtains

$$\langle E_{pair} \rangle \approx -2.3 \text{ MeV} ,$$

independently of A.

To the extent $\langle E_{pair} \rangle$ is independent of A, its absolute value is, of course, largely irrelevant. In the comparison of calculated masses with empirical ones, we have thus arbitrarily set $\langle E_{pair} \rangle = -2.3$ MeV. The comparison will be discussed in the next section.

To obtain the smooth average of the total single-particle energy, $E(g)$, we have studied and generalized a prescription first introduced by Strutinski[7]. Consider the level density given by

$$G(e') = \sum_{\nu} \delta(e' - e_{\nu}) \quad .$$

One can form a smooth average level density by smearing out each energy level e_{ν} by a width γ and then taking the sum. We expect $G(e')$ to have short-range fluctuations with range λ, which should be of the order of shell spacing $\hbar\omega_0$, and also long-ranged variations, with characteristic range, L, of the order of the Fermi energy. The problem is then to smooth out the short-range fluctuations and to retain the long-range variations. Obviously one would expect that $\lambda < \gamma < L$. For the results to be physically meaningful, they should be independent of γ over a wide range of values between these limits. One would then write down the smoothed level density as

$$g(e) = \frac{1}{\gamma\sqrt{\pi}} \sum_{\nu} f_{corr} \exp(-u_{\nu}^2) \quad ,$$

$$u_{\nu} = \frac{e - e_{\nu}}{\gamma} \quad ,$$

where f_{corr} is a correction factor to the simple gaussian smearing of levels that will ensure that the long-range variation is retained. Thus, if the long-range variation can be written down as a polynomial of order m, an expression can be explicitly written down for f_{corr}.

Requiring the order m to be six (or in fact, even up to seven), one has

$$f_{corr} = 1 + (\frac{1}{2} - u_{\nu}^2) + (\frac{3}{8} - \frac{3}{2} u_{\nu}^2 + \frac{1}{2} u_{\nu}^4)$$

$$+ (\frac{5}{16} - \frac{15}{8} u_{\nu}^2 + \frac{5}{4} u_{\nu}^4 - \frac{1}{6} u_{\nu}^6) + \cdots \quad .$$

With this prescription, $g(e)$ will have the same smooth polynomial behavior as $G(e)$ up to sixth or seventh order. Any error will be in the eighth order.

The smooth total single-particle energy is then

$$E(g) = \int^{E_F} 2\, e\, g(e)\, de \quad ,$$

with the Fermi energy E_F given by

$$N \text{ (or } Z) = \int^{E_F} 2\, g(e)\, de \quad .$$

E_{Shell} is then defined as the difference between total single-particle energy calculated on the original level density and that on the smoothed level density

$$E_{Shell} = E(G) - E(g) \quad .$$

In Figs. 14 and 15, we show this quantity as a function of smearing width γ for neutrons of Pu^{242} and Pb^{208}, respectively. Similar figures are valid for protons. It is obvious that the keeping of terms in f_{corr} up to only second order introduces a serious folding

error and the result is strongly dependent on r, but when we include terms up to sixth order, the result is rather r-independent except when r is too small or too large as discussed before. For a fixed value of $r \sim \lambda$ (say $r = 0.8$ in the Figure), corrections introduced by the various orders can be estimated to be reduced with the factor $(\lambda/L)^m$. Thus the change from the zeroth to the second order result is $\approx$60 MeV; from the second to the fourth order is $\approx$1 MeV, and from the fourth to sixth order, only $\approx \frac{1}{60}$ MeV. Hence we find that our calculation converges very well to a unique value for the shell contributions.

The expression for the total potential energy also requires the liquid drop energy E_{LD}. For this we take directly from the work of Myers and Swiatecki[11]

$$E_{LD} = -a_1(1 - \kappa I^2)A + a_2(1 - \kappa I^2)A^{2/3} + \text{Coulomb Energy} \quad ,$$

$$I = \frac{N - Z}{A} \quad .$$

The parameters are given by

$$a_1 = 15.4941 \text{ MeV}$$

$$a_2 = 17.9439 \text{ MeV}$$

$$\kappa = 1.7826 \quad .$$

We have discussed the Coulomb energy in a previous section and the Coulomb radius is taken as $1.2249\ A^{1/3}$ fm. The magnitude of this

Coulomb radius is conspicuously large. It might be partly due to the assumption that the isospin dependence proportional to I^2 is of the same relative magnitude in the volume and surface terms as shown in the above equation. These liquid drop parameters are determined also under the assumption of a particular simulated shell structure correction term. Although these parameters are by far the best available ones for our purposes, the introduction of the more realistic shell structure term based on our potential makes it desirable in the future to redetermine these parameters. In this redetermination the isospin parameter κ may be taken to have different values for the volume and surface terms.

In summary, we have thus replaced the smoothed part of the total potential energy surface by the results of the liquid-drop model. All local shell structure variations (the local wiggles of the energy surface) have, however, been retained.

It is thus important to verify that the equilibrium deformations, shown earlier to be in good agreement with experiments, remain the same. Indeed the changes in ε and ϵ_4 are in most cases less than 0.01 in absolute value. This is not unexpected, because we know the liquid-drop part of the total potential energy is a smoothly varying function, always predicting ground states to be at zero deformation. Any deformation of ground states will be completely due to the local fluctuations of the shell effect, which have been retained.

6. NUCLEAR MASSES

In Fig. 16, we compare empirical and theoretical masses† with reference to the liquid-drop masses at zero deformation. Thus the top curve gives the experimental values minus the respective spherical liquid-drop masses in MeV. Immediately below, the theoretical values at ground state equilibrium deformations are plotted. These contain all the effects of distortions and shell structure. The differences between theoretical and experimental values are exhibited as the third and lowermost graph in the figure. They reflect on the appropriateness both of the liquid drop parameters chosen and of the nuclear shell and pairing fields employed. Although the comparison shows encouraging agreements, there are three points of deviations

(i) The overall trend seems to be towards too small theoretical masses with large $\underline{A}$ values.

(ii) There appear to be relatively large discrepancies connected with the doubly-closed shells of ^{208}Pb. The theoretical binding energy is underestimated by about 2 MeV below and around $\underline{A} = 208$.

(iii) The isospin dependence within each band of isotopic masses shows a marked discrepancy especially for large $\underline{A}$ values.

First of all, as mentioned in the last section, it may be desirable to readjust the Myers-Swiatecki liquid drop parameters. Masses of spherical and deformed nuclei could be affected differently. If we further assume different isospin dependence (symmetry energy coefficients) for volume and surface terms, we would probably be able to improve on the theory on all the three points listed above.

On the other hand, the underestimate of binding near doubly closed shells may reflect on the details of the single-particle calculations. The pairing energy calculated on the basis of the simple BCS model employed collapses near closed shells, but actually there still remains some pairing energy of the order of one MeV as can be brought out by an RPA calculation. The presence of low-lying 3^- [a] state in ^{208}Pb indicates the existence of other correlations. The underestimate in binding for A between 190 and 200 may be associated with the neglect of the rotational asymmetry degree of freedom which is believed to play a role in this region.

The masses for the superheavy nuclei beyond the present experimental region show a broad shell structure at $Z = 114$ and $N = 184$ to 196. It is not as strong as the ^{208}Pb shell, but may be a bit underestimated as in the Pb region. As shown below, this shell is the main reason to believe that there may exist in this region an island of relative stability which may be explored experimentally.

7. POTENTIAL ENERGY SURFACES

From the minimum of a potential-energy surface we can obtain the ground-state mass and distortion which are discussed above. A further study of the potential-energy surface will bring out more features of physical interest, in particular those connected with spontaneous-fission barriers and shape (or spontaneous-fission) isomers. Let us discuss first of all the possible errors of these surfaces.

Two representative energy surfaces are exhibited in Figs. 17a,b. The separate contributions from the liquid-drop terms and the shell plus pairing energies are exhibited in Figs. 18 and 19. For small distortions from the spherical shape we expect the $(\varepsilon, \varepsilon_4)$ parameterization as used to be adequate. However at large distortions higher multipoles will be important in the calculations of saddle point energies[26,34]. Since for larger values of fissility parameter[†] x, the liquid-drop saddle points occur at smaller distortions and vice versa, we expect higher multipoles to be important for lighter nuclei whose values of x are small, and that the $(\varepsilon, \varepsilon_4)$ parameterization should be sufficient for heavier nuclei which have large values of x. Thus when we compare the liquid drop saddle point energies in our $(\varepsilon, \varepsilon_4)$ scheme with the more general parameterization used in ref.[34] we find for U, with its saddle point at $\varepsilon \approx 0.85$, that our value is too high by 0.6 MeV; for Pu, whose saddle point is at $\varepsilon \approx 0.75$, by 0.3 MeV; and for nuclei heavier than Cm ($Z = 96$) the error is less than 0.1 MeV. In particular for superheavy nuclei

($Z \approx 114$, $A \approx 298$), the error due to the restricted parameterization should be small.

The potential-energy surface plots show that the importance of the ϵ_4 degree of freedom as ϵ is increased. Although in the ground states both positive and negative values of ϵ_4 occur, the saddle point always occurs for a positive ϵ_4, representing a smaller waistline relative to the spheroid, which develops as ϵ increases (compare Fig. 1). In Fig. 6, one may study the effect of the ϵ_4 degree of freedom on the barrier of ^{254}Fm. Obviously its inclusion is necessary to give a reasonable barrier.

The further inclusion of the rotational asymmetric degree of freedom appears to reduce the saddle point energies. Thus, as reported by V. V. Pashkevich[35], the energies of the saddle points closest to the ground state for nuclei between ^{240}Pu and ^{256}Fm are reduced by amounts ranging from 0.4 MeV to 2.1 MeV. We have also made some calculations which include the P_6 degree of freedom. This is relatively unimportant but is found to lower the barriers by 0.2-0.3 MeV for most actinide elements. (As to the P_3 degree of freedom see below.)

In Figs. 20a-m we exhibit the barriers obtained for isotopes of $Z = 92$ to $Z = 114$ as a function of ϵ with minimization of energy with respect to ϵ_4 at each point. This type of plot represents a cut through the two-dimensional topographical map in the (ϵ, ϵ_4) plane along the potential energy minimum path with the energies projected onto the ϵ axis. Two plots are shown for the two alternative assumptions of the pairing strength: G equal to a constant and G proportional to the nuclear surface area. As pointed out in

the section on pairing energy we find the second alternative to be more adequate. This first alternative gives much too high fission barriers for U, Pu and Cm. However with a surface dependent pairing strength the barrier heights are within a few MeV of those obtained from experimental data analyzed in terms of the conventional liquid-drop barrier energy.

7.1. THE STRUCTURE OF SPONTANEOUS FISSION BARRIERS OF HEAVY AND SUPERHEAVY NUCLEI

The conventional liquid-drop barrier has the ordinary one-hump shape, but because of shell effects at moderate deformations, structures can be found in the realistic spontaneous fission barrier. These shell effects are understood to be the result of an extra shell binding that occurs at some moderate deformation and are of exactly the same type as the shell effects that appear for spherical shapes. Gross shell effects at larger distortions were considered by Geilikman[36] and later by Myers and Swiatecki[11] more realistic ones by Strutinski[7]. It was Strutinski who first emphasized that they will cause a double-humped fission barrier; such a double hump is also indicated in our 1966 calculations[12].

As a general feature, we note that in our plots of potential energy barriers, there exist in general three minima in energy. For the actinides the lowest one is at the prolate side of the spherical. For the superheavy nuclei as well as those in the Pb region the lowest minimum is at zero deformation. This should obviously corre-

spond to the ground state of the nucleus. An oblate minimum also occurs which in the actinide case is usually more than 5 MeV higher. This minimum has been shown by Arseniev, Malov, Pashkevich and Soloviev[37] to be a spurious minimum. When the rotational asymmetric (γ) degree of freedom is included, this "minimum" is found to be a maximum in the γ direction leading down to the lower ground state through a path provided by this extra degree of freedom. For lighter nuclei in the rare earth region this minimum is not much higher than the ground state minimum. In some cases, it may be actually lower and should be taken as the ground state. It is of particular interest to find the points on the mass surface, i. e. the N and Z values where a transition from a prolate to an oblate ground state takes place. A third minimum occurs at a strongly prolate shape usually at $\varepsilon \approx 0.60\text{-}0.75$ for the actinides. Of course, because of the fine details of shell effects at various deformations, other structures of the fission barrier may be discerned and some of these may be important for mass regions other than those considered here.

We can study the effect of shell corrections to the liquid drop barrier as shown in Fig. 21. For the actinides, even though the liquid drop definitely favours a spherical ground state, shell correction makes it deformed ($\varepsilon \approx 0.2$). The ground state minimum appears associated with the crossing of the shells N and $N+1$ while the secondary minimum appears associated with the crossing of shells N and $N+3$ and $N+2$. For lighter actinides the first hump is the lowest while for the heavier ones the second one dominates. The shift in magnitude between the two humps reflects mostly details of shell structure. Some role is played

by the systematic change in the fissility parameter x.

The results are collected in Table 2 where we tabulate the heights of the two humps of the barrier as well as of the secondary minimum in between, relative to the ground state. In particular is the second barrier hump probably overestimated and generally uncertain as at the large distortions in question the $(\varepsilon,\varepsilon_4)$ parametrization is insufficient.

For the superheavy nuclei region ($Z \approx 114$ and $N \approx 184$) the ground state occurs at zero deformation and the secondary minimum occurs at $\varepsilon \approx 0.4$. Since there is practically no liquid drop barrier in this region, the entire barrier is a shell structure effect (see Fig. 21). For the rare earth region, values of x are in general small so that saddle points are at very large ε. One may expect shell effects to be negligible at such large deformations.

It should be pointed out that for a particular element, a change in the number of neutrons may change the picture dramatically. The effect of the neutron number N on the fissility parameter is thereby of less significance than the shell structure effects associated with N. An example is the following result from the present preliminary investigations. For Z between 102 and 114 and for N less than 176, all the nuclei appear to have ground states near $\varepsilon = 0.3$. Since these nuclei have large x values the fission barriers exhibit only one hump (the second occurs below the ground state energy). There is also a minimum at zero deformation which lies higher than the ground state. But as N is increased, this minimum is getting lower until at

$N \approx 176$-178, the ground state minimum becomes associated with spherical shape. Hence for $N \lesssim 176$ we have a deformed ground state with a one-humped barrier. But for $N \gtrsim 178$, we have a spherical ground state with a double humped barrier with the secondary minimum at $\varepsilon \approx 0.3$. Obviously this latter case has a much thicker fission barrier and the nuclide in should be much more stable against spontaneous fission.

7.2. SHAPE (FISSION) ISOMERS

The existence of the double-humped structure with a secondary minimum in between the humps is strongly supported by the discovery of shape or fission isomers. This isomeric state corresponds to the secondary minimum which has a different shape from that of the ground state and whose energy exceeds that of the ground state by several MeV. The isomeric state may decay by gamma emission to the ground state or by spontaneous fission through the second hump barrier[38]. The gamma transition to the ground state is, however, highly hindered by the presence of the first hump. Obviously the gamma half life is roughly inversely proportional to the penetration probability of the first hump. In the rare-earth region the first hump is often nonexistent or very poorly developed and the second peak overwhelming. No fission isomer is therefore possible. For the heavier actinides the first hump is large so that gamma transition is greatly hindered and the isomeric state decays by fission through the second hump. The different barriers against fission of the ground state and the shape isomeric state is reflected in the very different half lives.

Experimentally these isomeric states are found in nuclei with $236 \lesssim A \lesssim 246$. They are thus found to decay by spontaneous fission rather

than gamma transitions. The first fission isomer, in ^{242}Am, was discovered by Polikanov et al.[39] and by Flerov et al.[40] with a fission half life of 140 ms. Since then a number of other cases have been found[41,42] with half lives ranging from milliseconds to nanoseconds. The isotope ^{242}Am seems to have an extraordinary long isomeric fission half life. This has been studied recently by Nix and Walker[38] who also speculated about the possible explanations. The excitation energies of these isomeric states appear to lie between 2 and 4 MeV. Relevant data are shown in Table 3 together with our theoretical results taken from Table 2. As pointed out before, our theoretical values are not expected to be quantitative predictions, but rather just an indication of the trends. On the other hand the three cases where comparison can be made exhibit a surprising agreement between theory and experiments.

Table 3

Additional evidence appears to support the existence of states associated with the barrier indentation. This evidence[42] is based on the study of the variation of the cold-neutron fission cross section for elements in the region $231 \leq A \leq 242$. Superposed on the fine structure of, say, a few eV, occurring at about 6-7 MeV of excitation, and relating to compound states associated with the equilibrium shape, there appears a sequence of resonances with a spacing of, on the average, about 100 eV and a width of a few eV†. The quantity D_{II}/D_I varies from about 500 in ^{235}U to about 50 in ^{241}Pu, where D_{II} refers to the spacing of the resonance type states and D_I to the spacing of the normal equilibrium shape states. Presently one interprets the resonance states as the states of the second energy minimum, as

suggested by Lynn[42]. Using the standard level density formulas one may estimate the second minimum to lie 1.5 - 3 MeV above the ground state for the various nuclei between ^{235}U and ^{242}Am. All these facts appear to be in qualitative agreement with the predictions of these present model calculations.

7.3. THE OCTUPOLE DEGREE OF FREEDOM

As is well known, nuclei between Th and Cf exhibit strong assymmetry in the fission mass distribution. In this region of elements the ratio of the most probable masses in the heavy and light group varies from 1.5 to 1.2. It appears highly plausible a priori that this fact is associated with a path to fission that involves the P_3 degree of freedom[14]. However, the bifurcation point between a symmetric and an assymmetric path may occur rather late in the fission process. A term proportional to $\varepsilon_3 P_3$ has been included in the potential, as suggested above, in complete analogy to the P_4 case. Preliminary results of calculations involving a set of ε_3-values, $\varepsilon_3 = 0, 0.02, 0.04, \ldots 0.10$ have been obtained near the first barrier peak ($\varepsilon = 0.40, \varepsilon_4 = 0.04$), at the secondary minimum ($\varepsilon = 0.63, \varepsilon_4 = 0.07$) and at the secondary peak [$\varepsilon = 0.85, \varepsilon_4 = 0.12$]. All these points indicate stability towards ε_3-distortions. However, the stability is decreasing with distortion. Furthermore, only slightly removed from the second peak at [$\varepsilon = 0.85, \varepsilon_4 = 0.16$] there occurs an ε_3 instability particularly for the lighter actinides. The investigation is being continued.

8. BARRIER PENETRATION AND MICROSCOPIC THEORY OF THE FISSION PROCESS

A problem of foremost importance in connection with the stability of a nucleus against spontaneous fission is that of the dynamical inertial mass associated with the penetration of the fission barrier.

Let us assume for the moment that the problem is one-dimensional and that ϵ is the relevant co-ordinate. According to the simple WKB theory the probability for the penetration of a barrier is given by the expression

$$P = \exp\left\{-2\int_{\epsilon'}^{\epsilon''}\sqrt{\frac{2B}{\hbar^2}(W(\epsilon) - E)}\,d\epsilon\right\} \equiv \exp(-K) ,$$

where B is the inertial mass associated with fission, E is the initial excitation energy of the nucleus towards fission, and $W(\epsilon)$ represents the barrier as obtained from a potential energy surface considered in the previous section. There exists an improved expression, as e.g. exhibited in P. O. Fröman and N. Fröman[43]:

$$P = (1 + \exp K)^{-1} .$$

This differs from the one above mainly for small K values, i.e. for energies E near the top of the fission barrier. In particular, when E is equal to the top of the barrier, the probability for penetration is 0.5. In our calculations below we consider only very small E values for spontaneous fission, so we use the previous expression, which should be adequate. In the integral above, if ϵ is dimensionless

as in our calculations, B will have the dimension of a moment of inertia. Thus if we scale the nuclear system simply according to its mass number, then B would be proportional to $A^{5/3}$. This scaling effect can be taken out by considering the quantity $BA^{-5/3}$.

The quantity P is the probability of penetration through the barrier for a given "assault" towards fission. The number of assaults, n, on the barrier per second is usually equated to the frequency of the beta-vibrational motion at the equilibrium point. Setting $n = 10^{20.38}$ corresponds to a vibrational frequency of $\hbar\omega_{vib.} \approx 1$ MeV. We have thus the half life given by

$$\tau = \frac{\ell n\, 2}{n} \cdot \frac{1}{P} = 10^{20.54} \exp K \quad \text{(seconds)} \quad .$$

The probability of penetration through a parabolic barrier of height S above the energy minimum and with a curvature C has been derived exactly by Hill and Wheeler[44]. We can obtain the same result by using Fröman and Fröman's expression for P. With $\omega_f = \sqrt{(C/B)}$ one finds for K:

$$K = \frac{2\pi(S - E)}{\hbar\omega_f} \quad .$$

Hence the Hill Wheeler expression is obtained:

$$P = \left[1 + \exp\left(\frac{2\pi(S - E)}{\hbar\omega_f}\right)\right]^{-1} \quad .$$

From the dependence of the penetrability on E, not only S but also an average $\hbar\omega_f$ is experimentally accessible. Empirical analysis gives S as dropping from 8 to 4 MeV when A goes from 230 to 250. And various empirical values of $\hbar\omega_f$ were found between 300-400 KeV. As all such experimental analysis is based on the assumption of a one-humped barrier and not one with two-humps (which should be the case in this region of A), these estimates will have to be re-evaluated.

In the preliminary discussion above we used a one-dimensional description and furthermore the inertial parameter B entered as a completely phenomenological quantity. However, an estimate of this parameter may be obtained from the microscopic treatment of the nuclear fission process[3]. The detailed calculations of B are the subject of a separate paper[45]. Here, we shall only briefly describe the method of the calculation and quote the main results.

In the case of a one-dimensional collective motion the total energy of the nucleus is expanded in terms of the deformation parameter ϵ and its time derivative $\dot{\epsilon}$. The inertial parameter B_ϵ appears as a coefficient in front of the term $\frac{1}{2}\dot{\epsilon}^2$. The resulting formula for B_ϵ is

$$B_\epsilon = \frac{2\hbar^2\Sigma_3}{(2\Sigma_1^2)} \left(\frac{\partial Q}{\partial \epsilon}\right)^2 ,$$

with

$$\Sigma_n = \sum_{\nu\mu} \frac{\langle\nu|q|\mu\rangle^2 (U_\nu V_\mu + V_\nu U_\mu)^2}{(E_\nu + E_\mu)^n}$$

(where n = 1 or 3)

Here E_ν denotes quasiparticle energy equal to $\sqrt{((\varepsilon_\nu - \lambda)^2 + \Delta^2)}$; $\langle\nu|q|\mu\rangle$ are matrix elements of the single-particle quadrupole operator $q = 2r^2 P_2$, and U_ν, V_ν are the coefficients in the BCS trial wave function. Finally $\frac{\partial Q}{\partial \varepsilon}$ is the derivative of the total (mass) quadrupole moment Q with respect to the deformation parameter ε.

The resulting values for the inertial parameter are given in Table 4 for two deformations $\varepsilon = 0.2$ with $\varepsilon_4 = 0$ and $\varepsilon = 0.5$ with $\varepsilon_4 = 0.02$. It may be instructive to compare the calculated values of B with those following from the assumption of the irrotational flow in the liquid-drop picture of the nucleus. The corresponding formula for the inertial parameter B_{irr} has the form

$$B_{irr}(\varepsilon) = \frac{2}{15} AMR_0^2 \left(1 - \frac{1}{3}\varepsilon^2 - \frac{2}{27}\varepsilon^3\right)^{-\frac{4}{3}} \frac{\left(1 + \frac{2}{3}\varepsilon^2\right)}{\left(1 - \frac{2}{3}\varepsilon\right)^2} .$$

It can be concluded that the ratio $B_\varepsilon/B_{irr}(\varepsilon)$ is of the order of (6 to 11) for large deformations ($\varepsilon \approx 0.5$) and of the order of (4 to 9) around the equilibrium point (at $\varepsilon \approx 0.2$).

Apart from the rather strong ε-dependence of B, it also turns out to be a sensitive quantity with respect to the choice of the pairing force: a 5% change in G induces roughly a 20% change in B. The coupling of the fissioning collective motion to pairing vibration (see ref. [46]), which also has been included in our calculation, turns out to be of relatively minor importance. The change in the inertial parameter induced by this coupling is usually of the order of 6 to 15%.

Approximate preliminary results seem to indicate that the coupling of various multipole components in the collective motion may have an important influence on the effective inertial parameter and consequently on the penetrability of the fission barrier. In particular, the complete dynamical inclusion of the ϵ_4 degree of freedom tends to diminish the effective inertial parameter B and thus to increase the penetrability of the barrier.

9. NUCLEAR STABILITIES

There are three main decay processes of importance in this mass region: spontaneous fission, alpha decay, and beta decay (or electron capture). Alpha decay half lives can be estimated from the Q-values of the process, which are directly derived from the massss of parent and daughter nuclei. Similarly by comparing masses of adjacent isobars, beta stability can be determined. Since these processes involve only mass differences between nuclei one or two units of N or Z from each other, their half life estimations will be affected only by relative errors in the nuclear mass values. Hence the alpha and beta stabilities can be determined with reasonably reliability. For the actinide region (Table 5) we are able to reproduce the experimental Q-values of alpha decay to within ±0.2 MeV and beta stable nuclei are usually verified. The results for lead region are not so satisfactory. In the latter region the difference between experimental and theoretical Q-values for alpha decay approach 0.6 MeV. This fact reflects the inadequacy of our calculations to reproduce the entire shell effects on the nuclear masses near the lead region (see Section 6). The estimation of spontaneous-fission half lives, on the other hand, involves larger uncertainties as will be discussed in detail below.

Table 5

9.1. SPONTANEOUS FISSION HALF LIVES

In our calculation of spontaneous-fission half lives[47] we have avoided application of the more complicated dynamic calculations

involving the entire quantum mechanical time-dependent problem with several degrees of freedom describing the variation in shape. Instead, we have here made use of the one-dimensional WKB approximation from which the half life is given by

$$\tau = 10^{28.04} \exp K \quad \text{(years)} \ ,$$

where

$$K = 2 \int \sqrt{\frac{2B}{\hbar^2} (W(\underline{\varepsilon}) - E)} \ d\underline{\varepsilon} \ .$$

We have thus simplified the problem to a one-dimensional barrier penetration problem constructing a path on the energy surface by minimizing the potential energy with respect to $\underline{\varepsilon}_4$ for each $\underline{\varepsilon}$ and then projecting this path onto the $\underline{\varepsilon}$ axis. Superficially one might believe this to underestimate the path integral, but this is not necessarily true. It will definitely introduce uncertainties in the results. Also, as discussed earlier, the potential barrier thus obtained, $W(\underline{\varepsilon})$, will have errors at large $\underline{\varepsilon}$ since we consider only quadrupole and hexadecapole deformations whereas higher multipoles are important at large distortions. This effect will be especially large for light actinides whose barriers extend to rather large distortions. Shell effects will have their main impact near the ground states and will be washed out at larger distortions. Thus any errors in the shell calculations will distort and not just lower the entire potential energy and hence affect the half-life estimates.

Still we have to consider the actinide region as testing region for the fission half-life calculations, and our venture into the superheavy region is based on the outcome of the half-life reproductions in that region.

Measured fission half lives are available for even-even nuclei in the actinide region from $Z=90$ and up to $Z=104$. The barrier extends for the lighter of the actinide elements to larger distortions than those for which our parameterization is adequate and for which calculations have been completed. Nevertheless we have treated, through extrapolations, all the elements above $_{92}U$. The results are particularly unreliable for the lighter of these elements. In Table 6 we list the theoretical B values obtained from microscopic theory in ref.[45] for $\varepsilon = 0.2$, $\varepsilon_4 = 0.0$ and for $\varepsilon = 0.5$, $\varepsilon_4 = 0.02$, respectively. Assuming a linear ε-dependence of B based on these points we have evaluated the integral K theoretically and semiempirically using fission half lives. (A corrected K-value, K_{corr}, is obtained simply by adding to E the error in the equilibrium mass value.)

Table 6

The latter method employed reflects an extreme assumption that the error in energy at the equilibrium point does not propagate through the barrier but is localized at the particular equilibrium point.

As seen from Table 6, a comparison for the lighter actinides between experimental and theoretical half lives using B-values from the microscopic calculations does not appear very successful. In general the K-value is in error by about 30 %, probably mostly reflecting a theoretical

overestimate of the second barrier. As B increases linearly with ε according to microscopic theory, the second hump carries a large weight.

On the other hand, for the heavier actinides, where the second hump is less negligible, the half lives are reproduced satisfactorily on the basis of microscopic B-values.

To estimate fission half lives in the superheavy region we have made use of both microscopic-theory calculations from ref. [45] performed for nuclei near $A = 300$ and of two semiempirical values of B determined in the actinide region and extrapolated into the superheavy region. Due to the inherent uncertainty in the superheavy region we have been content with just using one average value of $BA^{-5/3}$ for the entire superheavy region. (the A-factor reproducing the simple volume effect) In the semiempirical case we have assumed that $BA^{-5/3}$ be the same for all heavy and superheavy nuclei, which, however, have different shell effects and different saddle point shapes. (We have attempted to study the empirical dependence of $BA^{-5/3}$ (derived from analysis of empirical half lives) on saddle point shapes in the actinide region by plotting against the fissility parameter x and also against the mean location of the barrier along ε axis. In both cases no simple trends were discerned.)

Several methods are used to estimate $BA^{-5/3}$. The first is based on the microscopic theory. These calculations are, of course, performed for the elements in question. From the inertial parameter at the highest saddle points for superheavy nuclei we found that they cluster within 30 % of a mean value. This estimate is shown as a

Fig. 22 straight vertical line in Fig. 22, where we have plotted, for $Z = 110$ and $Z = 114$, $\ln \tau$ against $(BA^{-\frac{5}{3}}/\hbar^2)^{\frac{1}{2}}$. The slope is $2^{\frac{3}{2}} \cdot \int (W(\xi) - E)^{\frac{1}{2}} d\xi \cdot A^{\frac{1}{2}}$ where the excitation energy E is taken as 0.5 MeV corresponding to the average of the "assault" energy of vibration, as discussed in the last section. A second estimate of $BA^{-5/3}$ is made semiempirically by using the barriers for the actinides obtained from our calculations and requiring these to give the correct experimental half lives. These values of $BA^{-5/3}$ are found to cluster within ≈30% limits about a mean value which is also shown in the figure. A third estimate is also empirical and is due to Moretto and Swiatecki[48]. These authors used liquid-drop barriers modified by Myers-Swiatecki shell correction term[11] and with the ground state masses and liquid-drop barriers adjusted to experimental values for each nuclide. They are able to estimate the mean value of $BA^{-5/3}$ for the actinides with only a 10 % spread. It was found that all of these three estimates lie within 30 % of each other, and in our estimation of spontaneous fission half lives we have taken the average value of the three estimates. It should be pointed out here that this value is more than seven times the irrotational liquid-drop value, which latter should be considered only as an extreme lower limit. This ratio, seven, turns out to be somewhat larger than the corresponding ratio for the rotational moment of inertia for deformed nuclei and also larger than the ratio for the quadrupole vibrational mass.

The spontaneous-fission half lives of the superheavy nuclei are discussed in the next subsection. The half lives for the actinides are

represented in Table 5 (in contrast to Table 6) based on one single adjusted value of $BA^{-5/3}$ as the ratio in powers of ten of the experimental to theoretical values. There appears to be a systematic underestimate of half lives on the neutron-poor side and an overestimation on the neutron-rich side. A readjustment of the liquid-drop parameters with independent volume and surface symmetry energy coefficients, as suggested before, may be able to take care of this systematic discrepancy.

Some attempts are being made to explore any possible improvments of our present method. These are further discussed in ref. [45].

9.2. ISLANDS OF STABILITY IN THE SUPERHEAVY REGION

The stability against alpha and beta decay as well as spontaneous fission† has been worked out for nuclei in the vicinity of $Z = 114$ and $N = 184$. The results are tabulated in Table 7, which is summarized in the half life contours of Fig. 23.

Table 7.

Fig 23

Some general features of this figure may be pointed out. The longest fission half-lives center rather symmetrically around ($Z = 114$, $N = 184$). It must be emphasized here that any stability against spontaneous fission in this region is due to the extra binding resulting from the shell effect so that as one goes away from $^{298}114$, the fission half-lives decrease rapidly. Without the shell effect, the alpha half-lives depend on the inclination of the $\Delta N = \Delta Z$ line (which is the direction of alpha decay) with respect to the direction of the beta stability valley. The shell effect essentially increases the alpha half-lives for nuclei with $Z < 114$ and $N < 184$ and decreases those for nuclei $Z > 114$ and $N > 184$. It also causes the kink shown.

The great uncertainty associated with the numbers obtained must be emphasized. First of all there is the uncertainty of the extrapolation of the shell model potential to an unknown mass region. Furthermore, a deviation of 30% in the estimate of the inertia parameter B corresponds roughly to a factor of 10^6 in the spontaneous fission half-lives, while a 1 MeV deviation in alpha energy corresponds to a factor 10^6 difference in alpha half-lives. An under-estimate of a given nuclear mass due to a local shell effect leads normally to an overestimate of the fission half-life. On the other hand, the error in alpha energy is comparatively small. For the actinide region (where we do not have the uncertainty due to extrapolation of parameters), Table 5, our alpha energies are within 5% of the experimental values corresponding to half-lives agreeing within a factor of ten, but our fission half-lives for some isotopes can be wrong by a factor as large as 10^6 either way.

All these uncertainties may move the contours of half-lives in Fig. 23, but the general pattern should remain the same as long as $\underline{Z} = 114$, $\underline{N} = 184$ is a well-developed magic nucleus. Thus, the main use of the figure is as a guide in the search for relatively long-lived nuclei in this region.

9.3. SURVIVING SUPERHEAVY ELEMENTS

Applying a "survival-of-the-fittest" test with respect to fission, alpha decay, and beta decay in the above region and taking the calculated numbers at their face value, one ends up with one possible candidate for survival in earthly matter, namely $^{294}110$, which has a total half life of about 10^8 years. However, due to the uncertainty of our numbers as discussed above, we cannot rule out that, instead, a nucleus close-by may have a better chance of survival.

Self-consistent field calculations of the electronic configurations[50,51] indicate that the elements with even $\underline{Z}$ from 106 up to 116 have chemical properties similar to those of W, Os, Pt, Hg, Pb, and Po, respectively (Fig. 24). So these superheavy elements, if they occur in nature, may be found in ores of their respective chemical homologues. However if the total half-life falls below $\sim 2 \times 10^8$ years, the detection in earthly matter is beyond the capabilities of our present techniques.†

A question may be asked whether such a long-lived superheavy element may be produced in nature in the first place. The indication†† is that such a superheavy element could well be formed by the so-called

r-process[52] in which a nucleus absorbs a large number of neutrons very rapidly and then undergoes successive beta decays, ending up as a much heavier relatively stable nucleus. Most very neutron rich isotopes seem to be sufficiently fission stable for this process, which also requires a condition of huge neutron flux and very high temperatures. This condition may have prevailed at some point in the history of the universe and may also exist in some massive stars and quasi-stellar radio objects at this present time. This at once raises the possibility of detecting superheavy nuclei in the primary cosmic radiation. According to the most optimistic estimates, the nuclei of interest in the primary cosmic radiation may have been produced 10^5 years ago, while elements in the solar system have an age of $\sim 5 \times 10^9$ years. If we take Fig. 23 at its face value, we see that in the study of the primary cosmic rays, one might be able to find a few more nuclei which live longer than 10^5 years.

A recent preliminary search at Berkeley for element 110 in a platinum ore has yielded negative results[53]. A study of very heavy nuclei in the primary cosmic rays has recently been carried out by P. H. Fowler, P. B. Price and R. W. Walker in a balloon experiment. The data are still under analysis.

10. POSSIBLE EXPERIMENTAL PRODUCTION OF SUPERHEAVY NUCLEI

10.1 HEAVY ION REACTIONS

The heaviest elements presently produced ($Z > 100$) are all synthesized by bombardment of target elements of sufficiently high atomic number with beams of heavy ions.† The heaviest ion presently available is $^{40}_{18}Ar$, but in the future ions as heavy as $^{}_{92}U$ may be accelerated.

By heavy-ion reactions one tends to reach elements far off on the neutron deficient side of the stability line. This is so because the stability line bends more and more towards the neutron-rich side relative to its initial 45° direction in the N-Z mass plane. Both target and projectile are therefore less neutron-rich than the center of the superheavy region ($Z = 114$, $N = 184$), near to which the stability line happens to pass.[54] Even by the choice of very neutron-rich targets[55] $^{248}_{96}Cm$ and very neutron-rich projectiles as $^{40}_{18}Ar$ as in the experiments by Thompson et al.[55] and Ghiorso et al.[56]

$$^{248}_{96}Cm + ^{40}_{18}Ar \rightarrow ^{284}114 + 4n \ ,$$

one obtains only $^{284}114$ whose half life we estimate to be much less than 10^{-10} seconds and ... beyond the sensitivity of the present experimental techniques. The unfortunate loss of four neutrons is necessary to take away the excess energy of the compound nucleus. This results from the high energy necessary to penetrate the Coulomb barrier between the heavy ion and the target nucleus. From our calculations,

it appears that one has to obtain an isotope of 114 heavier than 288 before the half life becomes long enough to make detection possible.

On the other hand, there are indications that the proton number 124 may be associated with a minor shell closing in our model. Hence the nucleus $^{308}_{124}184$ may have sufficiently strong shell binding effects to make it relatively stable against spontaneous fission. To make this nucleus one would need, for example a $^{64}_{28}Ni$ or a $^{86}_{36}Kr$ projectile:

$$^{248}_{96}Cm + ^{64}_{28}Ni \rightarrow ^{308}_{124} + 4n ,$$

$$^{226}_{88}Ra + ^{86}_{36}Kr \rightarrow ^{308}_{124} + 4n .$$

(As no calculations are completed in this region, all statements are only qualitative.)

The nucleus $^{308}_{124}$ is almost certainly beta unstable and would possess a rather short alpha half life. It is a quantitative question whether the half life is long enough to make detection possible. However, even if it undergoes alpha decay or electron capture very quickly, one may still get something rather interesting if it prefers electron capture to alpha decay. By successive electron capture before alpha decay, the nucleus may actually end up somewhere in the vicinity of $^{298}_{114}184$. And there is a good chance that one may obtain some rather long-lived nuclei with total half lives of one year or more. In such cases, one can let the bombardment of heavy ions on a target be made for as long a time as it is practical and then do chemistry on the target afterwards to detect any superheavy elements that may have been produced.

In this discussion we have not considered whether these reactions have a large enough cross-section to detectable. Experience in the heaviest actinide region is somewhat discouraging. Thus the production[57] of $^{260}104$ by bombardment of ^{242}Pu with ^{22}Ne has a cross-section of only 10^{-34} cm^2.

10.2. NEUTRON CAPTURE REACTIONS

An alternative way to produce superheavy nuclei is by means of the r-process. Heavy nuclei are exposed to a high flux of neutrons. There is a competition between (n, γ) and (γ, n) reactions. If conditions are favourable, the nuclei will capture a large number of neutrons and then beta decay, ending up as heavy nuclei of much higher Z, which in turn undergo the same process. Eventually they should reach the superheavy region. This process is mentioned in the preceeding section where we have commented about the possibility of such a process reaching the superheavy region. The conditions[52] for the r-process are a temperature of $\gtrsim 5 \times 10^9$ ^oK and an integrated neutron flux of $> 10^{27}$ neutrons per cm^2. The entire time scale is assumed to be of the order of seconds. Nuclear explosive devices have an integrated flux of about 10^{25} neutrons per cm^2. The latter time scale is, however, of the order of microseconds. This process thus proceeds even further into the neutron-rich region than the r-process. This latter method has also produced fewer heavy elements than expected. Indeed ^{257}Fm is the nucleus with the largest Z and A numbers that has been obtained[54]. In our model we do not expect

^{258}Fm to possess very much shorter half life than ^{257}Fm or ^{256}Fm, and it presents a serious theoretical problem why heavier nuclei are not produced. Until it is resolved, the suspicion remains that the same cause that blocks the element-generation path connected with nuclear "devices" may also be relevant for r-process path through which superheavy elements might be produced in the universe.

At the moment it appears that the most promising way to produce superheavy nuclei is still by means of heavy-ion reactions, especially when heavier projectiles than the presently existing argon beam become available.

ACKNOWLEDGEMENTS

One of the authors (SGN) is grateful to Dr. Isadore Perlman, head of Nuclear Chemistry Division of Lawrence Radiation Laboratory for the warm hospitality granted during his stay in the Laboratory.

We are indebted to Dr. Aage Bohr, Dr. Ben Mottelson, and Dr. Larry Wilets for valuable suggestions and criticism. The great interest in this work shown by Dr. Glenn Seaborg, Dr. Wladyslaw Swiatecki, and Dr. Stanley Thompson has been decisive for its line of direction. In particular we are grateful to Dr. Swiatecki for his helpful advice in all phases of this work. Important contributions to the investigations have earlier been made by Dr. Rayford Nix. We would like to acknowledge his help and the co-operation of Dr. Sven Björnholm in compiling the experimental data in Table 3.

We would also like to thank Drs. Thompson, Swiatecki, and Nix for critical comments on the manuscript.

FOOTNOTES

Page 6 † Octupole (P_3) distortions of nuclear potential in connection with ground state nuclei have earlier been considered by S.A.E. Johansson[14] and P. Vogel[15], and hexadecapole (P_4) distortions by C. Brihage and G. Reidemeister[16].

Page 14 † Provided G is constant, independent of distortion, the subtracted term corresponds to a trivial constant shift of the total energy.

Page 16 † As the product $G\rho$ is independent of A (ρ = level density), Δ is proportional to the cut-off range assumed. Requiring $\Delta \sim A^{-\frac{1}{2}}$ we are lead to the prescription above.

Page 19 † Preliminary results of such calculations by J. Bang and A. Stenholm Jensen are reported in Conf. Int. Symp. Nucl. Str., Dubna (1968) 98. The authors find single-particle effects (as compared with a classical homogeneous charge distribution) to be of order of one MeV. As polarization effects (coupling between shells N and $N \pm 2$) are neglected, they do not consider their results reliable except for small distortions.

Page 22 † The relation between β_λ and the conventional co-ordinate α_λ is given by

$$\beta_\lambda = \sqrt{4\pi/(2\lambda + 1)}\ \alpha_\lambda$$

The relation between (β_2, β_4) and (ϵ, ϵ_4) is illustrated in Fig. 9.

Page 26 + It is not immediately obvious that for a realistic nucleus the $A^{2/3}$ term will behave like the surface area upon distortion. Numerical studies of nucleons in rectangular, spherical, and cylindrical boxes[33] are consistent with this assumption.

Page 33 + Our calculations of masses are similar to those reported by P. A. Seeger and R. C. Perisho, Los Alamos Scientific Laboratory Report, LA-3751, 1967, which provided part of the original stimulus for undertaking calculations described in this section. These authors neglected the P_4 degree of freedom and in their fission calculations represented the liquid drop barrier by a cubic in ϵ. However, they allow for an adjustment of liquid drop parameters. Our inclusion of the P_4 degree of freedom appears to improve the mass fit considerably. No adjustment of liquid-drop parameters is made in the present paper.

Page 35 + The fissility parameter x may be defined as

$$x = \frac{Z^2/A}{50.88(1 - 1.7826\, I^2)}$$, using the Myers-Swiatecki liquid-drop parameters.

Page 42 + These numbers given are relevant for the particular case of ^{235}U. They are obviously different for odd-A, odd-odd or even-even cases. For a general discussion see the article by Lynn[42].

Page 53 + The spontaneous-fission half lives of superheavy nuclei were discussed in an earlier paper[47] of ours in collaboration with Dr. J. Rayford Nix. Since then, various improvements have been made in the calculations so that we believe the present results to be relatively more reliable. The material in this as well as the next subsection forms the major part of a letter[49] written in collaboration with Dr. Stanley G. Thompson.

Page 55 + We would like to thank Dr. Luciano Moretto for drawing our attention to this point.

Page 55 ++ We are grateful to Dr. P. A. Seeger for helpful discussions of the r-process.

Page 56 + Our estimate of masses along the prospective r-process path is, however, sensitive to the value assumed for the coefficient of the surface symmetry energy. Conceivably the value of this coefficient, after readjustment of all the liquid drop parameters, might be such as to make the generation of superheavy elements impossible. The isotopic trends of actinide fission half-lives, which we fail to reproduce adequately (Table 5), may be indicative of this.

Page 57 + For a more comprehensive review under this heading, see ref. [54]. Many of the ideas in this section have been first suggested by Dr. Wladyslaw J. Swiatecki.

REFERENCES

1. B. R. Mottelson and S. G. Nilsson, Mat. Fys. Skr. Dan Vid. Selsk 1 No. 8 (1959).
2. D. Bés and Z. Szymanski, Nuclear Physics 28 (1961) 92.
3. A. Bohr and B. R. Mottelson, monograph, to be published.
4. S. G. Nilsson, Mat. Fys. Medd. Dan. Vid. Selsk. 29, No. 16 (1955).
5. Z. Szymanski, Nuclear Physics 28 (1961) 421.
6. A. Sobiczewski, Nuclear Physics A93 (1967) 501.
7. V. M. Strutinsky, Nuclear Physics A95 (1967) 420.
8. C. F. von Weizsäcker, Z. Physik 96 (1935) 431.
9. H. A. Bethe and R. F. Bacher, Revs.Mod. Phys. 8 (1936) 193.
10. N. Bohr and J. A. Wheeler, Phys. Rev. 56 (1939) 426; See also "Deformation Energy of a Charged Drop", Part I - W. J. Swiatecki, Phys. Rev. 101 (1956) 651; Part II - Phys. Rev. 104 (1956) 993; Part III - Paper No. P/651, Proceedings of the Second United Nations International Conference on the Peaceful Uses of Atomic Energy, Geneva, 1958 (United Nations, Geneva, 1958); Part IV - S. Cohen and W. J. Swiatecki, Ann. of Phys. 19 (1962) 67; Part V - S. Cohen and W. J. Swiatecki, Ann. Phys. 22 (1963) 406.
11. W. D. Myers and W. J. Swiatecki, Nuclear Physics 81 (1966) 1; see also Proc. International Symposium on Why and How Should We Investigate Nuclei Far Off the Stability Line, Lysekil, Sweden, 1966, (Almqvist and Wiksell, Stockholm, 1967), p. 343; and Arkiv Fysik 36 (1967) 593.

12. C. Gustafson, I. L. Lamm, B. Nilsson, and S. G. Nilsson, Lysekil Symposium, 1966, op. cit., p. 613; and Arkiv Fysik 36 (1967) 613.

13. S. G. Nilsson, "Nuclear Structure, Fission, and Superheavy Elements," Institut D'Etudes Scientifiques De Cargése (Corsica), Summer Institute on Nuclear Physics, summer 1968; University of California Lawrence Radiation Laboratory Report UCRL-18355-Rev.

14. S. A. E. Johansson, Nucl. Phys. 22 (1962) 529.

15. P. Vogel, Phys. Lett. B25 (1967) 65.

16. C. Brihage and G. Reidemeister, Nucl. Phys. A100 (1967) 65.

17. H. Meldner, Lysekil Symposium, 1966, op. cit., p. 593; and Arkiv Fysik 36 (1967) 593.

18. A. Sobiczewski, F. A. Gareev, and B. N. Kalinkin, Phys. Lett. 22 (1966) 500.

19. V. M. Strutinski and Yu. A. Muzychka, Proc. International Conference on the Physics of Heavy Ions, 13-19 October 1966, Dubna, Vol. 2, p. 51.

20. C. Y. Wong, Phys. Lett. 21 (1966) 688.

21. E. Rost, Phys. Lett. 26B (1967) 184.

22. A. Bohr, B. R. Mottelson, and D. Pines, Phys. Rev. 110 (1958) 936.

23. H. C. Britt, F. A. Rickey, and W. S. Hall, Los Alamos Scientific Laboratory Report LA-DC-9562; L. Moretto and S. Thompson, to be published in Phys. Rev.

24. W. Stepien and Z. Szymanski, Phys. Lett. 26B (1968) 181.

25. R. C. Kennedy, L. Wilets, and E. M. Henley, Phys. Rev. Letters 12 (1964) 36.

"Further Studies in the Liquid-Drop Theory of Nuclear Fission", appendix, University of California, Lawrence Radiation Report, UCRL-17958 (July 1968)

26. J. R. Nix,

27. B. Nilsson, to be published.

28. D. L. Hendrie, N. K. Glendenning, B. G. Harvey, O. N. Jarvis, H. H. Duhm, J. Saudinos, and J. Mahoney, Phys. Lett. 26B (1968) 127; see also N. K. Glendenning, Proc. of the International School of Physics, Enrico Fermi, Varenna, Course XL, M. Jean editor (Academic Press, New York, 1968).

29. S. G. Nilsson, Nucleonic Structure of Equilibrium and Fission Deformations, International School of Physics "Enrico Fermi", Varenna, Course XL, M. Jean editor (Academic Press, New York, 1968).

30. G. F. Bertsch, Phys. Lett. 26B (1968) 130.

31. K. Kjällquist, Nuclear Physics 9 (1958/1959) 163.

32. K. Harada, Phys. Lett. 10 (1964) 80.

33. H. Hilf, private communication; E. Hilf and G. Sussmann, Phys. Lett. 21 (1966) 564; S. Knaak, G. Sussmann, E. Hilf, and H. Buttner, Phys. Lett. 23 (1966) 711; W. J. Swiatecki and C. F. Tsang, private communication.

34. S. Cohen, and W. J. Swiatecki, Ann. of Phys. (N.Y.) 22 (1963) 406-37.

35. V. V. Pashkevich, Conference International Symposium Nuclear Structure, Dubna (1968) 94.

36. B. T. Geilikman, Proceedings International Conference on Nuclear Structure, Kingston, 1960, (Toronto University Press, Toronto, 1960) p. 874; also "On The Secondary Shells for Large Nuclear

Deformations", I. V. Kurchatov Institute of Atomic Energy preprint (1968).

37. D. A. Arseniev, L. A. Malov, V. V. Pashkevich, and V. G. Soloviev, Dubna preprint E4-3703 (1968).

38. J. R. Nix and G. E. Walker, Los Alamos Scientific Laboratory report, LA-DC-10114 (November 15, 1968).

39. S. M. Polikanov, V. A. Druin, V. A. Karnaukov, V. L. Mikheev, A. A. Pleve, N. K. Skobolev, V. G. Subotin, G. M. Ter-Akopian, and V. A. Fomichev, Exp. Theor. Phys. 42 (1962) 1464; cf. also S. Björnholm, J. Borggreen, L. Westgaard, and V. A. Karnaukov, Nuclear Physics A95 (1967) 513.

40. G. N. Flerov, and S. M. Polikanov, Compt. Rend. Congr. Int. Phys. Nucl. (Paris 1964) Vol. I, p. 407.

41. S. Björnholm, private communication.

42. E. Lynn, report at the Conference on Nuclear Structure, Dubna, July, 1968.

43. P. O. Fröman and N. Fröman, J.W.K.B. Approximation, Contribution to the Theory (North-Holland Press, Amsterdam, 1965).

44. D. L. Hill and J. A. Wheeler, Phys. Rev. 89 (1953) 1102.

45. A. Sobiczewski, Z. Szymanski, and S. Wycech, S. G. Nilsson, J. R. Nix, and C.F. Tsang, Nuclear Physics, to be published

46. D. R. Bés, Mat. Fys. Medd. Dan. Vid. Selsk. 33 No. 2 (1961).

47. S. G. Nilsson, J. R. Nix, A. Sobiczewski, Z. Szymanski, S. Wycech, C. Gustafson, and P. Möller, Nuclear Physics A115 (1968) 545.

48. L. Moretto and W. J. Swiatecki, private communication.

49. S. G. Nilsson, S. G. Thompson, and C. F. Tsang, "Stability of Superheavy Nuclei and Their Possible Occurrence in Nature",

University of California Lawrence Radiation Laboratory Report UCRL-18531, and Phys. Letters 28B (1969) 458.

50. J. T. Waber, D. T. Cromer, and D. Liberman, "SCF Dirac-Slater Calculations of the Trans-Lawrencium Elements", Los Alamos Scientific Laboratory Report (to be published).

51. T. C. Tucker, L. D. Roberts, C. W. Nestor, Jr., T. A. Carlson, and F. B. Malik, "Calculation of the Electron Binding Energies and X-Ray Energies for the Superheavy Elements 114, 126, and 140 Using Relativistic SCF Atomic Wave Functions", Oak Ridge National Laboratory report (to be published).

52. E. M. Burbidge, G. R. Burbidge, W. A. Fowler, and F. Hoyle, Revs. Mod. Phys. 29 (1957) 547.

53. S. G. Thompson, R. C. Gatti, L. G. Moretto, H. R. Bowman, and M. C. Michel, paper in preparation.

54. G. T. Seaborg, Elements Beyond 100, Present Status and Future Prospects, Ann. Rev. Nucl. Sci. 18, (1968) 53-152.

55. S. G. Thompson, W. J. Swiatecki, R. C. Gatti, H. R. Bowman, L. G. Moretto, R. C. Jared, and R. M. Latimer, paper in preparation.

56. A. Chiorso, T. Sikkeland, and M. Nurmia, private communication.

57. G. N. Flerov, Yu. Ts. Oganesyan, Yu. V. Lobanov, V. I. Kuznetsov, V. A. Druin, V. P. Perelygin, K. A. Gavrilov, S. P. Tretiakova, and V. M. Plotko, Atomnaya Energ. 17 (1964) 310; translation: Soviet Atomic Energy 17 (1964) 1046; Phys. Letters 13, (1964) 73.

TABLE 1

A value	PROTONS		NEUTRONS	
	κ	μ	κ	μ
165	0.0637	0.600	0.0637	0.420
187	0.0620	0.614	0.0636	0.393
208	0.0604	0.628	0.0636	0.367
225	0.0590	0.639	0.0635	0.346
242	0.0577	0.650	0.0635	0.325
266	0.0559	0.665	0.0635	0.296
294	0.0534	0.686	0.0634	0.256

TABLE 2

Z	N	A	Ground State ε	Ground State ε_4	First Hump Height above g.s. MeV	Isomeric State ε	Isomeric State ε_4	Isomeric State Excitation above g.s. MeV	Second Hump Height above g.s. MeV
92	136	228	0.15	-0.06	3.4	flat region			5.3
	138	230	0.17	-0.06	3.6	flat region			6.1
	140	232	0.18	-0.06	4.0	0.59	0.06	2.9	7.5
	142	234	0.195	-0.05	4.9	0.585	0.05	2.5	8.1
	144	236	0.20	-0.05	5.6	0.605	0.06	2.4	8.9
	146	238	0.21	-0.04	6.1	0.60	0.07	2.7	9.5
	148	240	0.23	-0.03	6.8	0.64	0.06	3.2	10.0
94	138	232	0.18	-0.06	3.5	0.65	0.08	1.9	4.2
	140	234	0.19	-0.05	4.2	0.64	0.08	2.1	5.2
	142	236	0.20	-0.05	5.0	0.61	0.06	2.1	6.2
	144	238	0.215	-0.04	5.8	0.60	0.06	2.2	7.0
	146	240	0.22	-0.03	6.5	0.61	0.07	2.5	7.6
	148	242	0.225	-0.03	6.9	0.61	0.07	3.0	7.95
	150	244	0.23	-0.02	7.2	0.62	0.07	3.6	8.3
	152	246	0.23	-0.01	7.3	0.64	0.06	3.8	8.3
96	142	238	0.21	-0.04	5.1	0.63	0.07	1.5	4.0
	144	240	0.22	-0.04	6.05	0.61	0.07	1.65	4.9
	146	242	0.225	-0.03	6.7	0.60	0.07	2.2	5.5
	148	244	0.23	-0.02	7.4	0.615	0.07	2.8	6.0
	150	246	0.23	-0.01	7.6	0.625	0.07	3.1	6.2
	152	248	0.23	-0.01	7.7	0.65	0.07	3.5	6.4
98	146	244	0.22	-0.03	6.7	0.615	0.07	1.4	3.2
	148	246	0.23	-0.02	7.45	0.625	0.07	2.0	3.75
	150	248	0.23	-0.01	7.0	0.68	0.07	2.5	4.1
	152	250	0.23	0.00	8.0	0.695	0.08	2.7	4.4
	154	252	0.235	0.01	7.9	0.705	0.08	2.6	4.0
100	148	248	0.23	-0.01	7.7	0.73	0.08	1.2	1.8
	150	250	0.235	-0.01	7.9	0.72	0.08	1.5	2.1
	152	252	0.24	0.00	8.2	0.72	0.09	1.7	2.3
	154	254	0.24	0.01	8.1	0.73	0.09	1.6	2.1
	156	256	0.235	0.02	7.9	0.73	0.09	1.5	1.9

TABLE 3

Nucleus			Height of Barrier (MeV)			Exc. Energy of Sec. Min. (MeV)			D_{II}/D_I	Fission Isomer $T_{1/2}^{SF}$ (sec)	Ref.
Z	N	A	Expt	Theoretical 1st Hump	2nd Hump	From D_{II}/D_I	From thresh. meas.	Theory			
92	143	235	5.75			3			540		a
	144	236	5.8	5.6	8.9	2.4		2.4	260	1.1×10^{-7}	b
93	145	236	6.04								
94	142	236		5.0	6.2			2.1		$<2.10^{-9}$	c
	143	237								$\sim10^{-7}$	c
	144	238	5.3	5.8	7.0			2.2		$<2.10^{-9}$	c
	145	239	5.5							3.10^{-7}	c
	146	240	4.7	6.5	7.6	2.5		2.5	100	4.10^{-9}	d, c
	147	241	6.3			2.1			43	3.10^{-8}	e, b
	148	242	5.2	6.9	7.95			3.0		5.10^{-8}	b
	149	243	5.8			3.2			1900	6.10^{-8}	a, b
95	143	238									
	144	239					2.9			2.10^{-7}	b
	145	240					3.2			9.10^{-4}	b
	146	241	5.9				2.5			1.10^{-6}	b
	147	242	6.4			3.1	2.9		900	$1.4.10^{-2}$	f, b
	148	243									
	149	244	(6.2)							1.10^{-3}	b
(98	148	246		7.45	3.75		2.5	2.0		$(4.5.10^{-8})$	g

a. Harwell Group, AERE-M-2082

b. Cpoenhagen Group: Björnholm et al

c. Seattle Group: Vandenbosch et al

d. Saclay Group

e. Euratom Group: Weighman

f. Los Alamos Group: Seeger et al

g. Dubna Group

Expt. Barriers quoted from Myers and Swiatecki [11]

Table 4

Z	A	$\mathcal{E} = 0.20$; $\mathcal{E}_4 = 0.0$		$\mathcal{E} = 0.50$, $\mathcal{E}_4 = 0.02$	
		$B_\mathcal{E}$	$B_\mathcal{E}/B_{irr}(\mathcal{E})$	$B_\mathcal{E}$	$B_\mathcal{E}/B_{irr}(\mathcal{E})$
1	2	3	4	5	6
90	228	309.8	5.74	723.9	6.79
	230	266.4	4.86	1006.9	9.31
	232	247.7	4.46	1036.5	9.44
	234	271.4	4.82	970.4	8.72
	236	323.3	5.66	909.3	8.06
92	230	309.9	5.66	715.4	6.62
	232	260.7	4.70	1015.7	9.26
	234	237.8	4.22	1049.4	9.43
	236	261.7	4.58	976.4	8.65
	238	320.0	5.52	908.3	7.94
	240	365.9	6.22	915.3	7.89
	242	305.6	5.12	880.5	7.48
94	232	319.7	5.76	715.1	6.51
	234	266.5	4.73	1038.8	9.34
	236	241.0	4.22	1077.0	9.54
	238	266.1	4.59	995.7	8.70
	240	330.4	5.62	919.4	7.92
	242	379.9	6.38	923.4	7.85
	244	311.6	5.16	882.2	7.39
	246	297.7	4.86	856.1	7.08
96	238	243.0	4.19	1109.2	9.60
	240	268.8	4.58	1018.5	8.77
	242	336.0	5.64	932.8	7.92
	244	387.5	6.41	933.6	7.82
	246	315.1	5.15	885.1	7.32
	248	302.8	4.88	856.3	6.98
	250	271.4	4.32	780.9	6.28

Table 4 continued

1	2	3	4	5	6
98	244	353.6	5.86	981.1	8.22
	246	408.1	6.67	977.9	8.09
	248	331.9	5.35	918.1	7.49
	250	321.8	5.12	883.5	7.11
	252	288.6	4.53	796.9	6.33
	254	370.2	5.73	839.1	6.58
100	248	449.1	7.24	983.3	8.02
	250	368.2	5.85	912.7	7.35
	252	361.7	5.68	872.6	6.93
	254	327.1	5.06	778.2	6.10
	256	415.8	6.36	819.6	6.34
	258	495.1	7.47	796.9	6.09
102	252	331.2	5.20	917.3	7.29
	254	321.7	4.98	880.0	6.90
	256	279.7	4.28	786.9	6.09
	258	373.9	5.64	827.9	6.32
104	256	334.0	5.10	958.6	7.42
	258	289.6	4.36	865.1	6.61
	260	387.2	5.77	907.0	6.84
	262	473.1	6.96	879.0	6.54
106	258	402.9	6.08	1055.3	8.06
	260	361.2	5.38	960.1	7.24
	262	459.0	6.75	1004.0	7.47
	264	544.4	7.90	970.2	7.13

TABLE 5.

	138		140		142		144		146		148		150		152		154	
102															83.41 6.34 | 6 8.41		- | 3	
100											70.34 7.62 | 1 7.85		72.64 7.43 7.44		75.57 7.26 | 0 7.05		79.18 7.00 | 0 7.16	
98									60.29 7.17 7.13		62.73 6.67 | 2 6.79		65.88 6.42 | -3 6.27		67.66 6.24 | -4 6.03		74.06 6.02 | -6 6.12	
										59.53		62.65		66.56				
96					48.34 6.74 6.51		50.69 6.60 | 4 6.29		53.61 6.29 | 0 6.12		57.03 5.70 | -2 5.81		60.99 5.59 | -5 5.39		65.61 5.39 | -6 5.02			
				48.32				51.52				58.27		62.96				
94	37.21 6.60 6.59		39.17 6.17 6.20		41.66 5.82 | 4 5.77		44.89 5.74 | 3 5.56		48.70 5.34 | 2 5.17		52.97 4.95 | -2 4.92		57.79 4.65 | -6 4.53		63.73			
								46.65		51.17								
92	30.57		33.41 | 6		36.72 | 6		46.93 | 5		45.59 | 4		50.70						

-715-

TABLE 6.

		Theoretical		Experimental	Theoretical	
Z	A	K	K_{corr}	K	B(0.5)	P(0.2)
92	232	127	99	98	1040	260
	234	132	111	105	1050	240
	236	130	106	104	980	260
	238	127	102	105	910	320
94	236	120	101	83	1377	240
	238	119	103	91	1000	270
	240	118	98	92	900	330
	242	139	97	91	870	330
	244	144	106	90	820	300
96	240	103	76	81	1070	270
	242	117	79	82	950	340
	244	121	83	83	950	350
	246	131	93	83	890	320
	248	131	91	81	840	300
98	246	95	61	74	930	410
	248	114	71	75	900	330
	250	114	72	76	880	320
	252	106	59	71	870	290
100	248	73	33	59	930	450
	250	90	49		910	370
	252	88	49	68	870	360
	254	85	40	66	780	350
	256	86		58	680	410
102	252	47		51	900	320
	254	56	34	61	830	380
	256	53		56	790	280
	258	56		<46	810	370
104	256	46			960	330
	258	45			870	290
	260	51		48	910	390
	262	59			940	470

TABLE 7.

N

Z	178	179	180	181	182	183	184	185	186	187	188	189	
116	187.87 (1ms)(5.8) 1s(10.14)		190.36 1s(7.1) $\frac{1}{2}$ min(9.92)		193.14 10^{3}y(8.3) 10s(9.71)		195.42 10^{11}y(9.4) $\frac{1}{2}$ min(9.58)		201.30 10^{11}y(9.4) 0.1s(10.53)		206.55 1s(10.24)		305
115	185.02		185.75 10 min(8.89)		188.85 10h(8.58)		192.45 1d (8.45)		197.66 10s (9.39)$_{k}$		203.25 10 min(9.11)		304
114	178.01 1 min(5.4)	180.09	181.00 10^{2}y(7.0) 10d(7.97)	183.17 1y (7.71)	184.41 10^{3}y(8.3) 1y (7.55)	185.56 10^{2}y(7.20)	188.34 10^{10}y(9.5) 10y (7.40)	191.29 100d(7.87)	193.88 10^{10}y(9.4) 1d(8.34)	197.32 5h(8.49)	199.84 10^{10}y(9.4) 10s(8.09)	203.52 10d (8.00)	303
113	174.43		177.34 10y(7.33)		181.57 10^{3}y(6.20)		185.94 10^{3}y(6.58)		191.71 1y (7.53)		198.00 10y(7.29)		302
112	170.60 10^{-2}s(4.1)	173.03	174.43 1d (5.7) 1y (7.45)	176.93 10^{2}y(7.17)	178.51 10^{3}y(6.9) 10^{3}y(6.83)	180.99 10^{4}y(6.52)	183.11 10^{13}y(8.1) 10^{4}y(6.54)	186.40 10^{2}y(7.10)	189.32 10^{13}y(8.1) 1y (7.50)	193.09 100d(7.55)	195.94 10^{12}y(8.1) 10y(7.24)	199.95 10y(7.16)	301
111	168.88		172.54 10y(7.05)		176.83 10^{3}y(6.38)	179.47	181.75 10^{7}y(6.03)		188.28 10^{2}y(6.98)		195.23 10^{3}y(6.72)		300
110	164.54 (1ms)(3.2) 10y(7.20)	167.33	169.26 10min(4.3) 10^{2}y(6.35)	172.04 10^{4}y(6.40)	174.14 10^{3}y(5.5) 10^{6}y(6.14)	176.87 10^{9}y(5.63)	179.38 10^{11}y(6.8) 10^{8}y(5.76)	183.01 10^{3}y(6.24)	186.27 10^{10}y(5.7) 10^{2}y(6.73)	190.35 10^{2}y(6.86)	193.54 10^{9}y(6.8) 10^{4}y(6.45)	197.88 10^{4}y(6.35)	299
109	162.36		168.02	171.10	173.29	176.18	178.87 10^{11}y(5.24)	182.66	186.02 10^{5}y(6.21)		193.68		298
108	159.97 10^{3}y(6.33)	163.21	165.57 10s(5.2) 10^{4}y(6.25)	168.81	171.20 10y (4.3) 10^{8}y(5.57)	174.34	177.11 10^{8}y(5.8) 10^{13}y(4.89)	181.07 10^{9}y(5.39)	184.66 10^{8}y(5.9) 10^{6}y(5.86)	189.10	192.60 10^{7}y(5.8)		297
107					171.20	174.49	177.44						296
106					169.79 10d(3.9) 10^{11}y(4.97)	173.25	176.37 10^{7}y(5.3)						295
		284	285	286	287	288	289	290	291	292	293	294	

FIGURE CAPTIONS

Fig. 1. Nuclear shapes in the plane of the deformation parameters ε and ε_4. A sphere corresponds to $\varepsilon = 0$ and $\varepsilon_4 = 0$. Spheroids have their $\varepsilon_4 = 0$.

Fig. 2a. Single-proton levels $150 < A < 165$; $\kappa = 0.0637$, $\mu = 0.600$, $\varepsilon_4 = -0.04$.

2b. Single-neutron levels $150 < A < 165$; $\kappa = 0.0637$, $\mu = 0.420$, $\varepsilon_4 = -0.04$.

2c. Single-proton levels $175 < A < 190$; $\kappa = 0.0620$, $\mu = 0.614$, $\varepsilon_4 = 0.04$.

2d. Single-neutron levels $175 < A < 190$; $\kappa = 0.0636$, $\mu = 0.393$, $\varepsilon_4 = 0.04$.

2e. Single-proton levels $220 < A < 240$; $\kappa = 0.0590$, $\mu = 0.639$, $\varepsilon_4 = -0.04$.

2f. Single-neutron levels $220 < A < 240$; $\kappa = 0.0635$, $\mu = 0.346$, $\varepsilon_4 = -0.04$.

2g. Single-proton levels $250 < A < 260$; $\kappa = 0.0569$, $\mu = 0.655$, $\varepsilon_4 = 0.04$.

2h. Single-neutron levels $250 < A < 260$; $\kappa = 0.0635$, $\mu = 0.014$, $\varepsilon_4 = 0.04$.

2i. Single-proton levels $A \approx 298$; $\kappa = 0.0534$, $\mu = 0.686$, $\varepsilon_4 = 0$.

2j. Single-neutron levels $A \approx 298$; $\kappa = 0.0634$, $\mu = 0.256$, $\varepsilon_4 = 0$.

2k. Single-proton levels valid for first hump and secondray minimum, $A \approx 242$, $\kappa = 0.0577$, $\mu = 0.650$, $\varepsilon_4 = 0.04$.

2l. Single-neutron levels valid for first hump and secondary minimum, $A \approx 242$, $\kappa = 0.0635$, $\mu = 0.325$, $\varepsilon_4 = 0.04$.

Fig. 3a. Single-proton level diagram for spherical potential. Parameters are fitted to reproduce observed deformed single-particle level order at $A \approx 165$ and 242. Level order at $A = 208$, 290 is extrapolated linearly. E. Rost's predicted level order[21] for $A = 298$ is exhibited for comparison.

3b. Analogous to Fig. 3a, valid for neutrons.

Fig. 4a. Empirical odd-Z-even-even mass differences compared with theoretical Δ_p in rare earth region.

4b. Empirical odd-N-even-even mass differences compared with theoretical Δ_n in rare-earth region.

Fig. 5. Plot of ratios of calculated Δ_n and Δ_p for the case $G \approx S$ and for the case G = const. The two G-functions are normalized at $\epsilon = 0.25$. It is found that, apart from fluctuations, due to level density variations, Δ varies roughly as S^3 under the assumption $G \propto S$. In the figure we also exhibit for comparison a curve corresponding to $S^{3/2}$, the $\Delta(S)$ dependence suggested by the "slab model" of ref.[25].

Fig. 6. Effect of various terms in total energy as a function of deformation. Long-dashed curve marks simple sum of single-particle energies, for dotted curve Coulomb energy is added, for dot-dashed curve also pairing ($G \approx S$) is included, for short-dashed curve the Strutinsky normalization is applied. In all these cases it is assumed that $\epsilon_4 = 0$. In the last case (solid curve) also the effect of the ϵ_4-degree of freedom is included.

Fig. 7. Gap parameters (left scale) and total pairing energy (right scale) as functions of distortion ϵ for the two cases that G is constant and that G is proportional to the surface area.

Fig. 8. Empirical rare earth β_4-values (filled circles) obtained through the analysis of ref.[20] compared to the present calculations before the inclusion of the Strutinsky normalization. The effect of the latter is less than 0.01 in magnitude. Note that in the calculations coupling between shells N and $N \pm 4$ are neglected.

Fig. 9. Relation between coordinates ε, ε_4 and β_2, β_4. Note that the pure spheroid shape contains some β_4 (and in addition β_6 etc. not shown in figure).

Fig. 10a. Equilibrium distortion in the β_2- β_4-plane of a few representative nuclei in the actinide region. Case a gives pure within shell single-particle values, case b displays the effect of the added Coulomb energy, case c marks the additional effect of pairing while in case d also polarisation is included.

10b. Equilibrium β_4 distortions for nuclei in the actinide region for the four different cases given in Fig.10a.

Fig. 11. Same as Fig. 8 for equilibrium β_6-values in rare earth region. Errors in empirical β_6-values are at least 0.02. Theoretical β_6-values are sensitive to polarizations due to couplings between shells $N \rightarrow N \pm 4$ not presently included.

Fig. 12a. Equilibrium (ε, ε_4)-values in the rare earth region as of present calculations (Strutinsky normalization included).

12b. Equilibrium (ε, ε_4)-values in actinide region.

Fig. 13. Sum of single-particle, pairing and Coulomb energies <u>without Strutinsky normalization</u> as function of ε, ε_4. At large distortions the energy ultimately rises beyond + 15 MeV (limit for plot).

Fig. 14. Shell corrections evaluated by the Strutinsky method as a function of the shell-smearing parameter γ for case of neutrons of ^{242}Pu. Energies corresponding to three different distortions are considered. For $\gamma \approx 1.2\ \hbar\omega_0$ it is obvious that with fourth, or better, sixth-order correction terms included there is very satisfactory stability with respect to the choice of γ.

Fig. 15. Same as Fig. 14, but for neutrons of ^{208}Pb.

Fig. 16. Experimental and theoretical mass values for $150 < A < 340$ plotted relative to the spherical liquid drop value as of Ref. 11).

Fig. 17a. Total-energy surface in (ϵ, ϵ_4) plane for ^{252}Fm after application of the Strutinsky normalization. This figure corresponds to a somewhat earlier calculation and employs G = const and a different pairing cut-off than described in the present paper. More recent calculations are exhibited in Fig. 20.

17b. Same as Fig. 17a valid for ^{290}114.

Fig. 18a. Liquid-drop energy surface for ^{252}Fm.

18b. Liquid-drop energy surface for ^{290}114.

Fig. 19a. Shell and pairing energy contributions for ^{252}Fm. For further details see Fig. 17a.

19b. Same as Fig. 19a for ^{290}114.

Fig. 20a. Total energy minimized w.r.t. ϵ_4 for each ϵ as function of ϵ for isotopes of $_{92}$U. Dashed curve corresponds to

G set constant while the solid line is based on assumption that G is proportional to the nuclear surface area.

20b. Same as Fig. 20a for isotopes of $_{94}Pu$.

20c. Same as Fig. 20a for isotopes of $_{96}Cm$.

20d. Same as Fig. 20a for isotopes of $_{98}Cf$.

20e. Same as Fig. 20a for isotopes of $_{100}Fm$. The extra dot-dashed curve added for ^{256}Fm represents the new total energy for the case $G \approx S$ when the nuclear potential parameters are modified from those relevant for $A = 242$ to $A = 265$. As can be seen the barrier change is actually very small.

20f. Same as Fig. 20a for isotopes of $_{102}No$.

20g. Same as Fig. 20a for isotopes of $Z = 104$.

20h. Same as Fig. 20a for isotopes of $Z = 106$.

20i. Same as Fig. 20a for isotopes of $Z = 108$.

20j. Same as Fig. 20a for isotopes of $Z = 110$.

20k. Same as Fig. 20a for isotopes of $Z = 112$.

20ℓ. Same as Fig. 20a for isotopes of $Z = 114$.

20m. The two-peak barrier as a function of neutron number for $Z = 92$-100.

Fig. 21. Potential energy minimized with respect to ϵ_4 as a function of ϵ for various nuclei to illustrate the effect of shell structure on a liquid drop background. The broken curves correspond to liquid drop fission barriers. The solid curves are the barrier after inclusion of shell and pairing effects.

Fig. 22. Spontaneous fission half lives of $Z = 114$ and 110 isotopes as functions of the inertial parameter B for barrier penetration. Three estimates of B are given. For further explanations, see text.

Fig. 23. Contours of theoretical half-lives in the vicinity of $Z = 114$ and $N = 184$. The thick dark lines are contours of spontaneous fission half-lives. The broken lines are contours of alpha half-lives. Beta stable nuclei are shaded.

Fig. 24. Periodic Table exhibiting predicted locations of new elements.

TABLE CAPTIONS

Table 1. Values of κ and μ employed in the single-particle calculation corresponding to different regions of mass along the beta-stability line. The first column denotes the mass of the center of each region.

Table 2. Calculated properties of the two-humped spontaneous fission barriers and shape isomers from potential energy surfaces of the actinides. The deformations of the ground state and isomeric state are listed. The heights of the two humps and the excitation energy of the isomeric state are given in MeV above the ground state. It is assumed that the zero-point vibrational energies of the ground state and isomeric state are equal.

Table 3. Experimental properties of shape isomeric states. The first group of columns identifies the nucleus. The second group gives the experimental fission barriers based erroneous on the assumption of a one-humped structure. The excitation energy of the isomeric state is shown in the next group, estimated from threshold measurement and from (n,f) reasonance experiments. The next entry gives the ratio of distances between resonances in the isomeric state to the ground state. The last colum indicates the experimental spohtaneous fission half-lives of the isomers. Theoretical values are taken from Table 2.

We are grateful to Dr. S. Björnholm and Dr. J. R. Nix för their help in supplying us with the experimental data.

Table 4. Inertial parameters for nuclei in the actinide region. Columns 1 and 2 identify the nucleus, columns 3 and 5 list the values of the inertial parameter B in units of $\hbar^2$ MeV^{-1} for deformation $\varepsilon = 0.20$

and $\varepsilon_4 = 0.0$ and also $\varepsilon = 0.50$ and $\varepsilon_4 = 0.02$, respectively. Columns 4 and 6 present the ratio of B to the irrotational value $B_{irr}(\varepsilon)$. See ref. [45].

Table 5. Beta stability, alpha decay energies and spontaneous fission characteristics of the actinides. In each square classified by Z and N, the uppermost figure gives the mass excess on ^{12}C scale in MeV. If the nucleus is found to be beta-stable, this number is underlined. The two numbers below give the theoretical and experimental alpha decay energies respectively. The integer to the right is the ratio of the experimental spontaneous fission half life to the theoretical value. In the calculation we have taken the inertial parameter B to be the average of the three methods of estimation described in the text.

Table 6. Experimental and theoretical fission half-life parameters. The nuclide is identified by Z and A in the first two columns. Columns 3-5 give theoretical and experimental K-values (see section IV), the latter from empirical half-lives. The first K-value is calculated assuming a linear ε-dependence of B between the two calculated points. The second K-value is obtained after a correction for the error in the ground state mass value. The correction is assumed only to affect the equilibrium minimum. Columns 6-7 give the theoretical B-values calculated for $\varepsilon = 0.2$ ($\varepsilon_4 = 0$) and $\varepsilon = 0.5$ ($\varepsilon_4 = 0.02$).

The assumed linear dependence of B on ε weighs the second hump of the barrier heavily. As the height and width of this hump are

probably overestimated (see text) the uncorrected K-values come out very large.

Table 7. Table of masses, spontaneous-fission and alpha half-lives near Z = 114, N = 184. The upper number in each square gives the mass excess in ^{12}C scale (see ref. [11]) in MeV. In the line below is listed the spontaneous-fission half-life and in parenthesis the barrier height in MeV. The bottom line in each square gives the alpha half-life and the alpha Q-value (in parenthesis). Beta-stable nuclei are underlined.

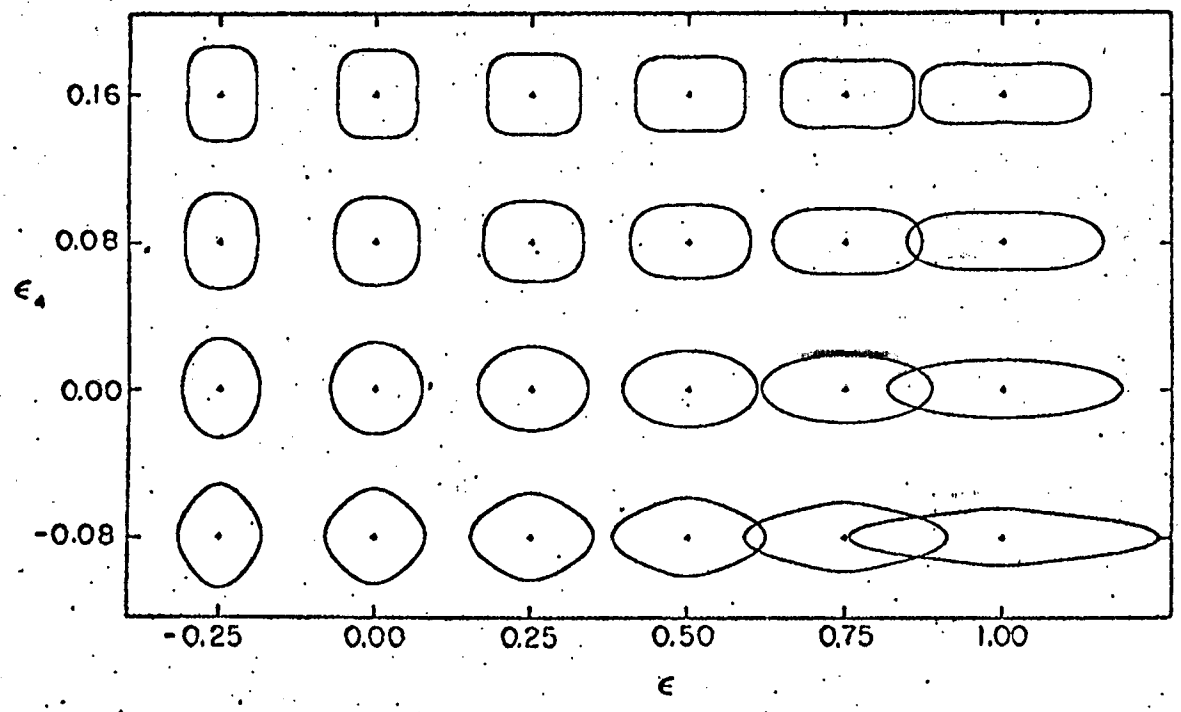

XBL6011-7120

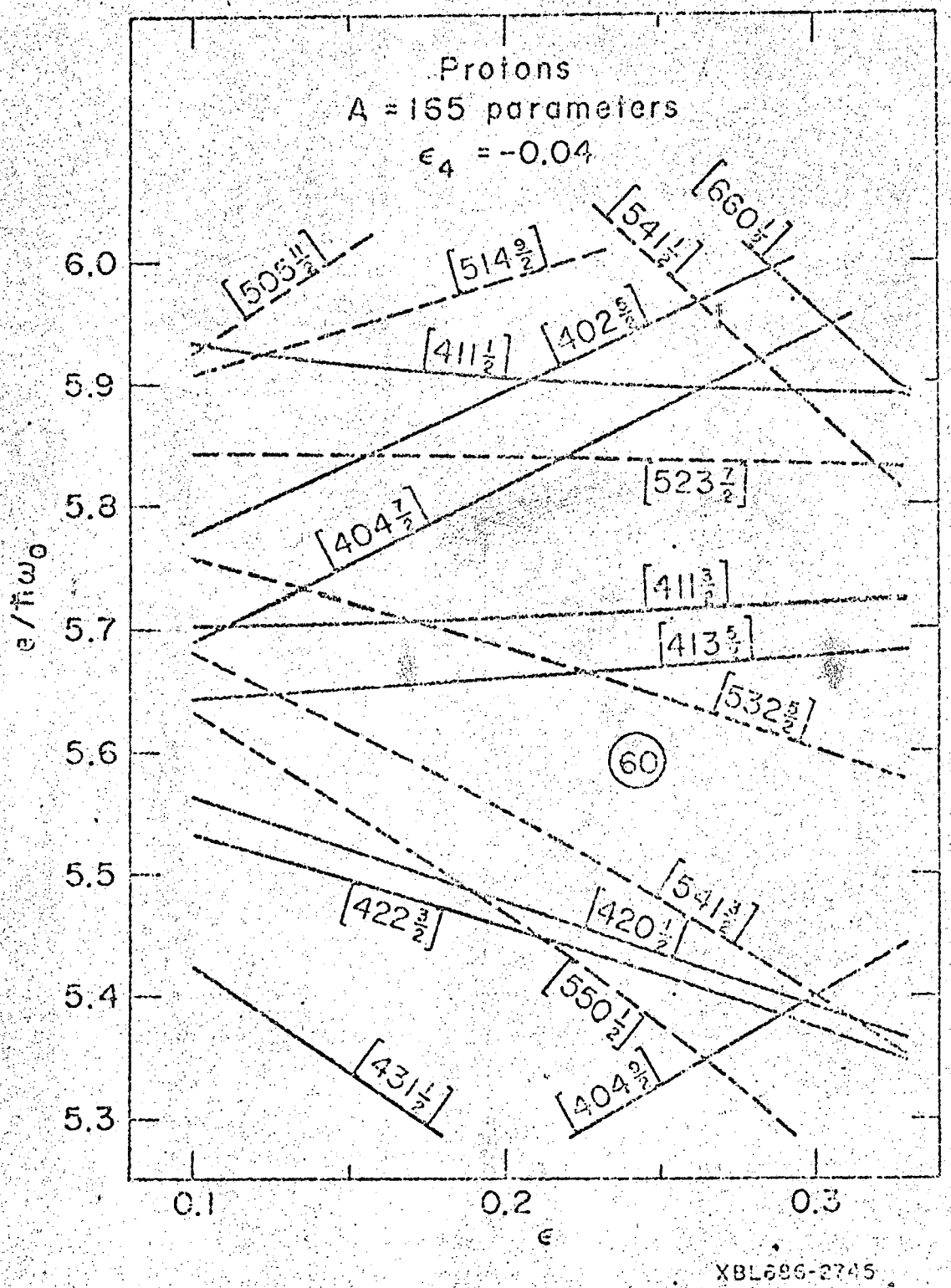
Protons
A = 155 parameters
ϵ_4 = -0.04
$[505\frac{11}{2}]$
$[514\frac{9}{2}]$
$[541\frac{1}{2}]$
$[660\frac{1}{2}]$
$[411\frac{1}{2}]$
$[402\frac{5}{2}]$
$[523\frac{7}{2}]$
$[404\frac{7}{2}]$
$[411\frac{3}{2}]$
$[413\frac{5}{2}]$
$[532\frac{5}{2}]$
60
$[541\frac{3}{2}]$
$[422\frac{3}{2}]$
$[420\frac{1}{2}]$
$[550\frac{1}{2}]$
$[431\frac{1}{2}]$
$[404\frac{9}{2}]$
6.0
5.9
5.8
5.7
5.6
5.5
5.4
5.3
$e/\hbar\omega_0$
0.1
0.2
0.3
ϵ
XBL696-2745

Fig. 3

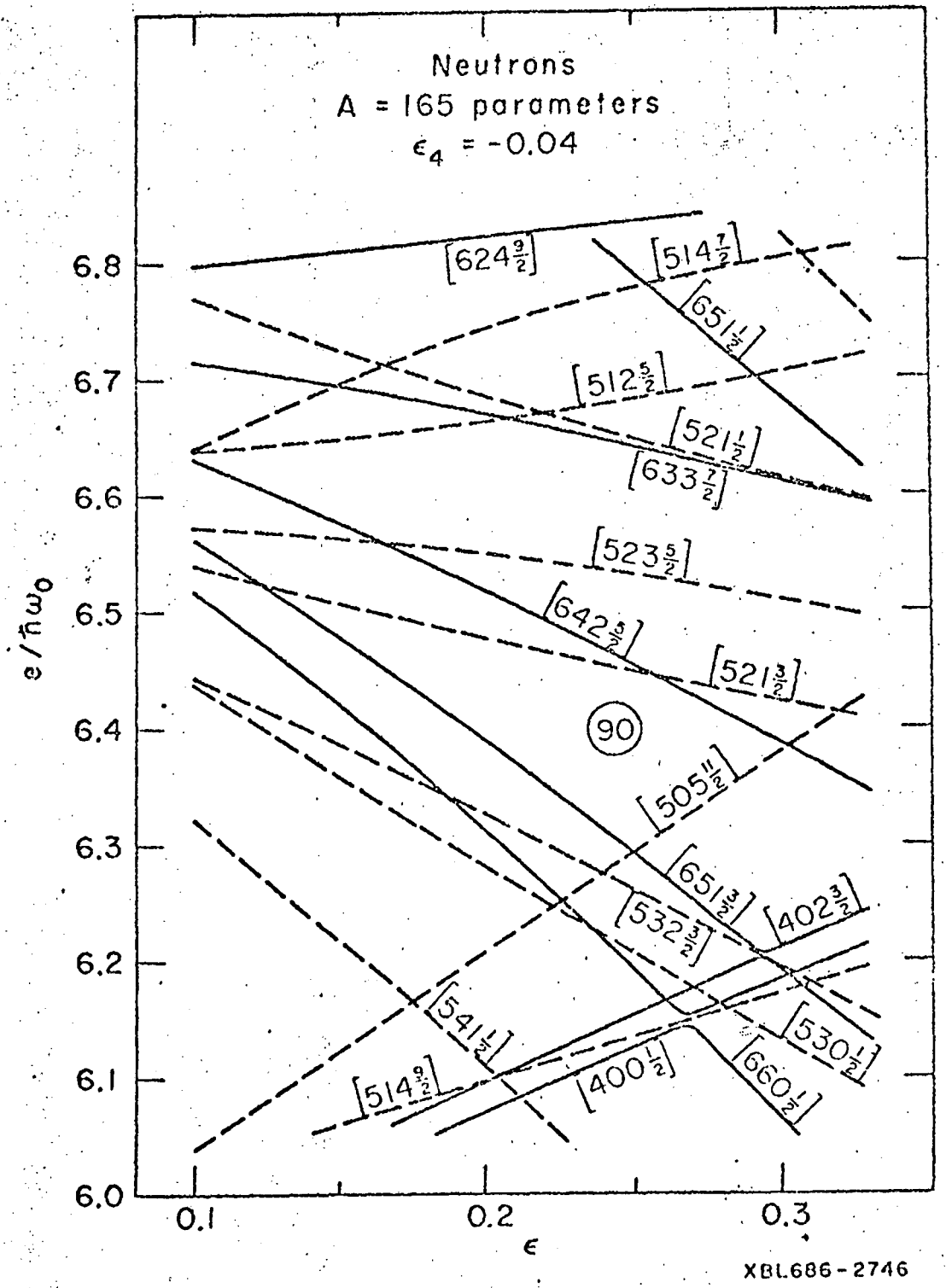
Neutrons
A = 165 parameters
ϵ_4 = -0.04
$[624\frac{3}{2}]$
$[514\frac{7}{2}]$
$[651\frac{1}{2}]$
$[512\frac{5}{2}]$
$[521\frac{1}{2}]$
$[633\frac{7}{2}]$
$[523\frac{5}{2}]$
$[642\frac{5}{2}]$
$[521\frac{3}{2}]$
90
$[505\frac{11}{2}]$
$[651\frac{3}{2}]$
$[532\frac{3}{2}]$
$[402\frac{3}{2}]$
$[541\frac{1}{2}]$
$[530\frac{1}{2}]$
$[514\frac{9}{2}]$
$[400\frac{1}{2}]$
$[660\frac{1}{2}]$
6.8
6.7
6.6
6.5
6.4
6.3
6.2
6.1
6.0
$e/\hbar\omega_0$
0.1
0.2
0.3
ϵ
XBL.686-2746

FIG. 9.15.

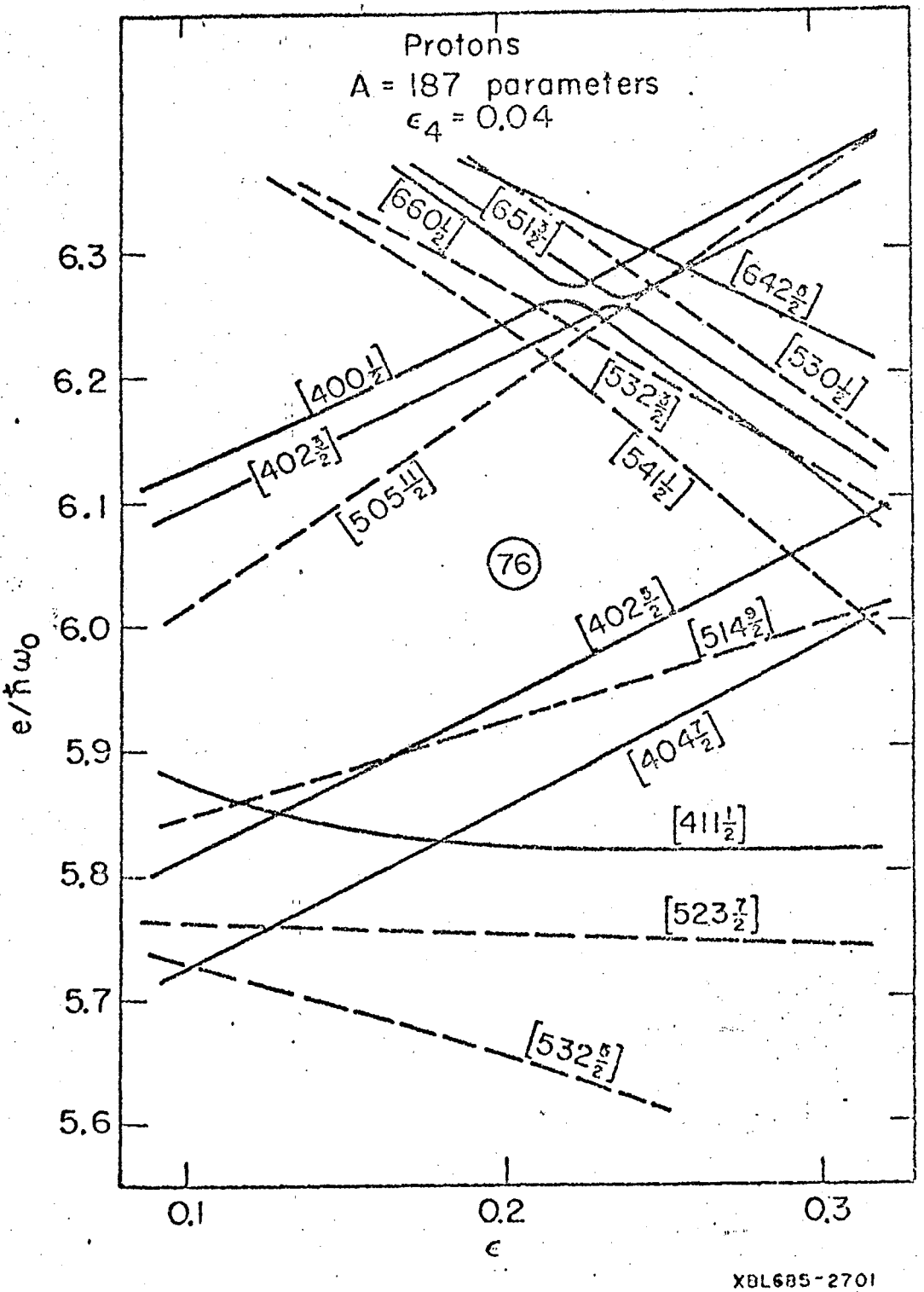
Protons
A = 187 parameters
ϵ_4 = 0.04
$[660\frac{1}{2}]$
$[651\frac{3}{2}]$
$[642\frac{5}{2}]$
$[530\frac{1}{2}]$
$[400\frac{1}{2}]$
$[402\frac{3}{2}]$
$[505\frac{11}{2}]$
$[532\frac{5}{2}]$
$[541\frac{1}{2}]$
76
$[402\frac{5}{2}]$
$[514\frac{9}{2}]$
$[404\frac{7}{2}]$
$[411\frac{1}{2}]$
$[523\frac{7}{2}]$
$[532\frac{5}{2}]$
6.3
6.2
6.1
6.0
5.9
5.8
5.7
5.6
$e/\hbar\omega_0$
0.1
0.2
0.3
ϵ
XBL685-2701

FIG 9 c

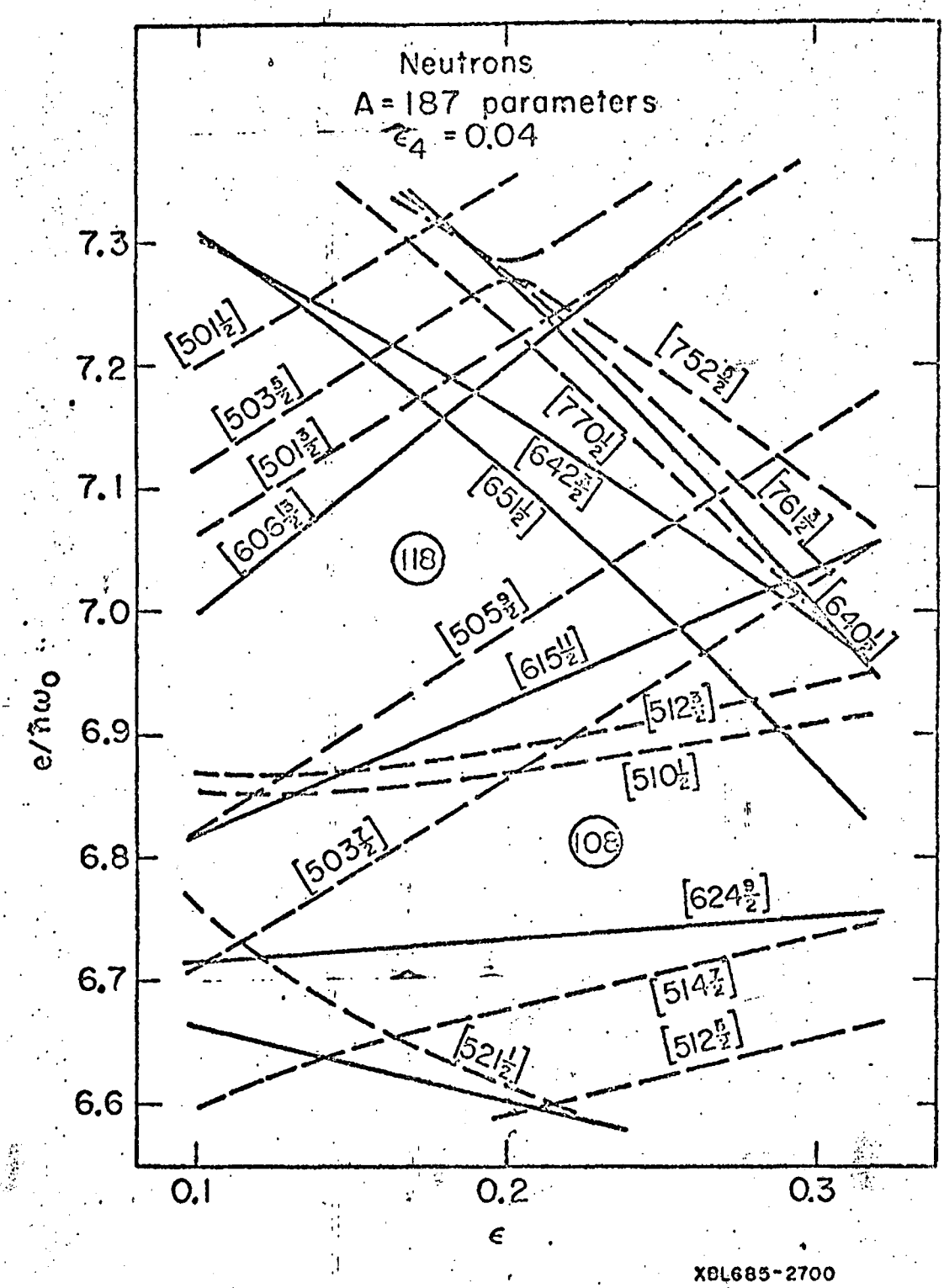
Neutrons
A = 187 parameters
ϵ_4 = 0.04
7.3
7.2
7.1
7.0
6.9
6.8
6.7
6.6
$e/\hbar\omega_0$
0.1
0.2
0.3
ϵ
[501 1/2]
[503 5/2]
[501 3/2]
[606 5/2]
[651 1/2]
[642 5/2]
[770 1/2]
[752 3/2]
[761 3/2]
[640 1/2]
118
[505 9/2]
[615 11/2]
[512 3/2]
[510 1/2]
108
[503 7/2]
[624 9/2]
[514 7/2]
[512 5/2]
[521 1/2]
XBL685-2700

FIG 2.d

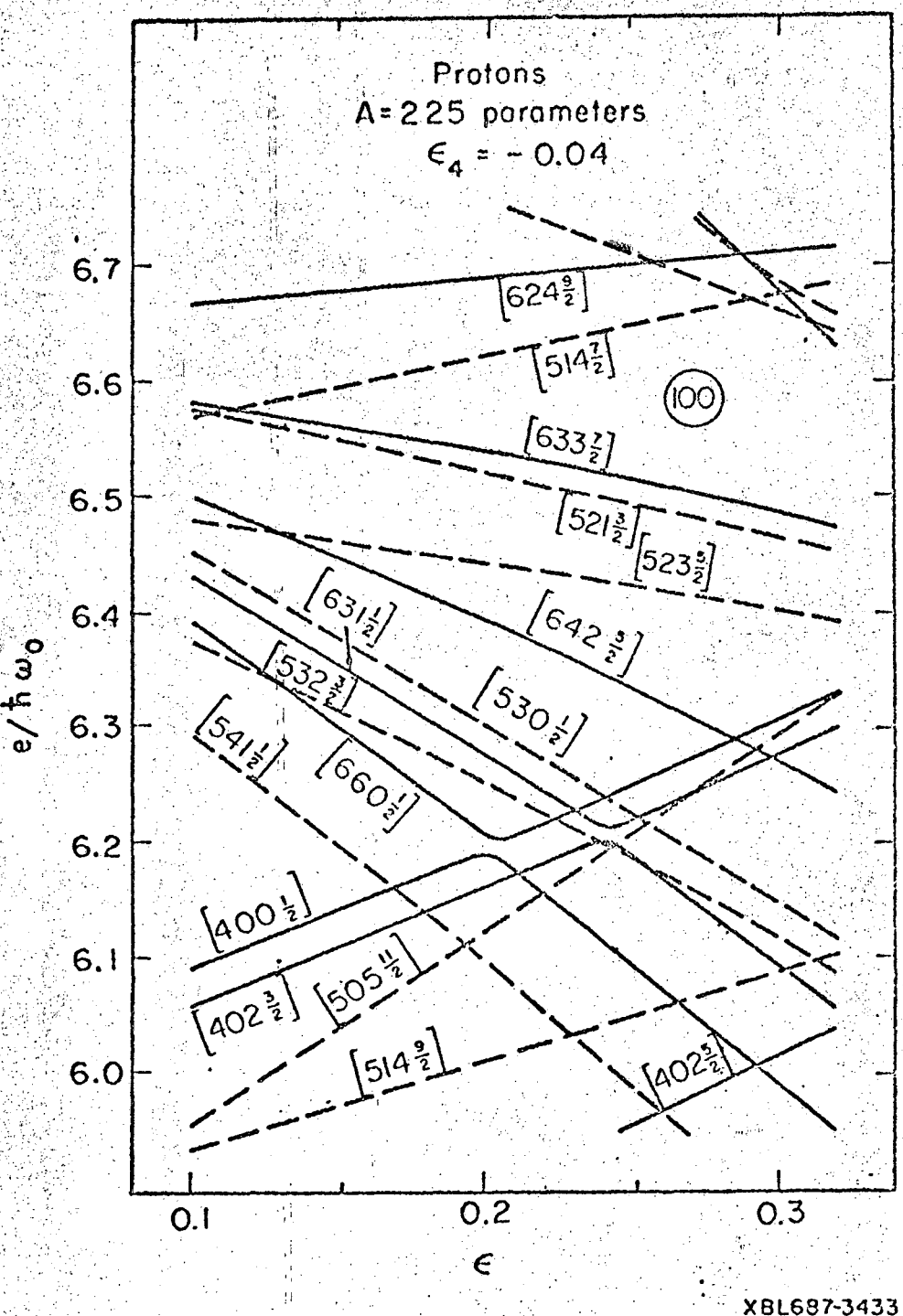
Protons
A=225 parameters
$\epsilon_4 = -0.04$
$e/\hbar\omega_0$
6.7
6.6
6.5
6.4
6.3
6.2
6.1
6.0
0.1
0.2
0.3
ϵ
[624 9/2]
[514 7/2]
(100)
[633 7/2]
[521 3/2]
[523 5/2]
[631 1/2]
[642 5/2]
[532 3/2]
[530 1/2]
[541 1/2]
[660 1/2]
[400 1/2]
[402 3/2]
[505 11/2]
[514 9/2]
[402 5/2]
XBL687-3433

FIG 2

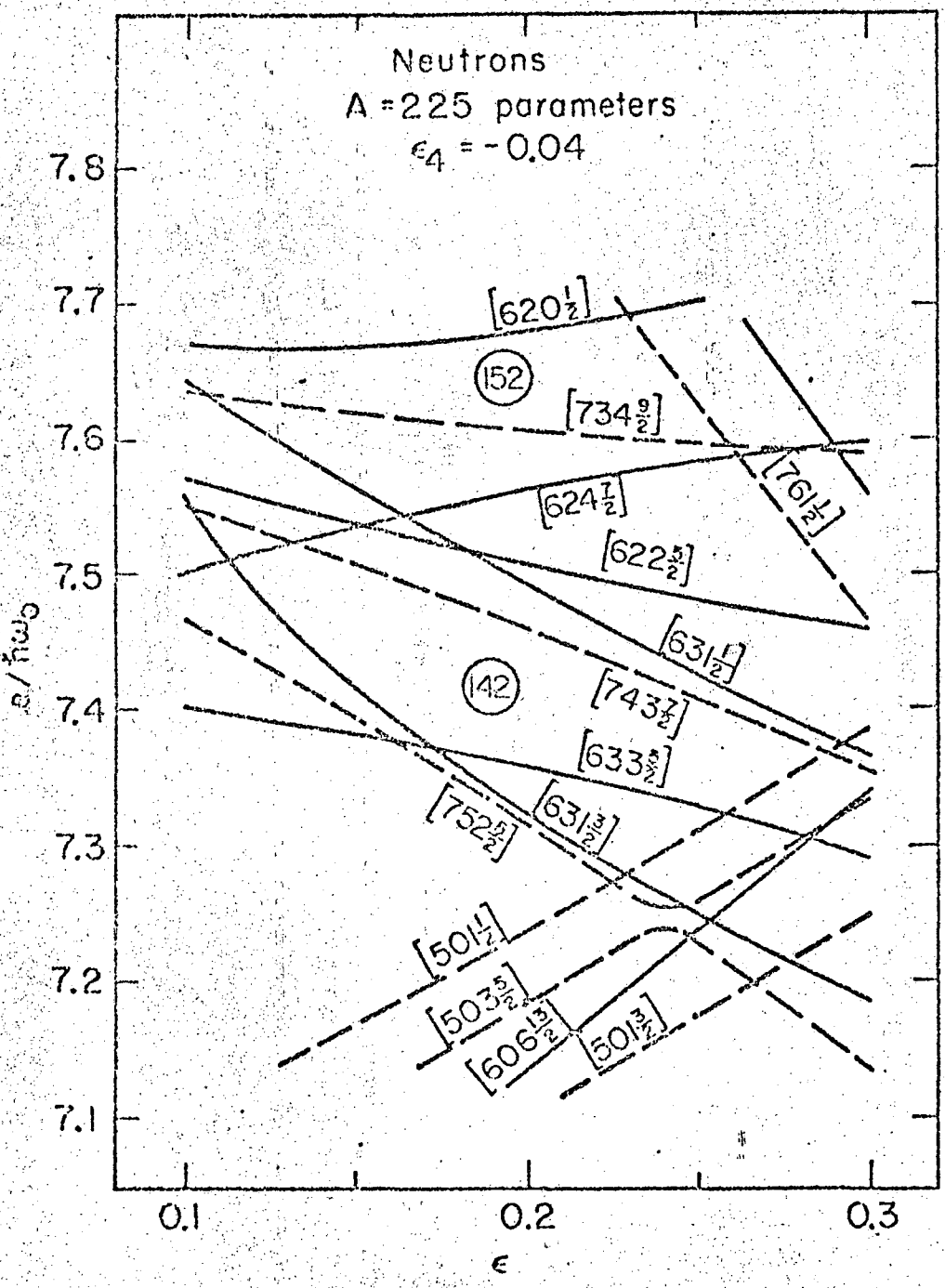
Neutrons
A = 225 parameters
$\epsilon_4 = -0.04$
$[620\frac{1}{2}]$
(152)
$[734\frac{9}{2}]$
$[624\frac{7}{2}]$
$[761\frac{1}{2}]$
$[622\frac{5}{2}]$
$[631\frac{1}{2}]$
(142)
$[743\frac{7}{2}]$
$[633\frac{5}{2}]$
$[752\frac{5}{2}]$
$[631\frac{3}{2}]$
$[501\frac{1}{2}]$
$[503\frac{5}{2}]$
$[606\frac{13}{2}]$
$[501\frac{3}{2}]$
7.8
7.7
7.6
7.5
7.4
7.3
7.2
7.1
$e/\hbar\omega_0$
0.1
0.2
0.3
ϵ
XBL685-2702

Fig 2 f.

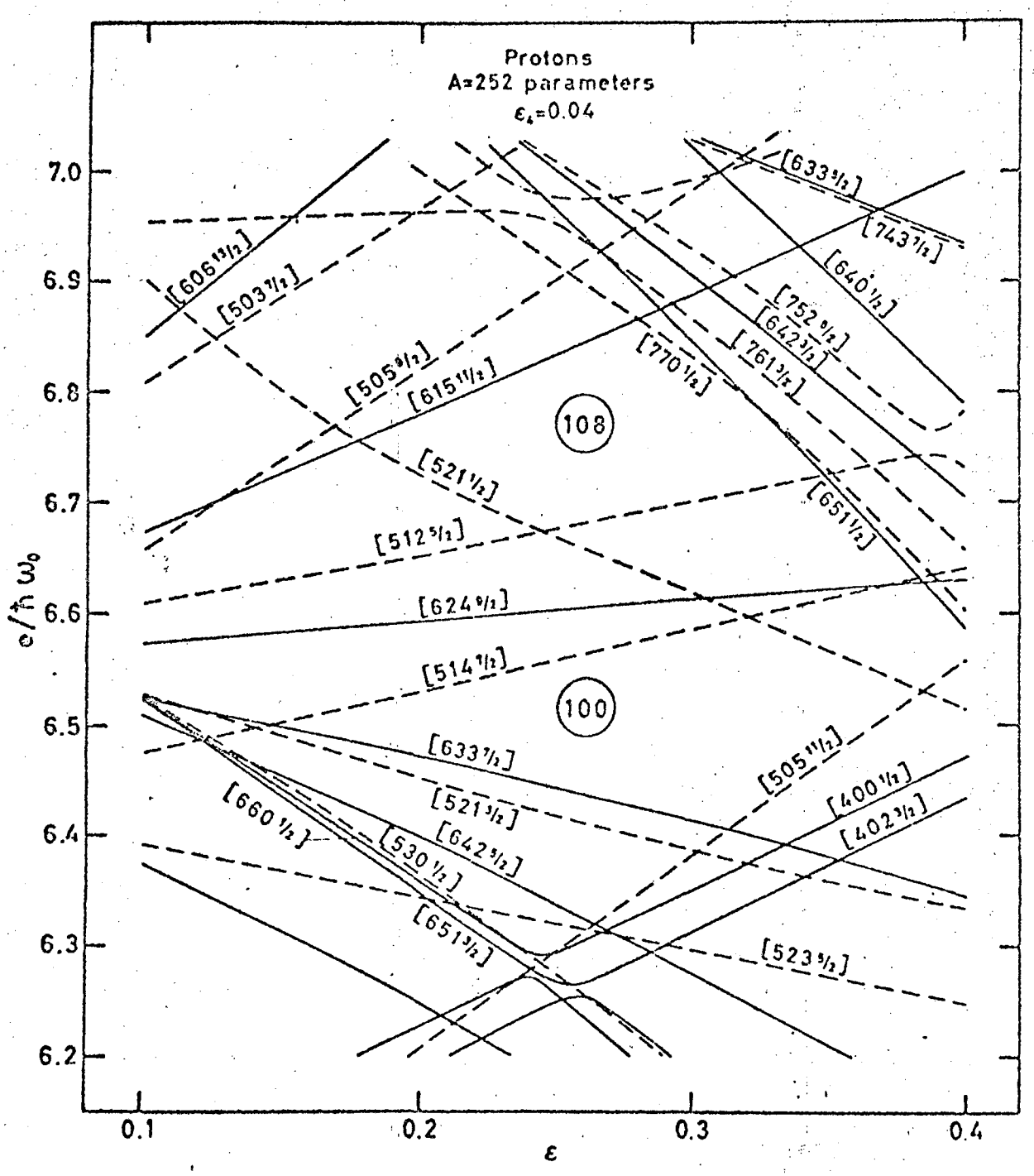
Protons
A=252 parameters
ε_4=0.04
7.0
6.9
6.8
6.7
6.6
6.5
6.4
6.3
6.2
$e/\hbar\omega_0$
0.1
0.2
0.3
0.4
ε
108
100
[606 11/2]
[503 7/2]
[505 9/2]
[615 11/2]
[521 1/2]
[512 5/2]
[624 9/2]
[514 7/2]
[633 7/2]
[521 3/2]
[660 1/2]
[642 5/2]
[530 1/2]
[651 3/2]
[505 11/2]
[400 1/2]
[402 3/2]
[523 5/2]
[633 3/2]
[743 1/2]
[640 1/2]
[752 5/2]
[642 3/2]
[761 3/2]
[770 1/2]
[651 1/2]

FIG 29

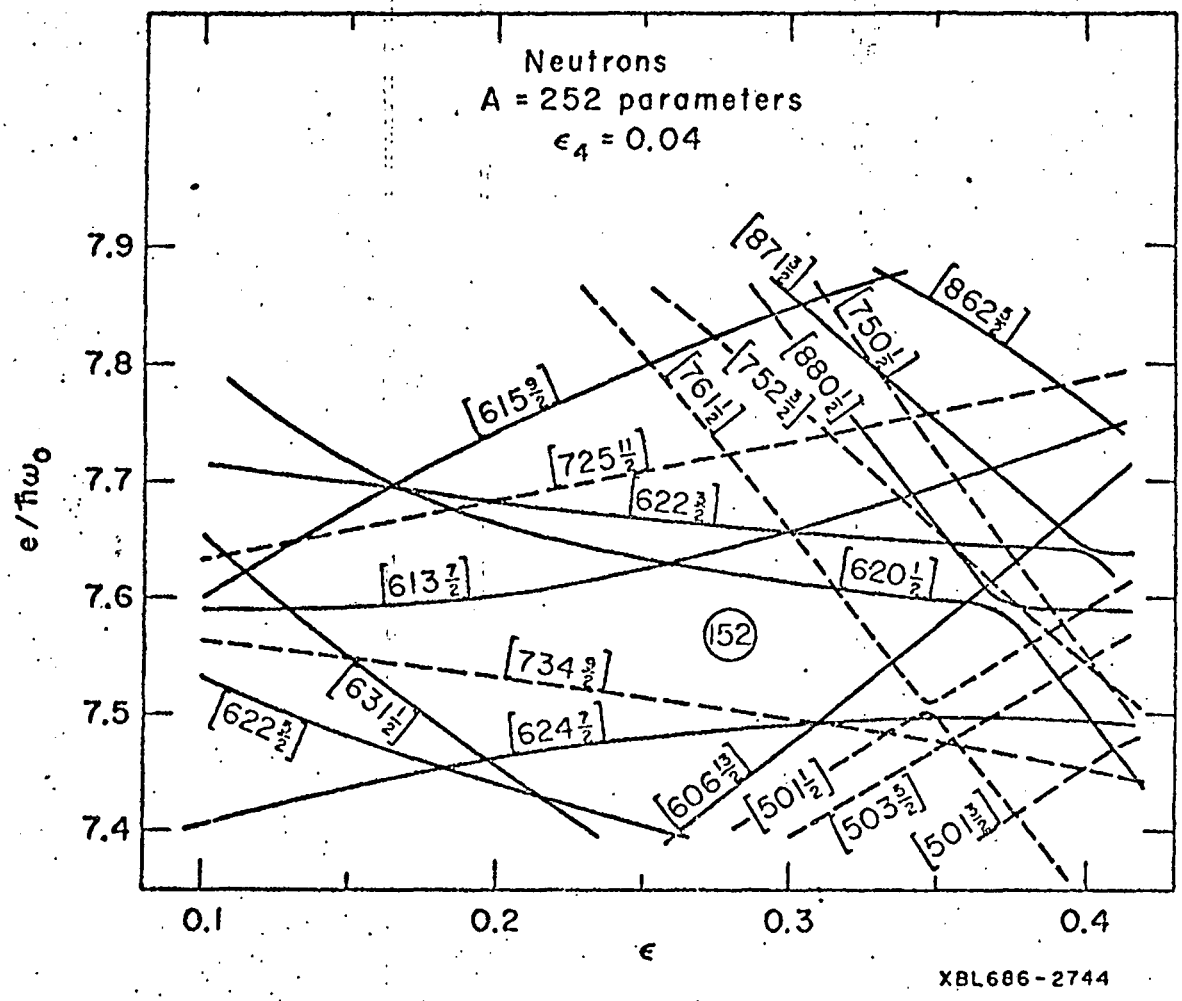
Neutrons
A = 252 parameters
ϵ_4 = 0.04
$e/\hbar\omega_0$
7.9
7.8
7.7
7.6
7.5
7.4
0.1
0.2
0.3
0.4
ϵ
[615 9/2]
[725 11/2]
[622 3/2]
[613 7/2]
[734 9/2]
[631 1/2]
[622 5/2]
[624 7/2]
[606 13/2]
[761/2]
[752 3/2]
[880 1/2]
[871 13/2]
[750 1/2]
[862 5/2]
[620 1/2]
[501 1/2]
[503 5/2]
[501 7/2]
152
XBL686-2744

FIG 2 h

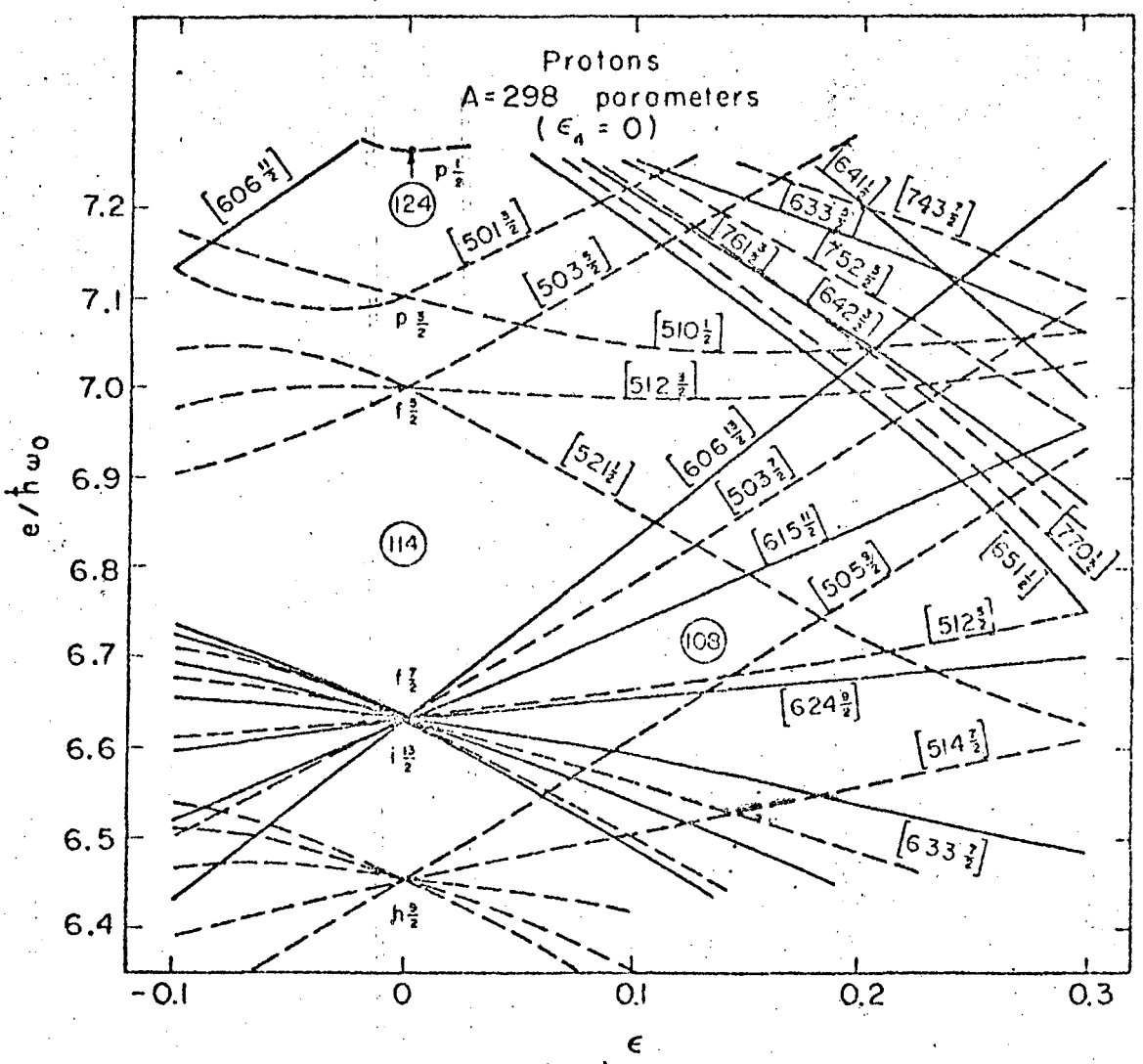

XBL687-3434

FIG 9 i

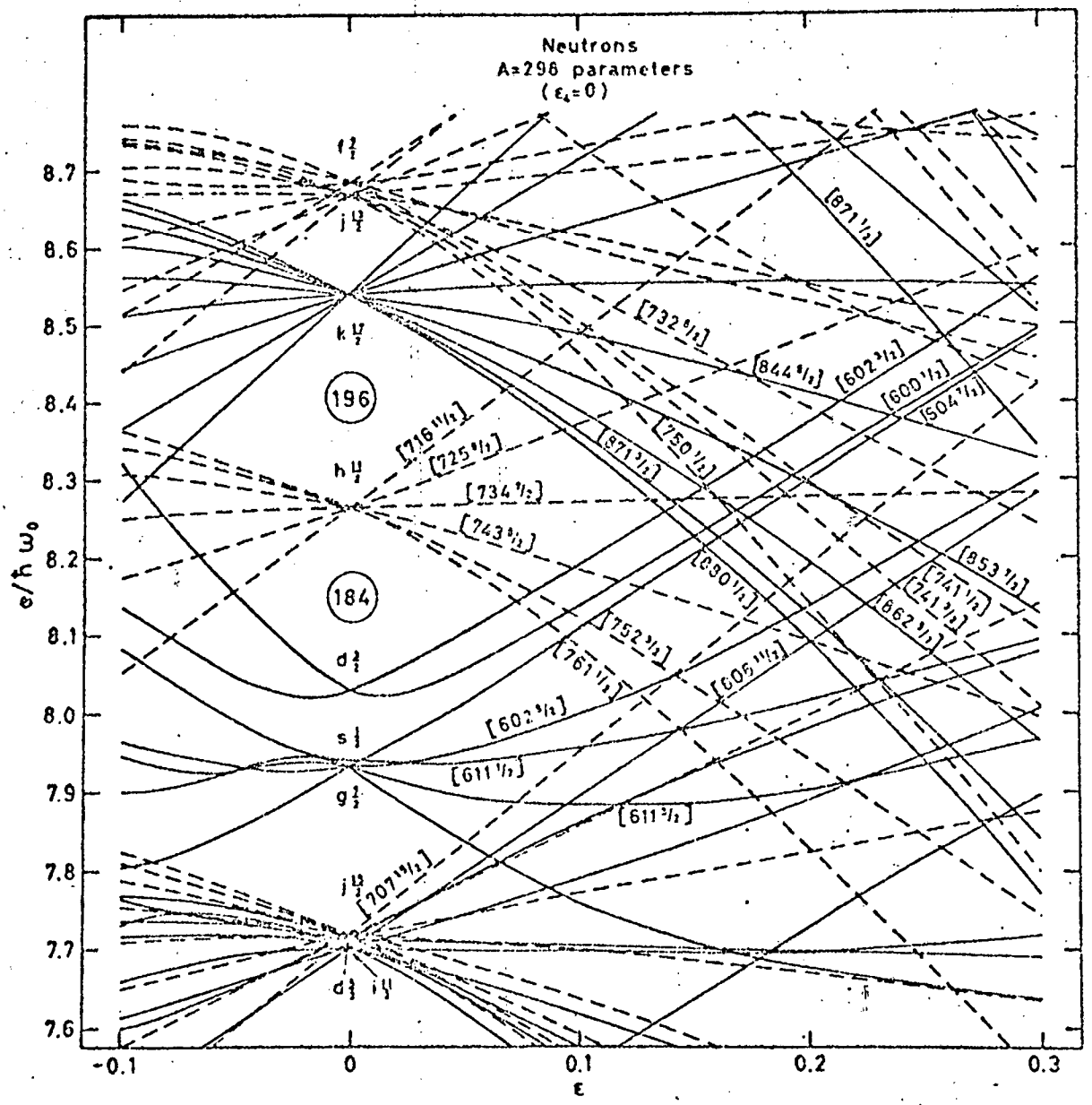
Neutrons
A=296 parameters
(ε₄=0)
e/ħω₀
ε
196
184
f 7/2
i 13/2
k 17/2
h 11/2
d 3/2
s 1/2
g 7/2
j 15/2
i 13/2
[871 1/2]
[732 1/2]
[844 1/2]
[602 1/2]
[600 1/2]
[504 1/2]
[716 11/2]
[725 1/2]
[734 1/2]
[743 1/2]
[750 1/2]
[871 3/2]
[853 1/2]
[741 1/2]
[741 3/2]
[662 3/2]
[752 3/2]
[761 1/2]
[606 11/2]
[602 3/2]
[611 1/2]
[611 3/2]
[707 11/2]

FIG. 2.

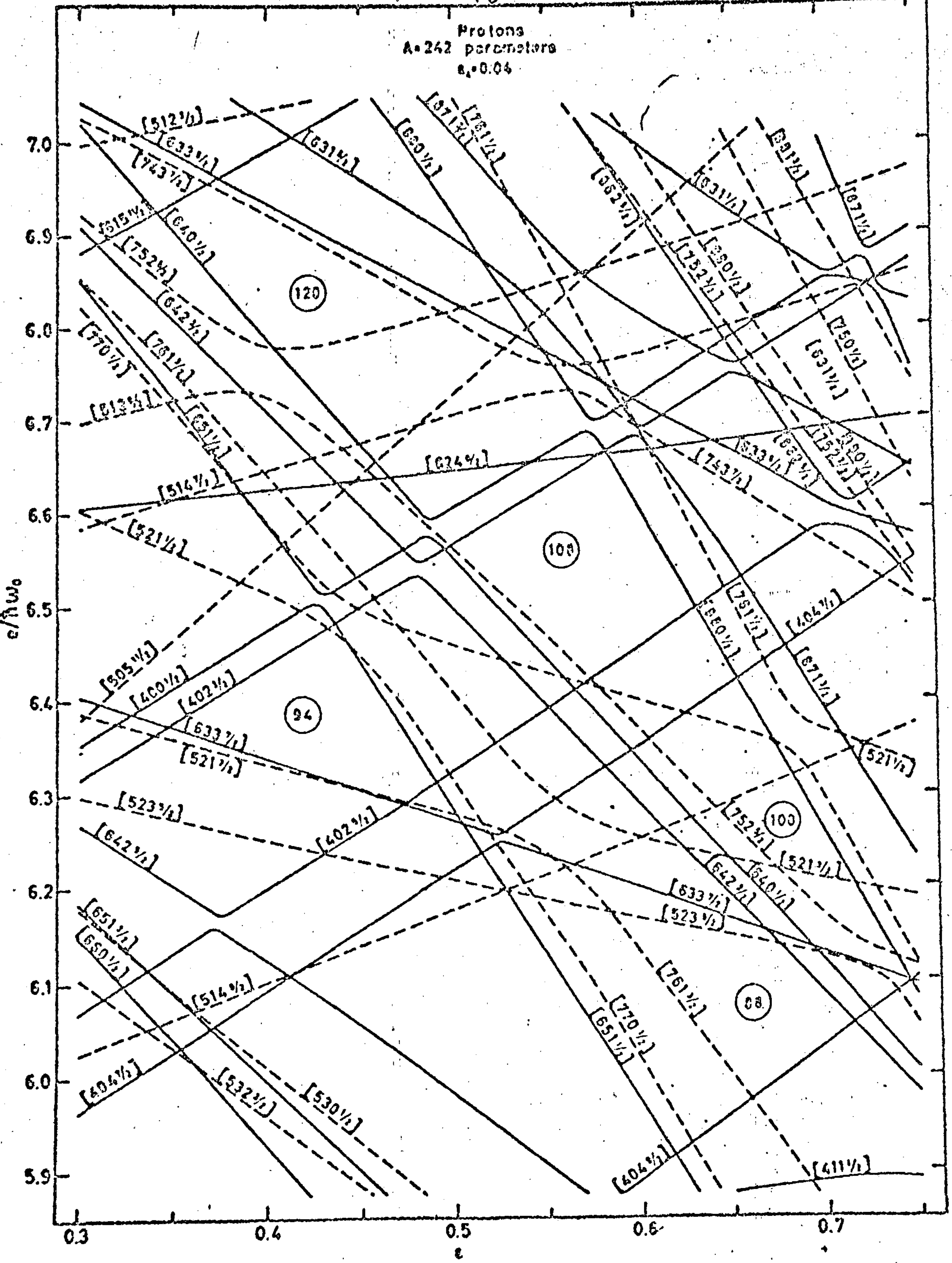
Protons
A=242 parameters
ε4=0.04
e/ħω0
ε
7.0
6.9
6.8
6.7
6.6
6.5
6.4
6.3
6.2
6.1
6.0
5.9
0.3
0.4
0.5
0.6
0.7
120
108
94
100
88

2 K

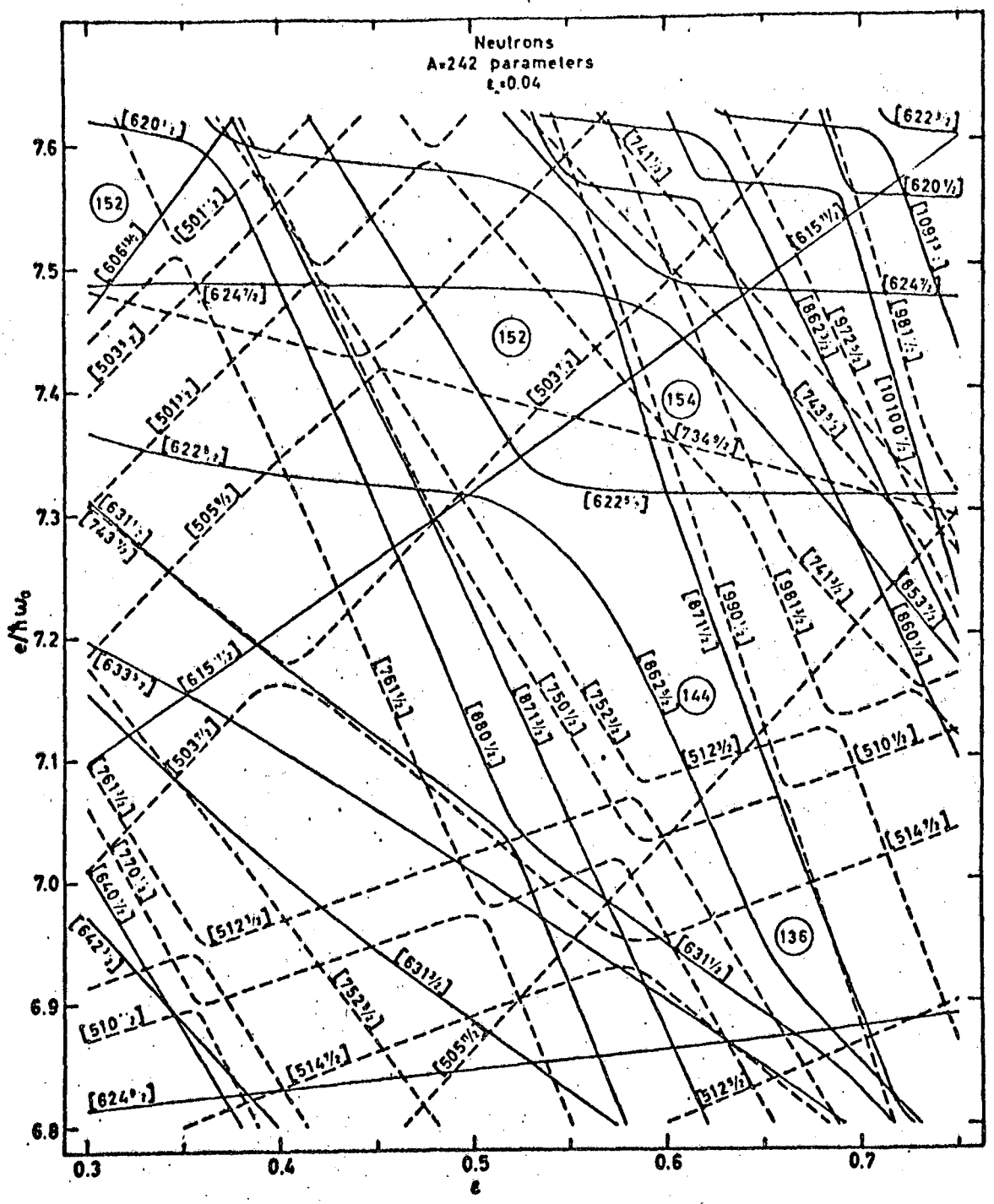
Neutrons
A=242 parameters
ε=0.04
e/ħω₀
ε
7.6
7.5
7.4
7.3
7.2
7.1
7.0
6.9
6.8
0.3
0.4
0.5
0.6
0.7
152
154
144
136
[620 1/2]
[501 1/2]
[606 3/2]
[624 7/2]
[503 3/2]
[622 5/2]
[631 1/2]
[743 1/2]
[505 5/2]
[633 3/2]
[615 3/2]
[503 7/2]
[761 1/2]
[770 1/2]
[640 7/2]
[642 5/2]
[510 5/2]
[624 9/2]
[514 7/2]
[512 3/2]
[752 3/2]
[631 1/2]
[505 11/2]
[880 1/2]
[871 1/2]
[750 1/2]
[752 1/2]
[741 1/2]
[734 9/2]
[622 5/2]
[671 1/2]
[990 1/2]
[862 1/2]
[512 1/2]
[512 5/2]
[615 1/2]
[862 1/2]
[922 1/2]
[1010 0 1/2]
[981 1/2]
[1091 1/2]
[624 7/2]
[622 1/2]
[620 1/2]
[743 1/2]
[741 1/2]
[981 1/2]
[853 1/2]
[660 1/2]
[510 1/2]
[514 7/2]
[631 1/2]

FIG 21

Protons

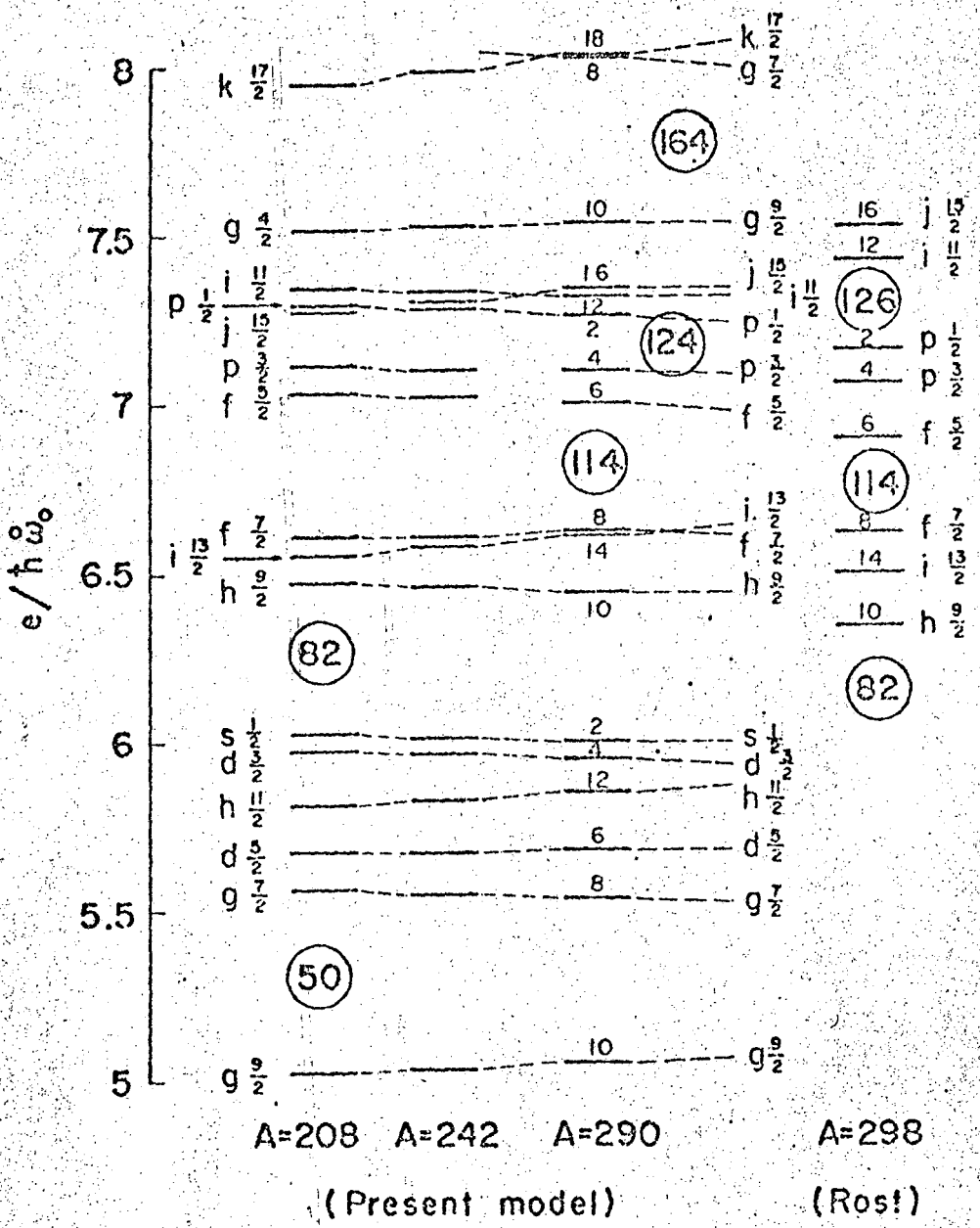

XBL682-1807

FIG. 3a

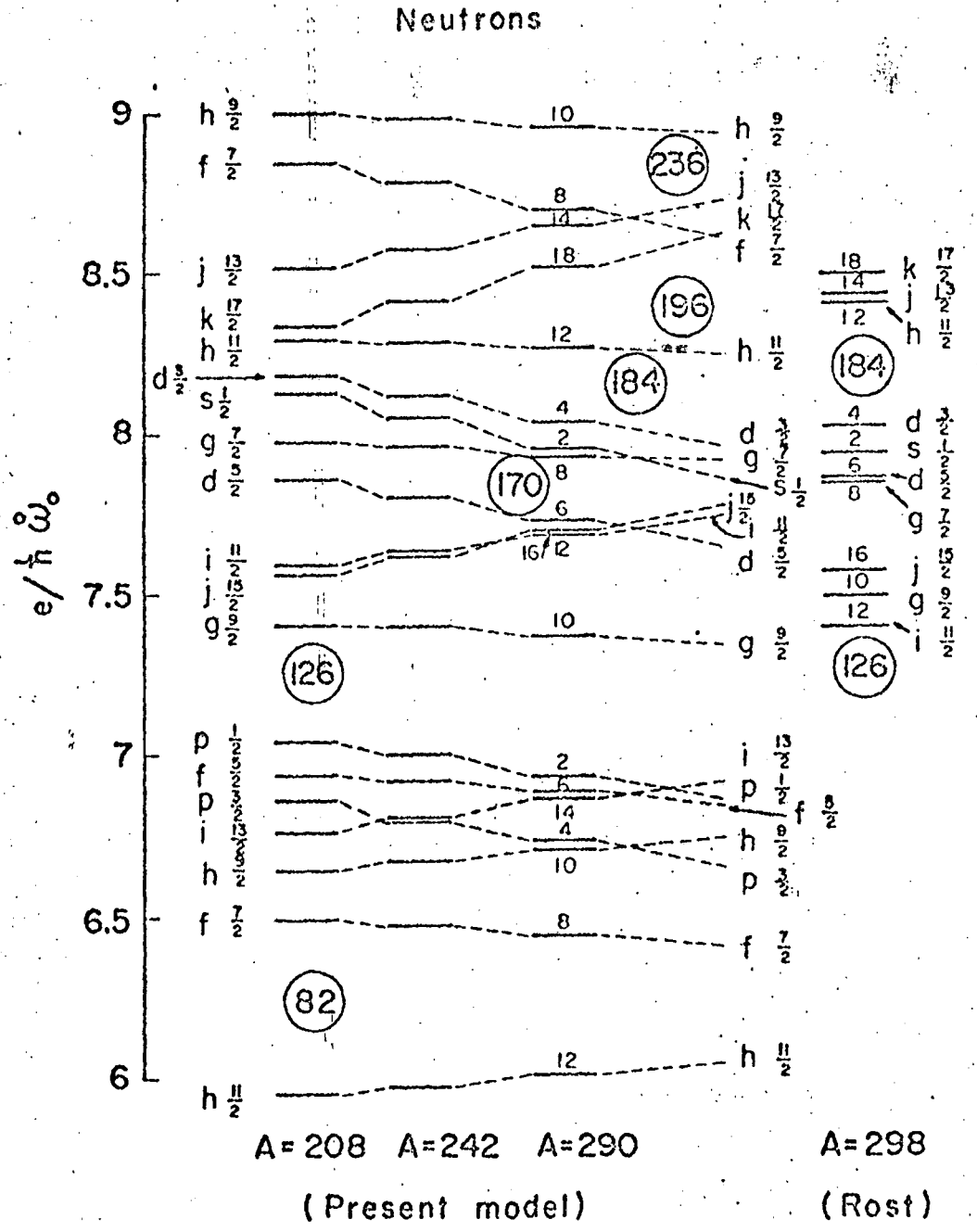

XBL682-1803

FIG 3b

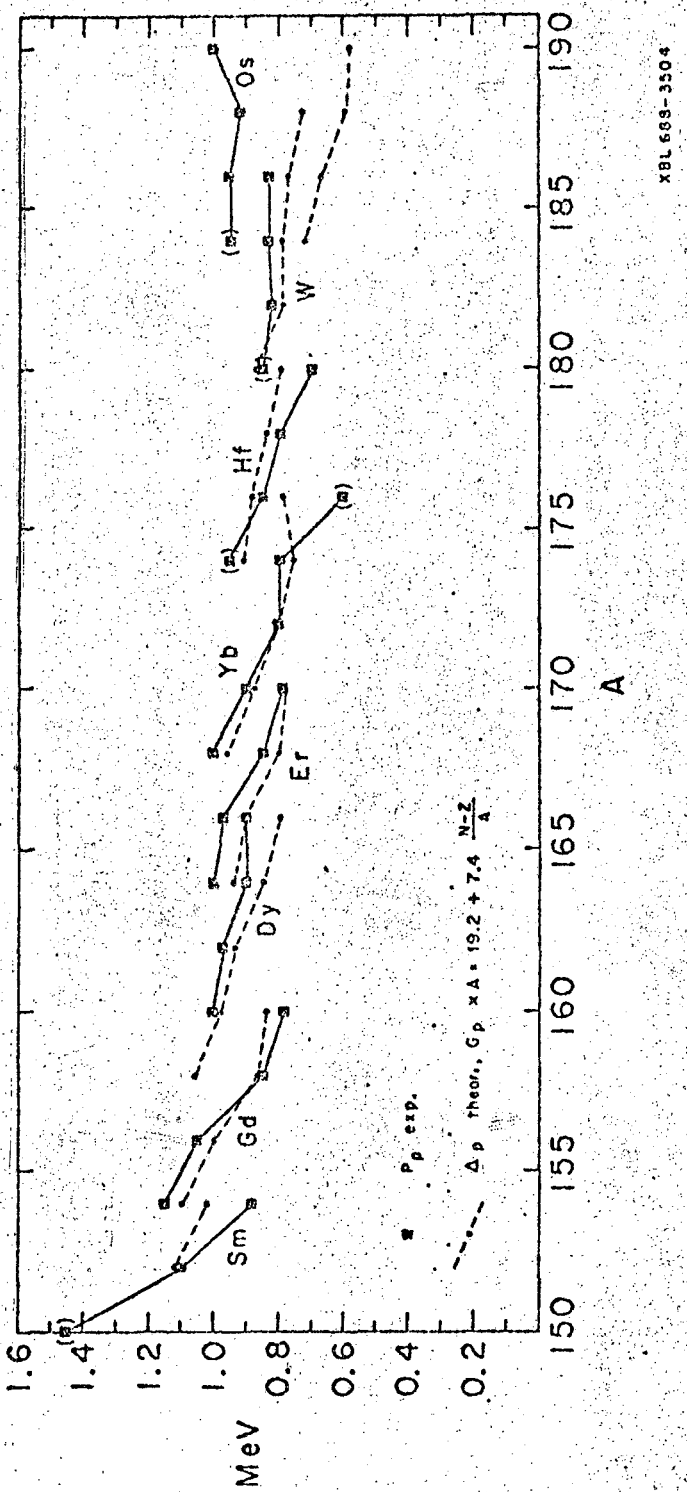
Os
W
Hf
Yb
Er
Dy
Gd
Sm
MeV
A
1.6
1.4
1.2
1.0
0.8
0.6
0.4
0.2
150
155
160
165
170
175
180
185
190
P_p exp.
Δ_p theor., $G_p \times A = 19.2 + 7.4 \frac{N-Z}{A}$
XBL 683-3504

FIG. 42

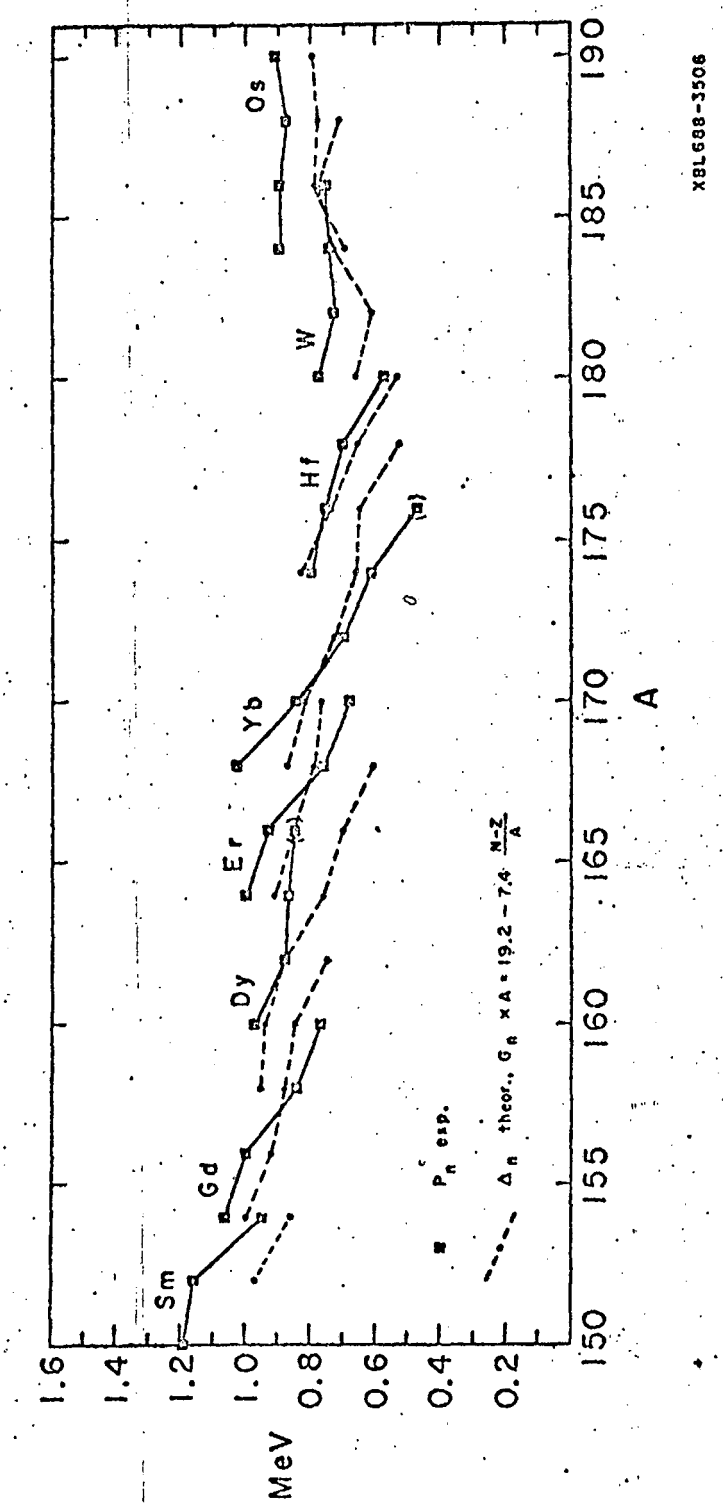
Os
W
Hf
Yb
Er
Dy
Gd
Sm
MeV
A
1.6
1.4
1.2
1.0
0.8
0.6
0.4
0.2
150
155
160
165
170
175
180
185
190
P_n exp.
Δ_n theor., $G_n \times A = 19.2 - 7.4 \frac{N-Z}{A}$
XBL688-3508

FIG 4b

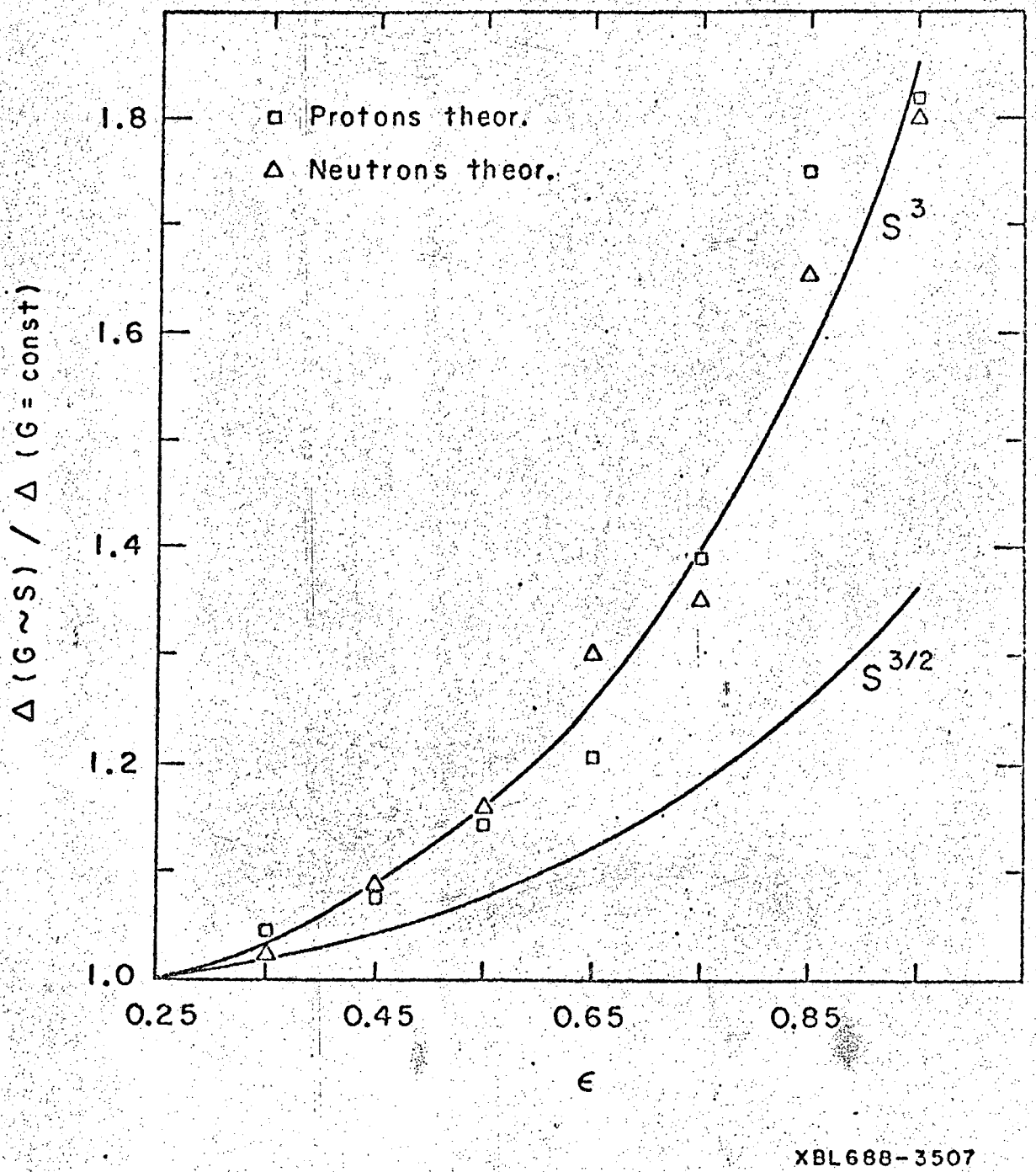
Protons theor.
Neutrons theor.
S^3
S^3/2
Δ (G ~ S) / Δ (G = const)
1.8
1.6
1.4
1.2
1.0
0.25
0.45
0.65
0.85
ϵ
XBL688-3507

FIG 5

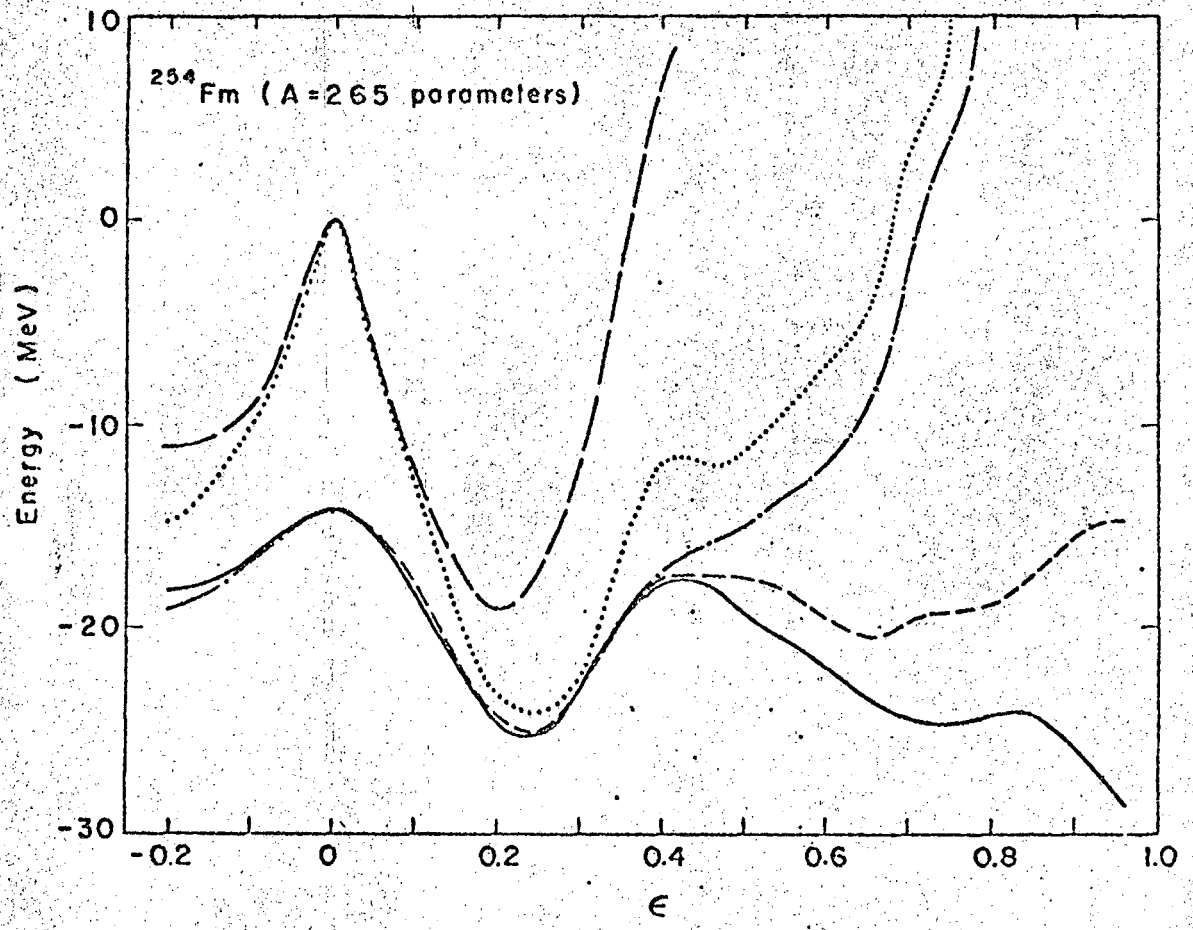

XBL687-3436

FIG 6

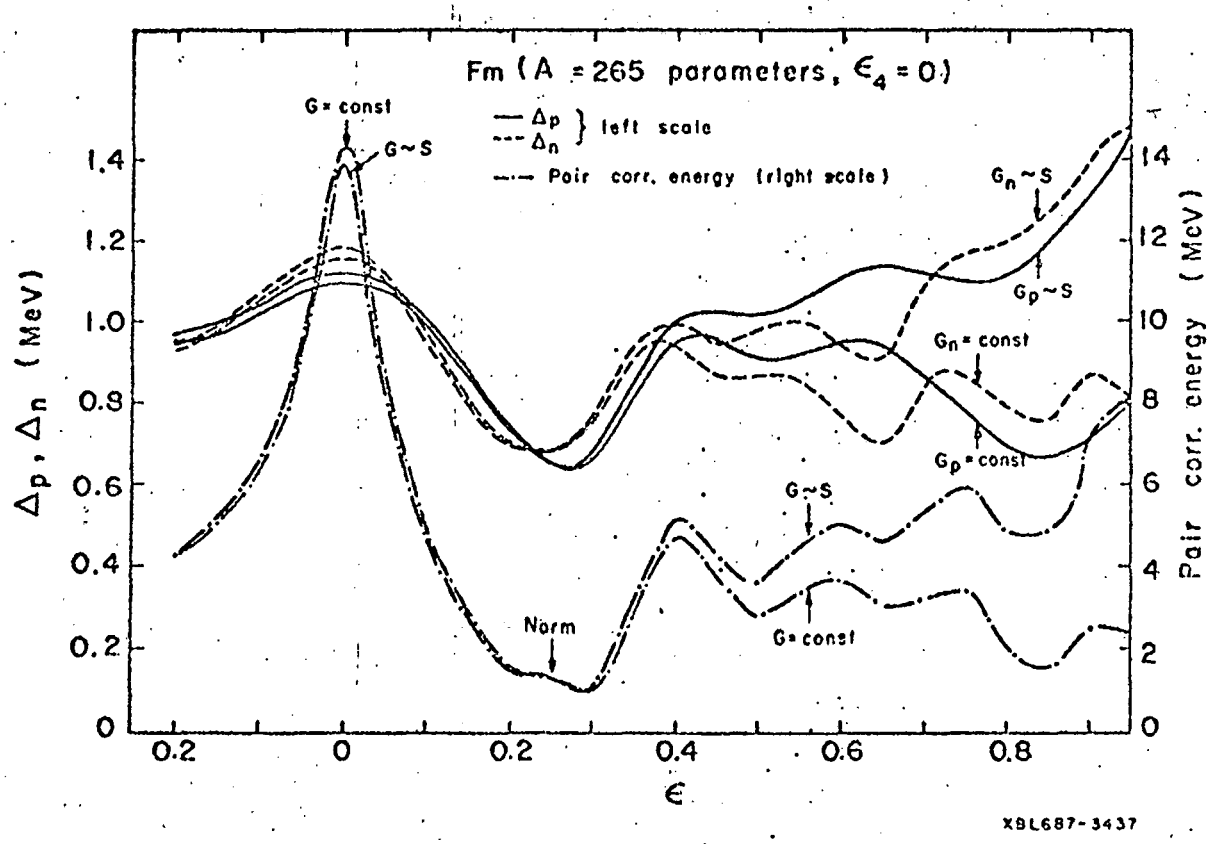
Fm (A = 265 parameters, $\epsilon_4 = 0$)
G = const
G~S
Δ_p } left scale
Δ_n
Pair corr. energy (right scale)
G_n~S
G_p~S
G_n = const
G_p = const
G~S
G = const
Norm
Δ_p, Δ_n (MeV)
Pair corr. energy (MeV)
ϵ
XBL687-3437

FIG. 7

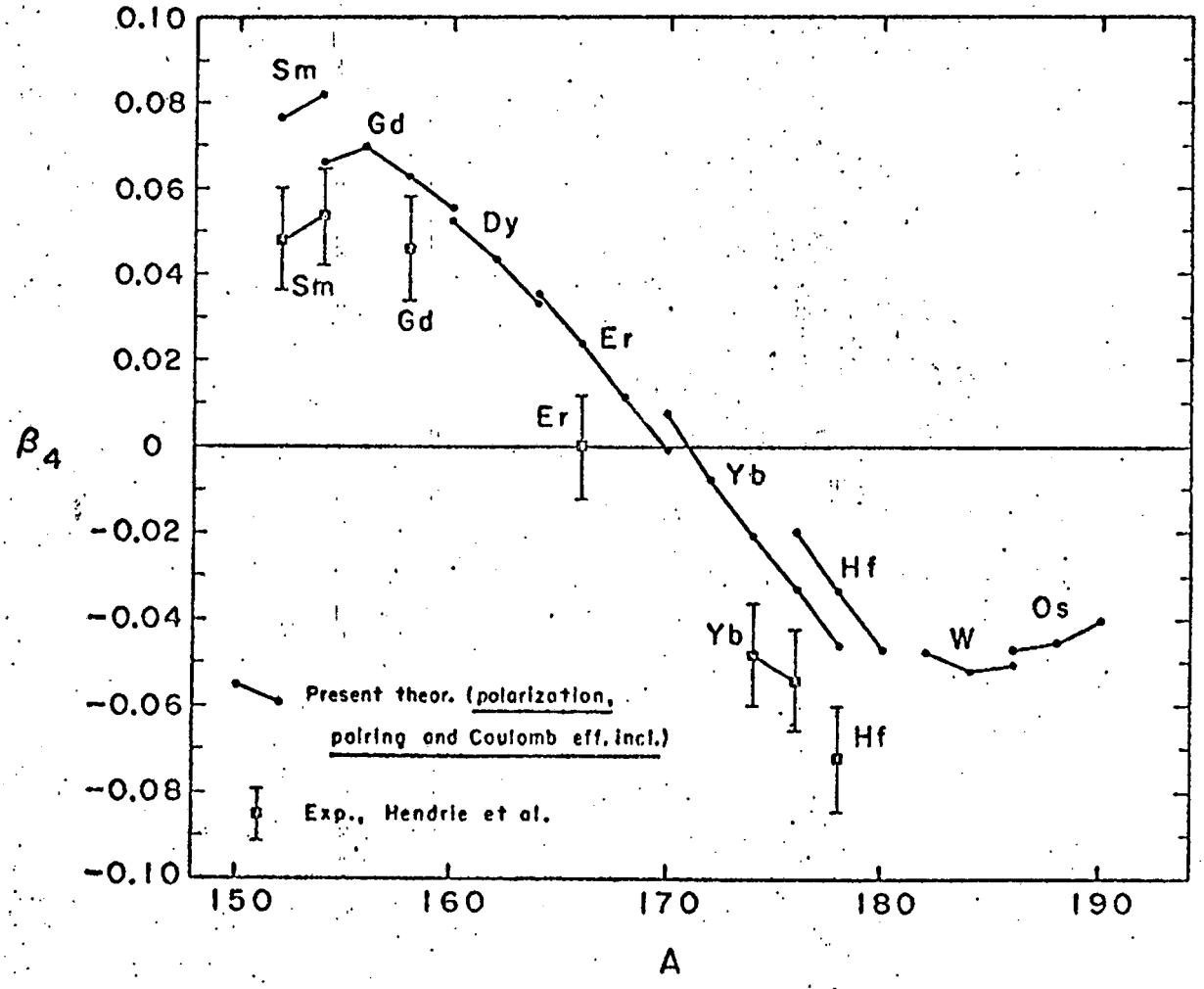
0.10
0.08
0.06
0.04
0.02
0
-0.02
-0.04
-0.06
-0.08
-0.10
β_4
150
160
170
180
190
A
Sm
Gd
Dy
Er
Yb
Hf
W
Os
Sm
Gd
Er
Yb
Hf
Present theor. (polarization, pairing and Coulomb eff. incl.)
Exp., Hendrie et al.
XBL688-3505

FIG 8

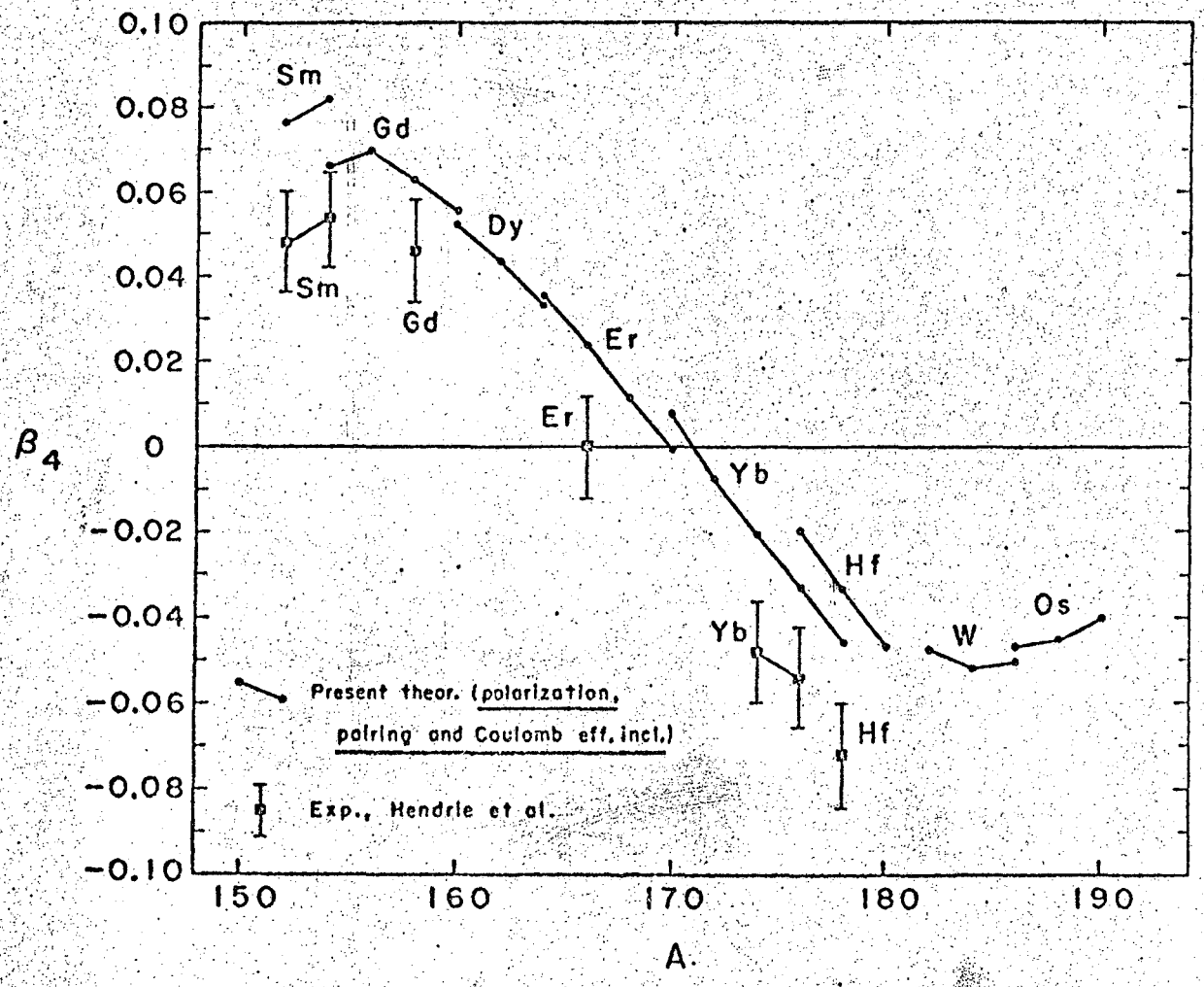

XBL688-3505

FIG 8

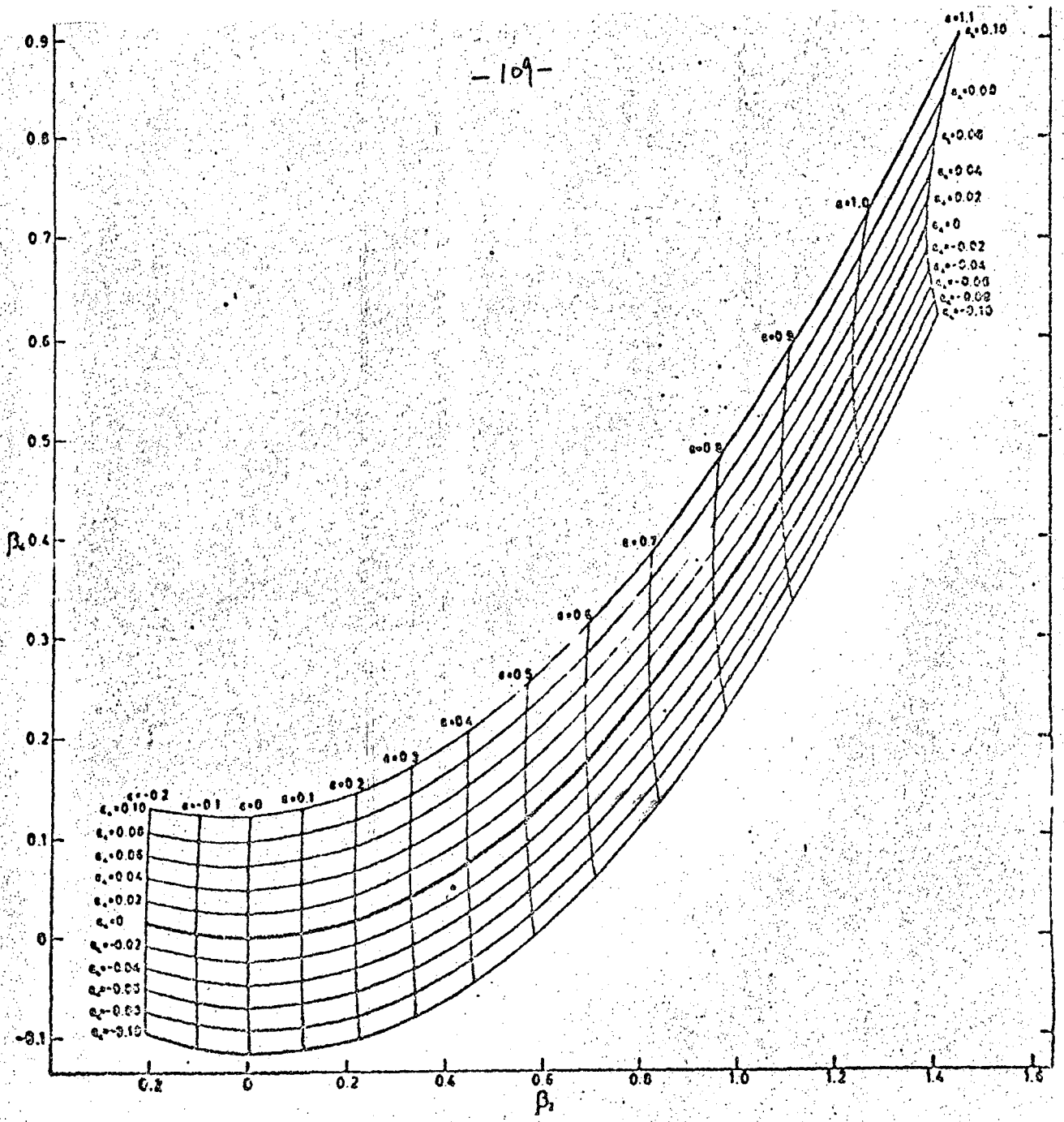
0.9
0.8
0.7
0.6
0.5
0.4
0.3
0.2
0.1
0
-0.1
β_4
-0.2
0
0.2
0.4
0.6
0.8
1.0
1.2
1.4
1.6
β_2
ε=1.1
ε=1.0
ε=0.9
ε=0.8
ε=0.7
ε=0.6
ε=0.5
ε=0.4
ε=0.3
ε=0.2
ε=0.1
ε=0
ε=-0.1
ε=-0.2
ϵ_4=0.10
ϵ_4=0.08
ϵ_4=0.06
ϵ_4=0.04
ϵ_4=0.02
ϵ_4=0
ϵ_4=-0.02
ϵ_4=-0.04
ϵ_4=-0.06
ϵ_4=-0.08
ϵ_4=-0.10

FIG. 9

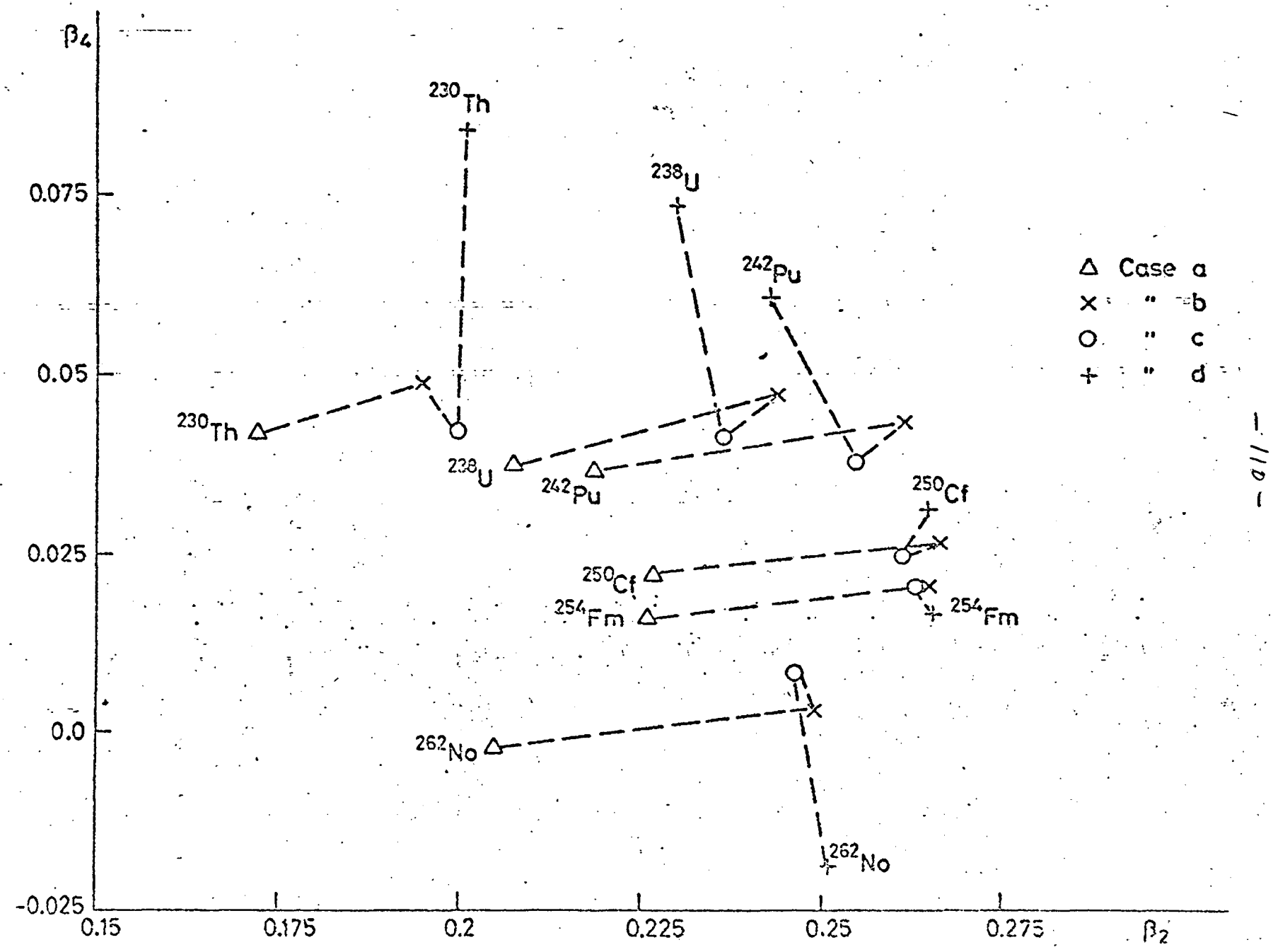
β4
0.075
0.05
0.025
0.0
-0.025
0.15
0.175
0.2
0.225
0.25
0.275
β2
230Th
238U
242Pu
250Cf
254Fm
262No
Δ Case a
× " b
○ " c
+ " d

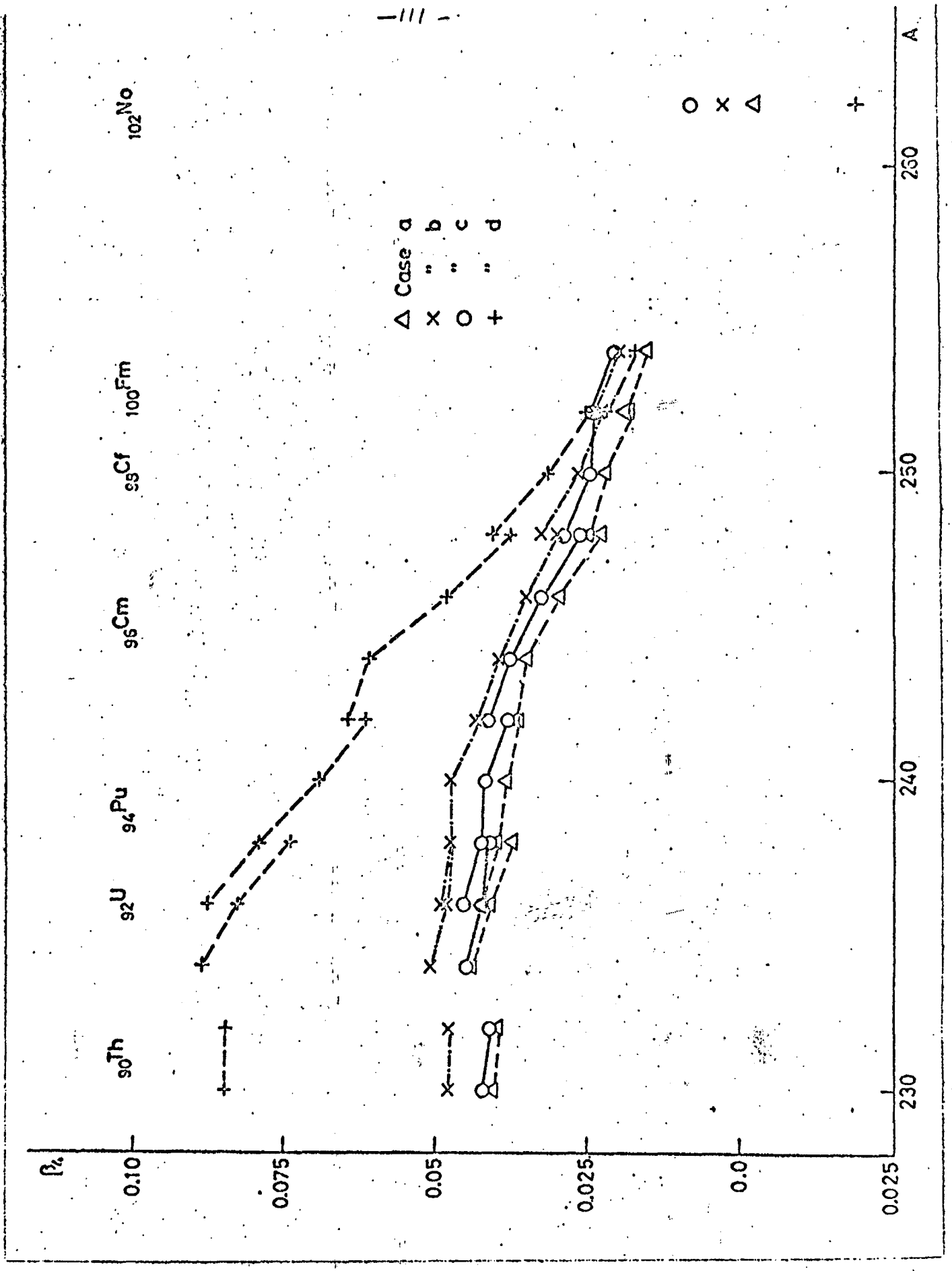
$_{90}$Th
$_{92}$U
$_{94}$Pu
$_{96}$Cm
$_{98}$Cf
$_{100}$Fm
$_{102}$No
Case a
b
c
d
β_4
0.10
0.075
0.05
0.025
0.0
0.025
230
240
250
260
A

FIG 10 b

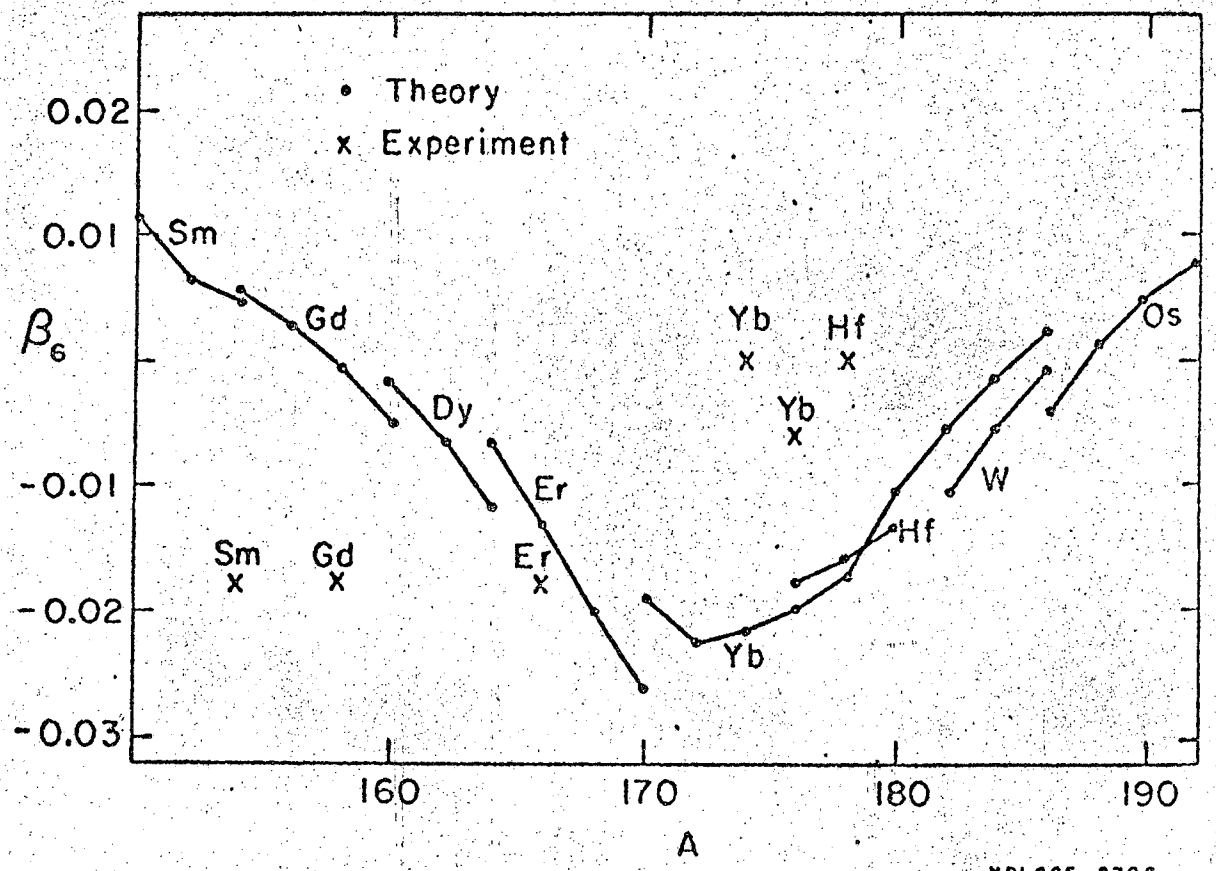
• Theory
x Experiment
0.02
0.01
β_6
-0.01
-0.02
-0.03
Sm
Gd
Dy
Er
Er
Sm
Gd
Yb
Hf
Yb
Yb
Hf
W
Os
160
170
180
190
A
XBL665-2706

FIG 11

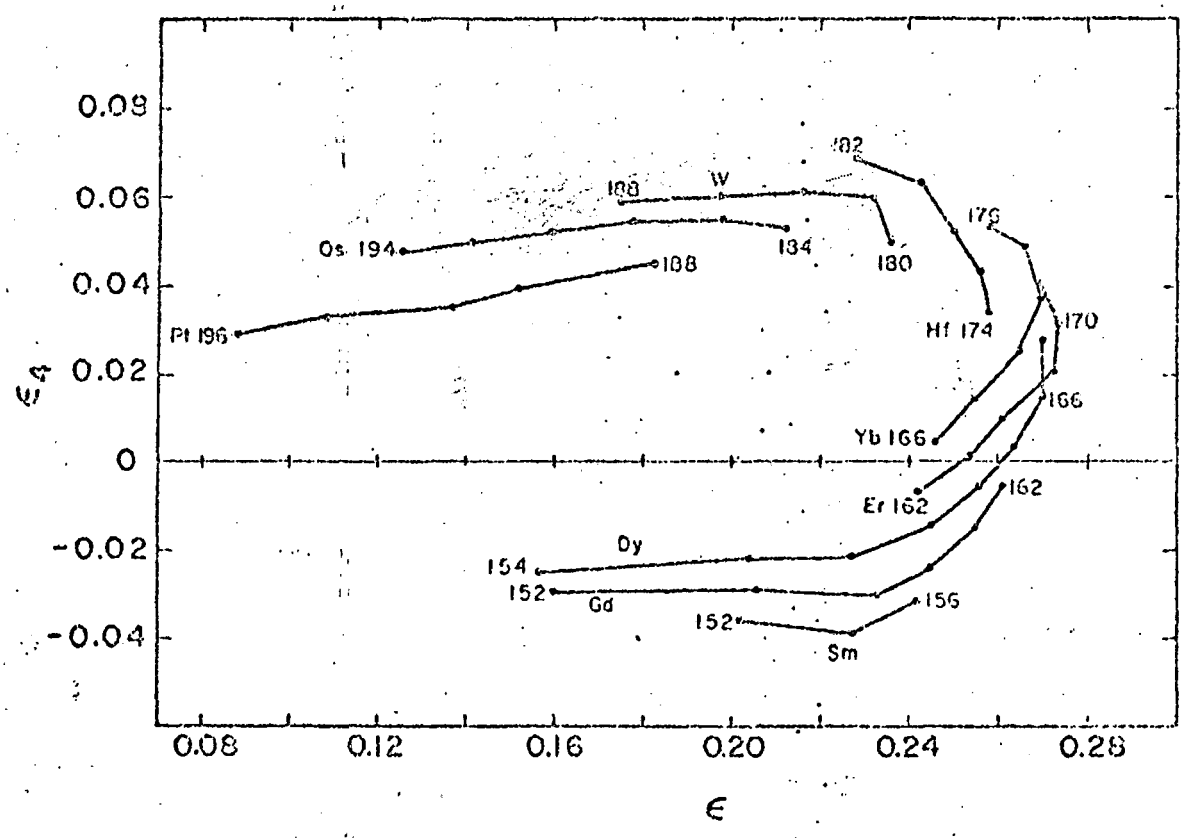
0.08
0.06
0.04
0.02
0
-0.02
-0.04
γ
0.08
0.12
0.16
0.20
0.24
0.28
ε
Pt 196
Os 194
188
W
184
180
182
178
Hf 174
170
166
Yb 166
Er 162
162
Dy
154
152
Gd
152
Sm
156
XBL6d7-3439

FIG 12a

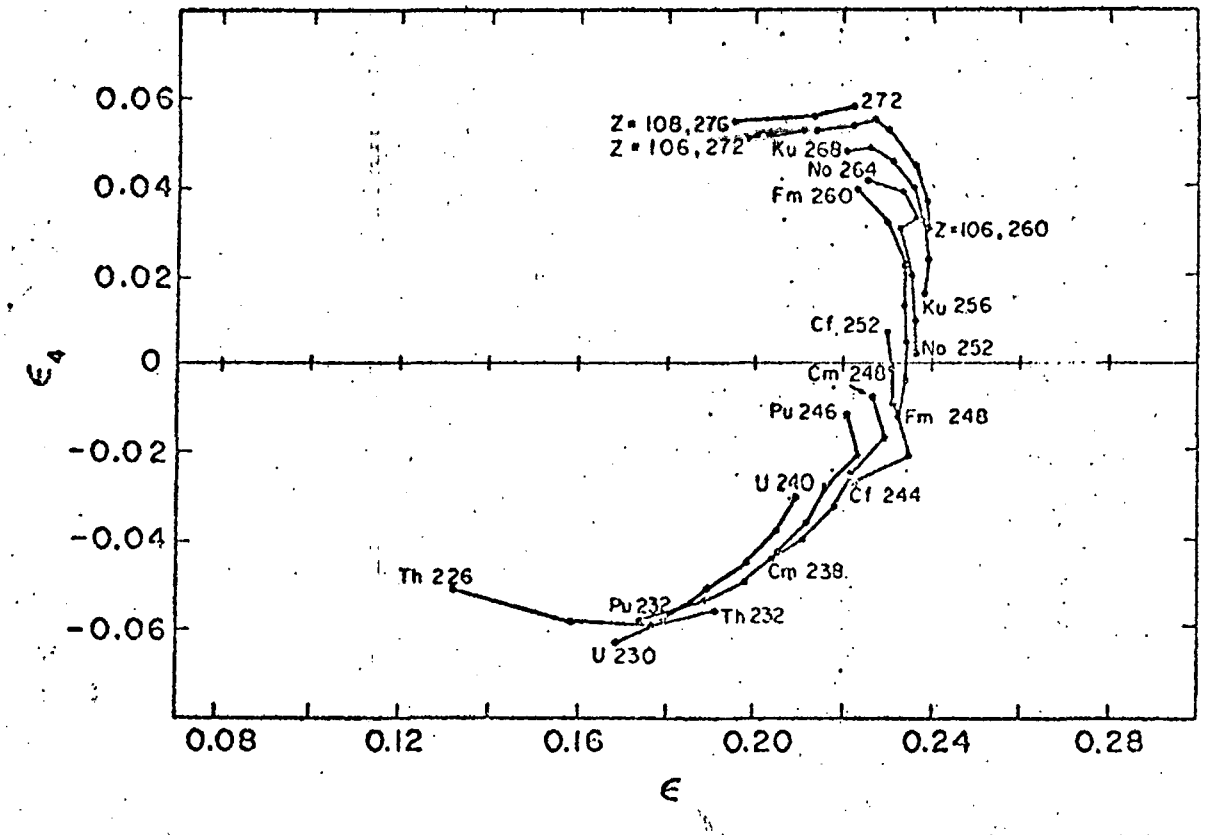
0.06
0.04
0.02
0
-0.02
-0.04
-0.06
ϵ_4
0.08
0.12
0.16
0.20
0.24
0.28
ϵ
Z = 108, 276
Z = 106, 272
272
Ku 268
No 264
Fm 260
Z = 106, 260
Ku 256
Cf 252
No 252
Cm 248
Fm 248
Pu 246
U 240
Cf 244
Cm 238
Th 226
Pu 232
Th 232
U 230
XBL687-3438

FIG 12 b.

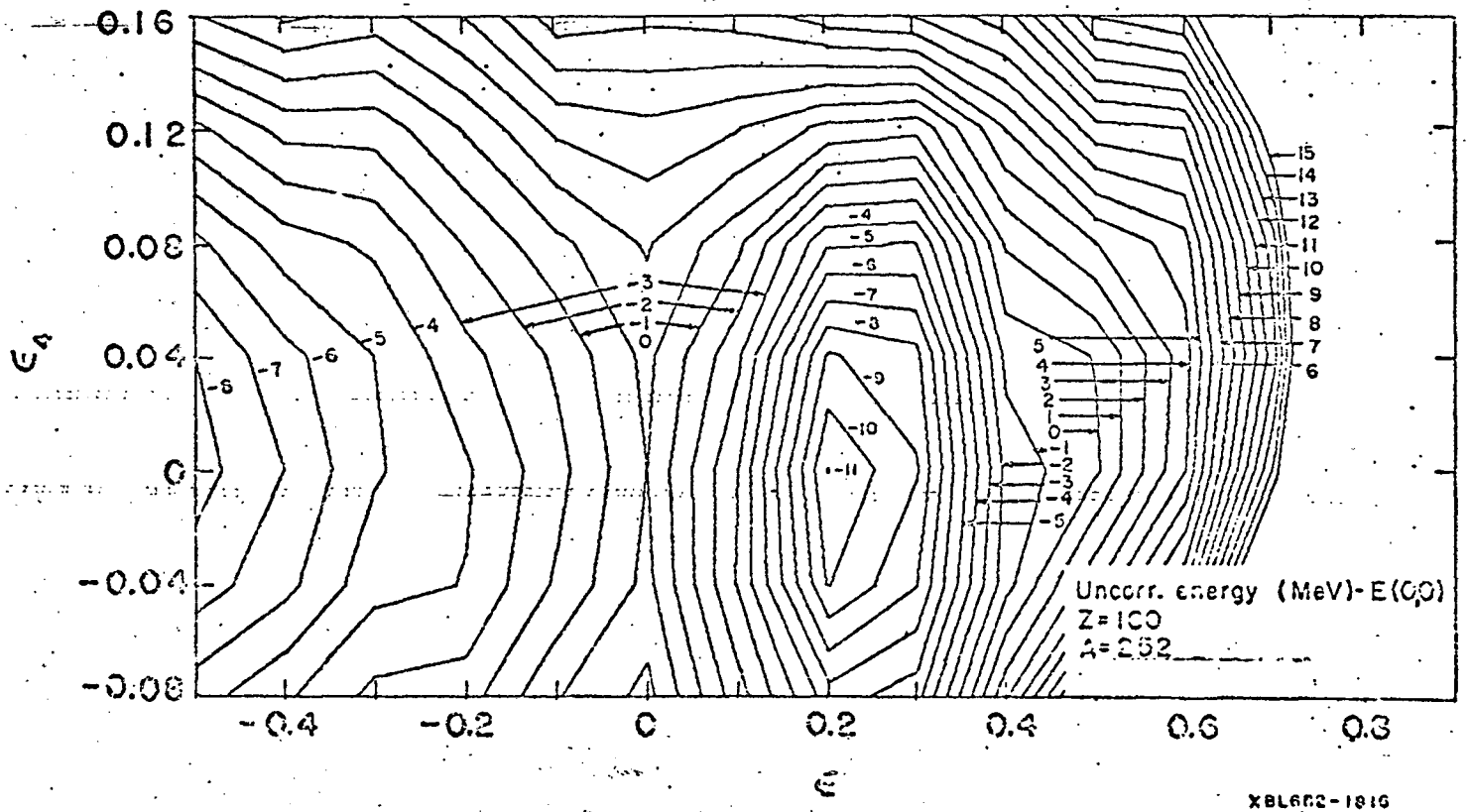
0.16
0.12
0.08
0.04
0
-0.04
-0.08
ϵ_4
-0.4
-0.2
0
0.2
0.4
0.6
0.8
ϵ
Uncorr. energy (MeV)-E(0,0)
Z=100
A=252
XBL682-1816

FIG 13

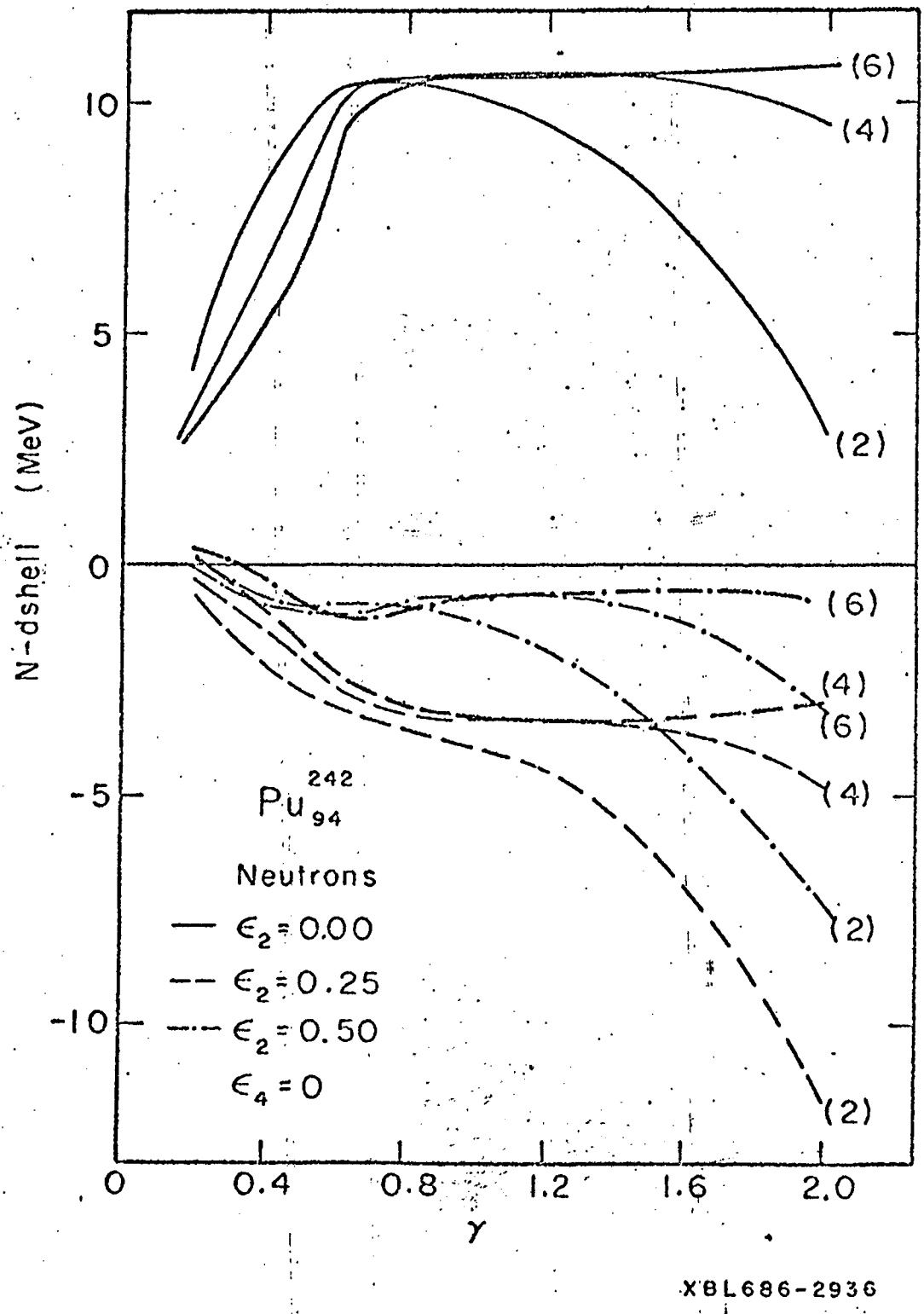
N-dshell (MeV)
10
5
0
-5
-10
0
0.4
0.8
1.2
1.6
2.0
γ
(6)
(4)
(2)
(6)
(4)
(6)
(4)
(2)
(2)
Pu_{94}^{242}
Neutrons
$\epsilon_2 = 0.00$
$\epsilon_2 = 0.25$
$\epsilon_2 = 0.50$
$\epsilon_4 = 0$
XBL686-2936

FIG 14

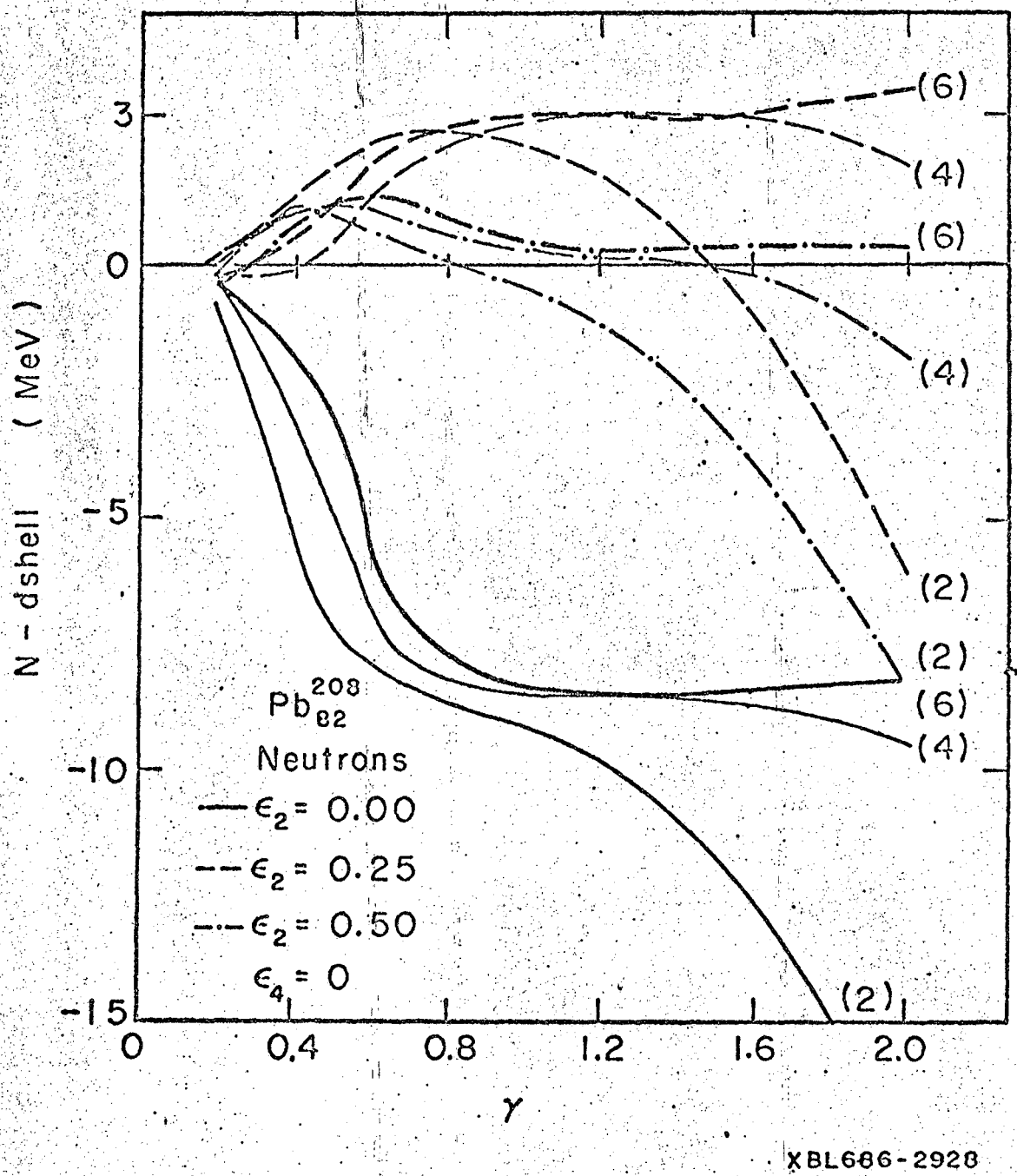
N - dshell (MeV)
3
0
-5
-10
-15
0
0.4
0.8
1.2
1.6
2.0
γ
(6)
(4)
(6)
(4)
(2)
(2)
(6)
(4)
(2)
$Pb^{208}_{\epsilon 2}$
Neutrons
$\epsilon_2 = 0.00$
$\epsilon_2 = 0.25$
$\epsilon_2 = 0.50$
$\epsilon_4 = 0$
XBL686-2928

FIG 15

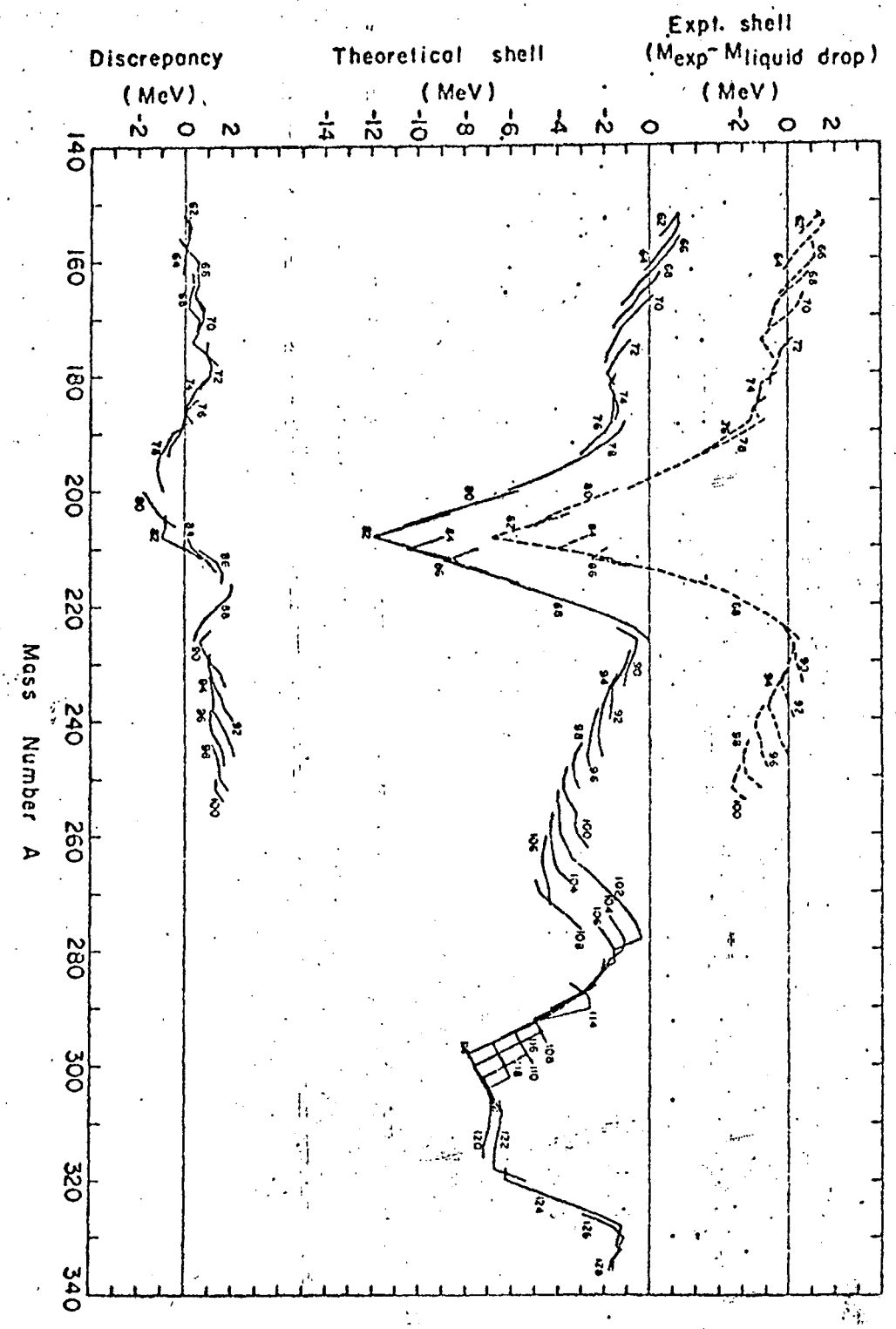
Discrepancy
(MeV)
Theoretical shell
(MeV)
Expt. shell
(Mexp - Mliquid drop)
(MeV)
Mass Number A

FIG 16

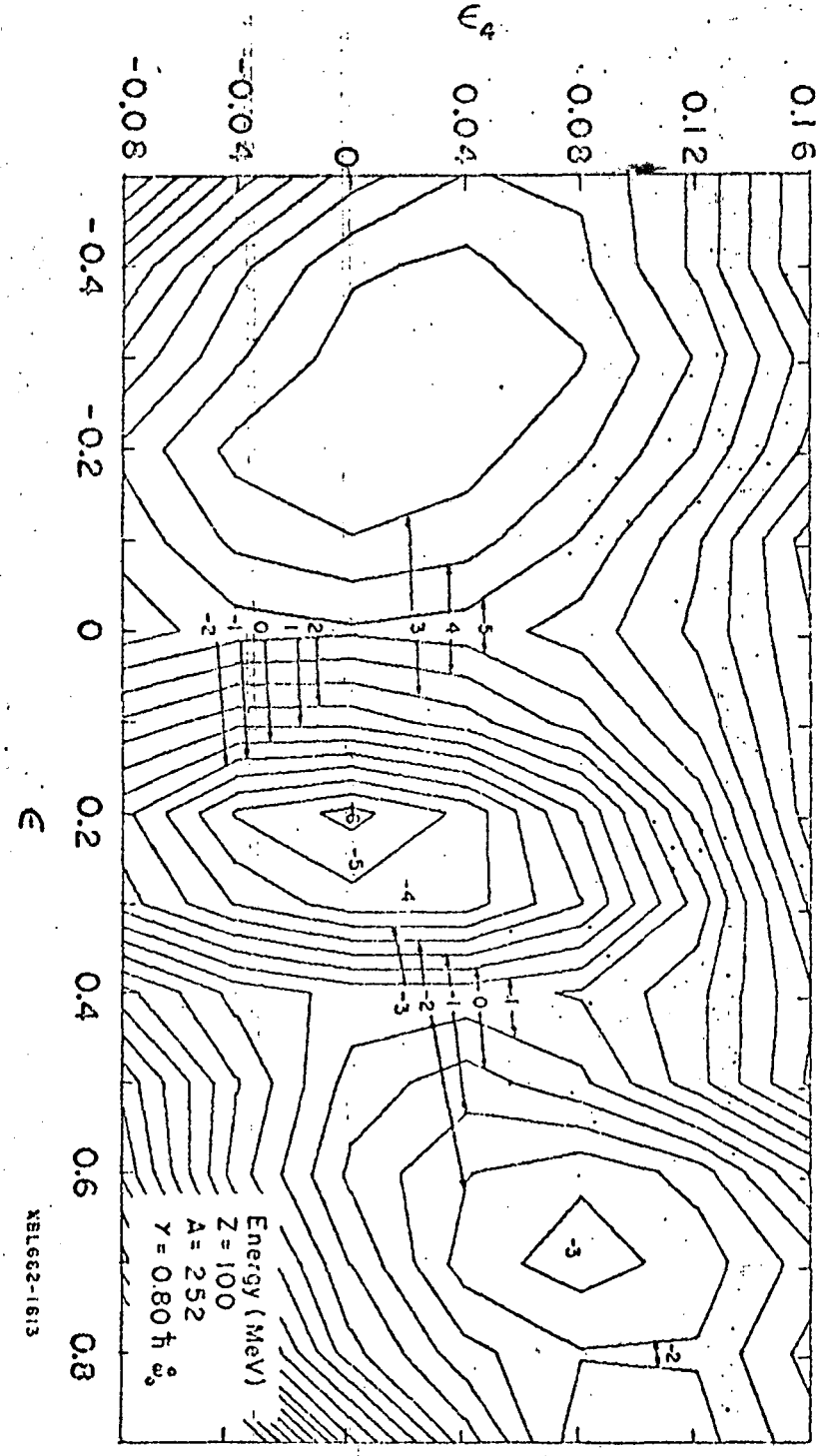
ϵ_4
-0.08
-0.04
0
0.04
0.08
0.12
0.16
-0.4
-0.2
0
0.2
0.4
0.6
0.8
ϵ
Energy (MeV)
Z = 100
A = 252
γ = 0.80 ħ ω₀
XBL662-1613

FIG. 17a

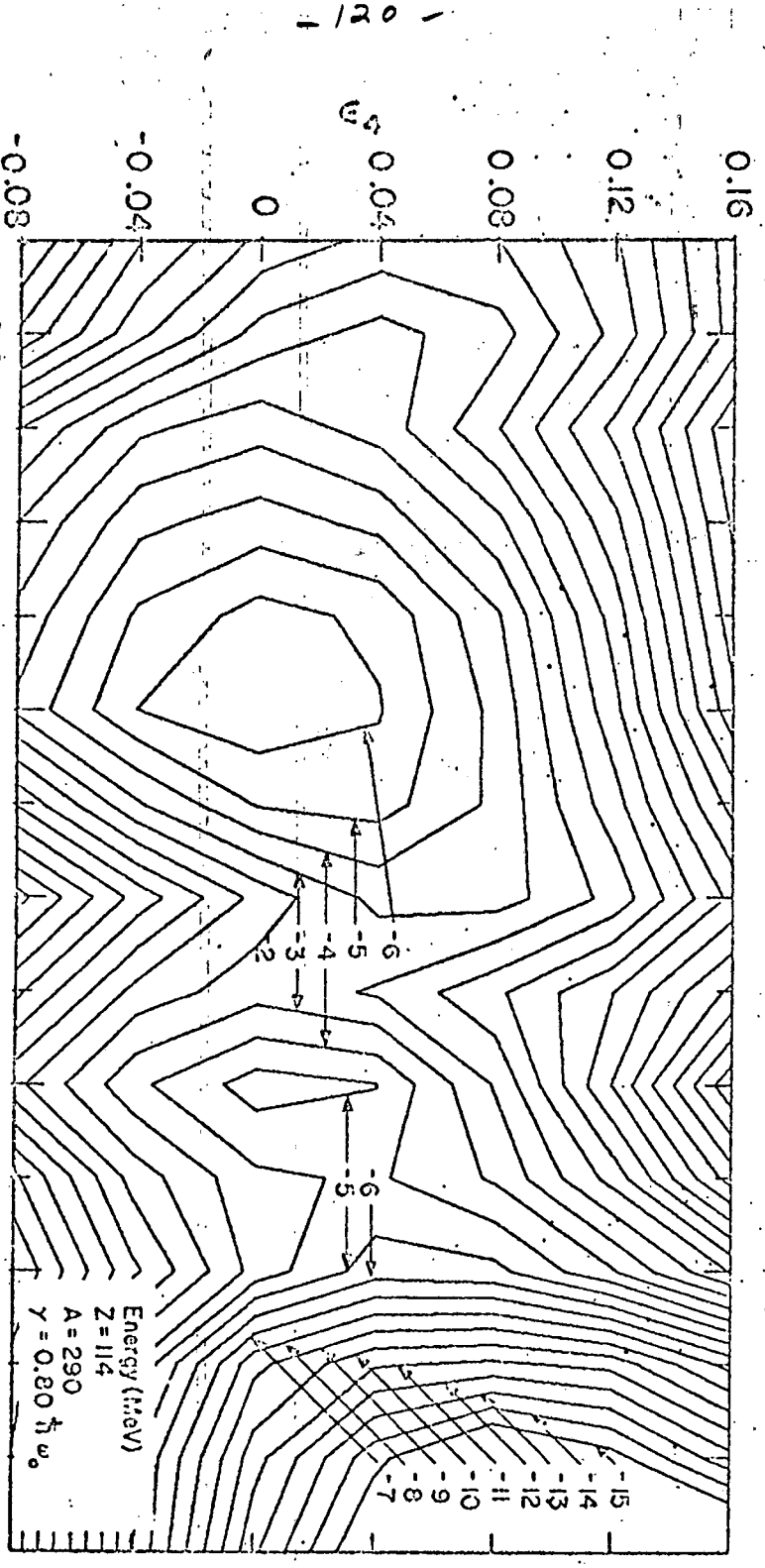
ε_4
0.16
0.12
0.08
0.04
0
-0.04
-0.08
ε
-0.4
-0.2
0
0.2
0.4
0.6
0.8
-2
-3
-4
-5
-6
-5
-6
-7
-8
-9
-10
-11
-12
-13
-14
-15
Energy (MeV)
Z = 114
A = 290
γ = 0.80 ħω₀

FIG 17b

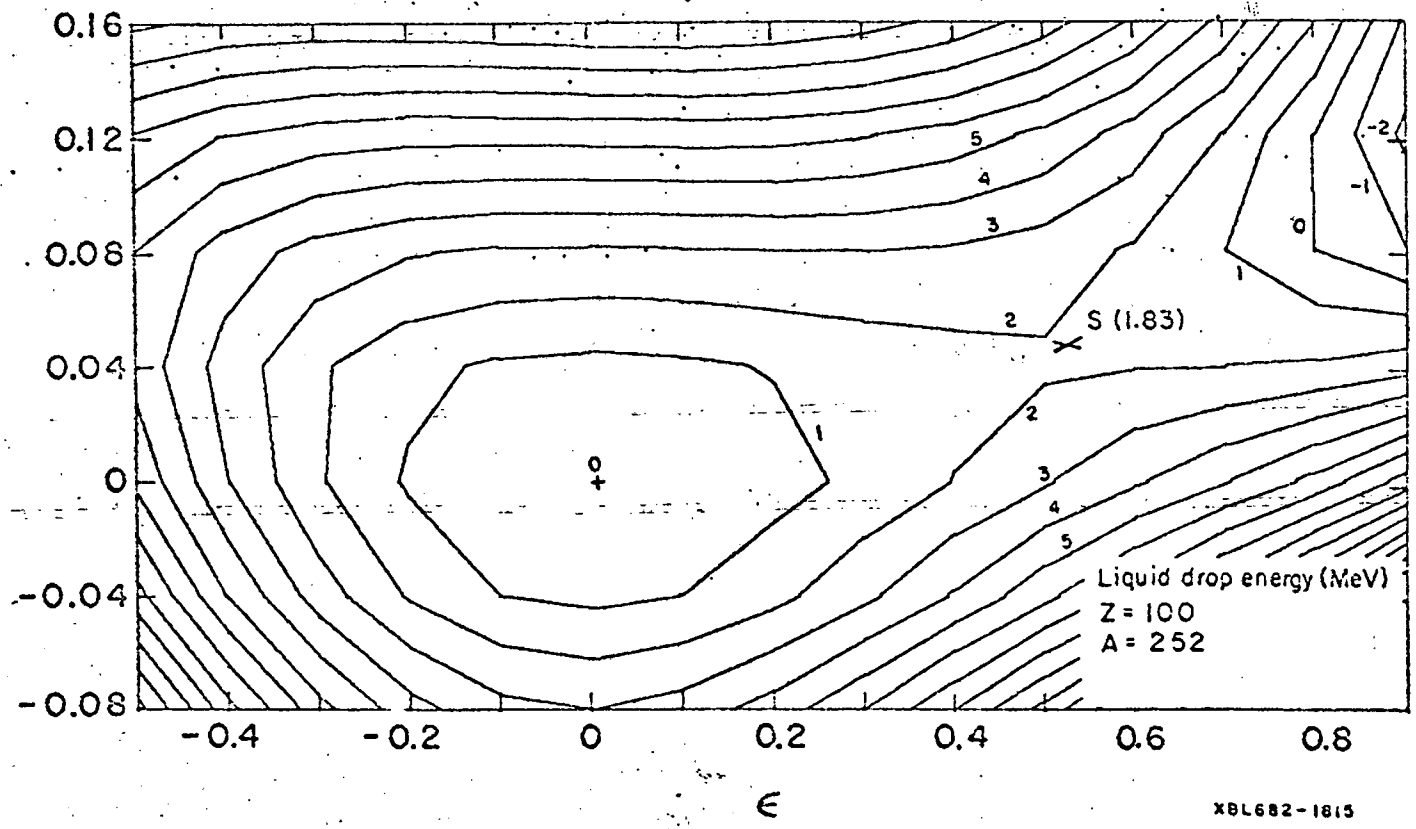
0.16
0.12
0.08
0.04
0
-0.04
-0.08
ϵ_4
-0.4
-0.2
0
0.2
0.4
0.6
0.8
ϵ
S (1.83)
0+
Liquid drop energy (MeV)
Z = 100
A = 252
XBL682-1815

FIG 18a

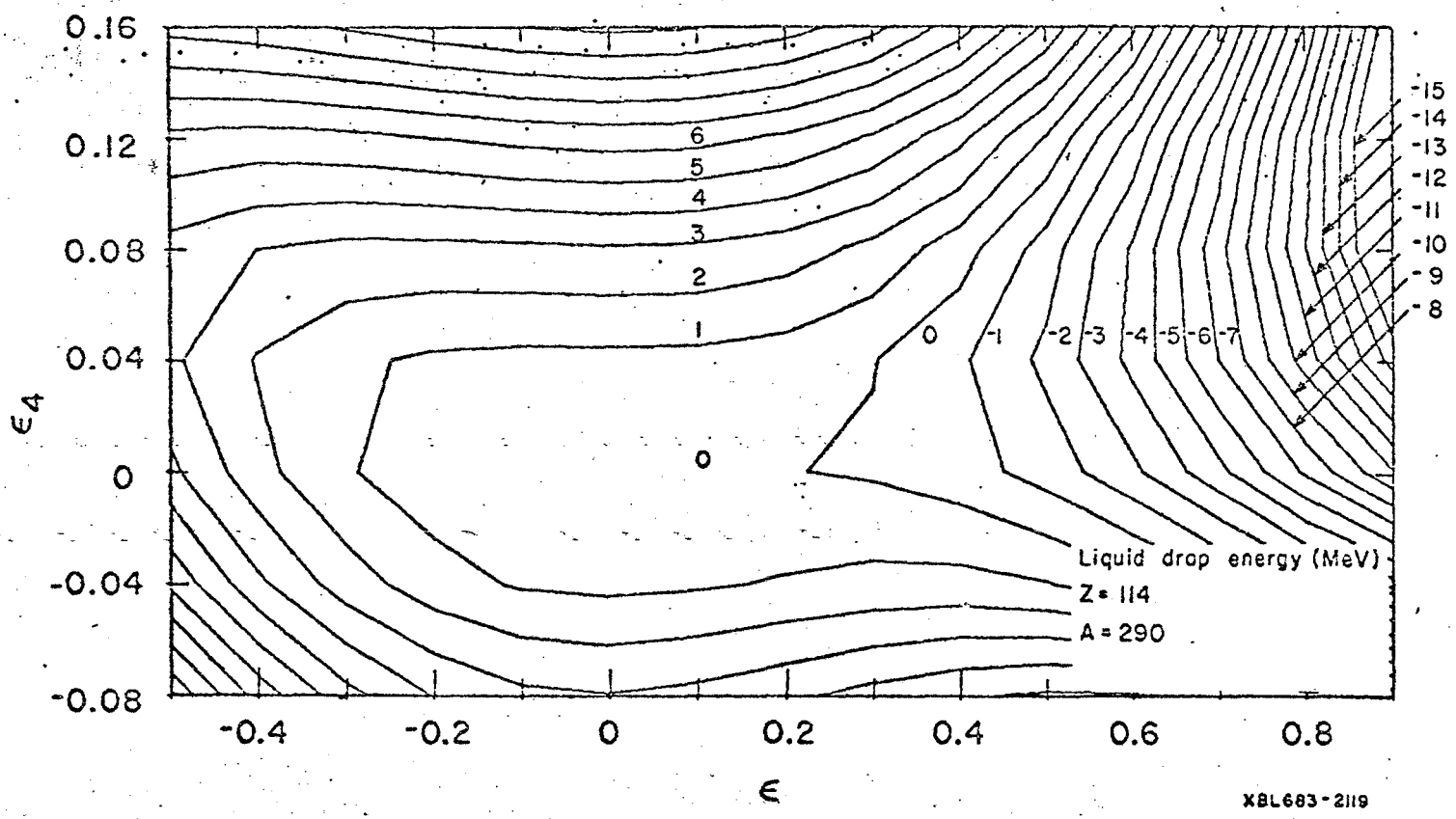
0.16
0.12
0.08
0.04
0
-0.04
-0.08
ϵ_4
-0.4
-0.2
0
0.2
0.4
0.6
0.8
ϵ
6
5
4
3
2
1
0
0
-1
-2
-3
-4
-5
-6
-7
-15
-14
-13
-12
-11
-10
-9
-8
Liquid drop energy (MeV)
Z = 114
A = 290
XBL683-2119

Fig 18b

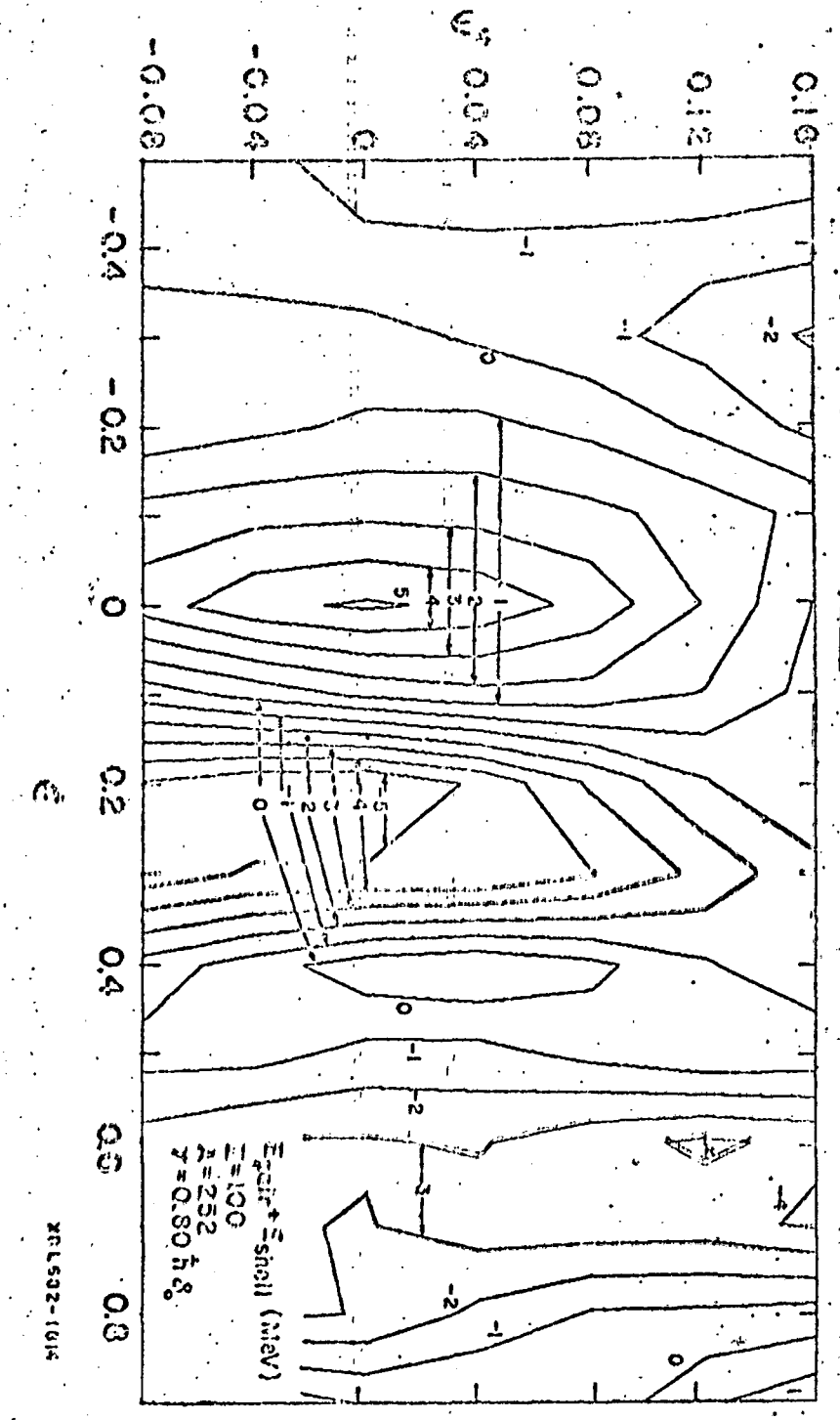
-0.08
-0.04
0
0.04
0.08
0.12
0.16
ψ_s
-0.4
-0.2
0
0.2
0.4
0.6
0.8
ξ_s
E_{edge}=Small (MeV)
E=100
λ=252
γ=0.80 h_s
XGL582-1614

FIG 19 a

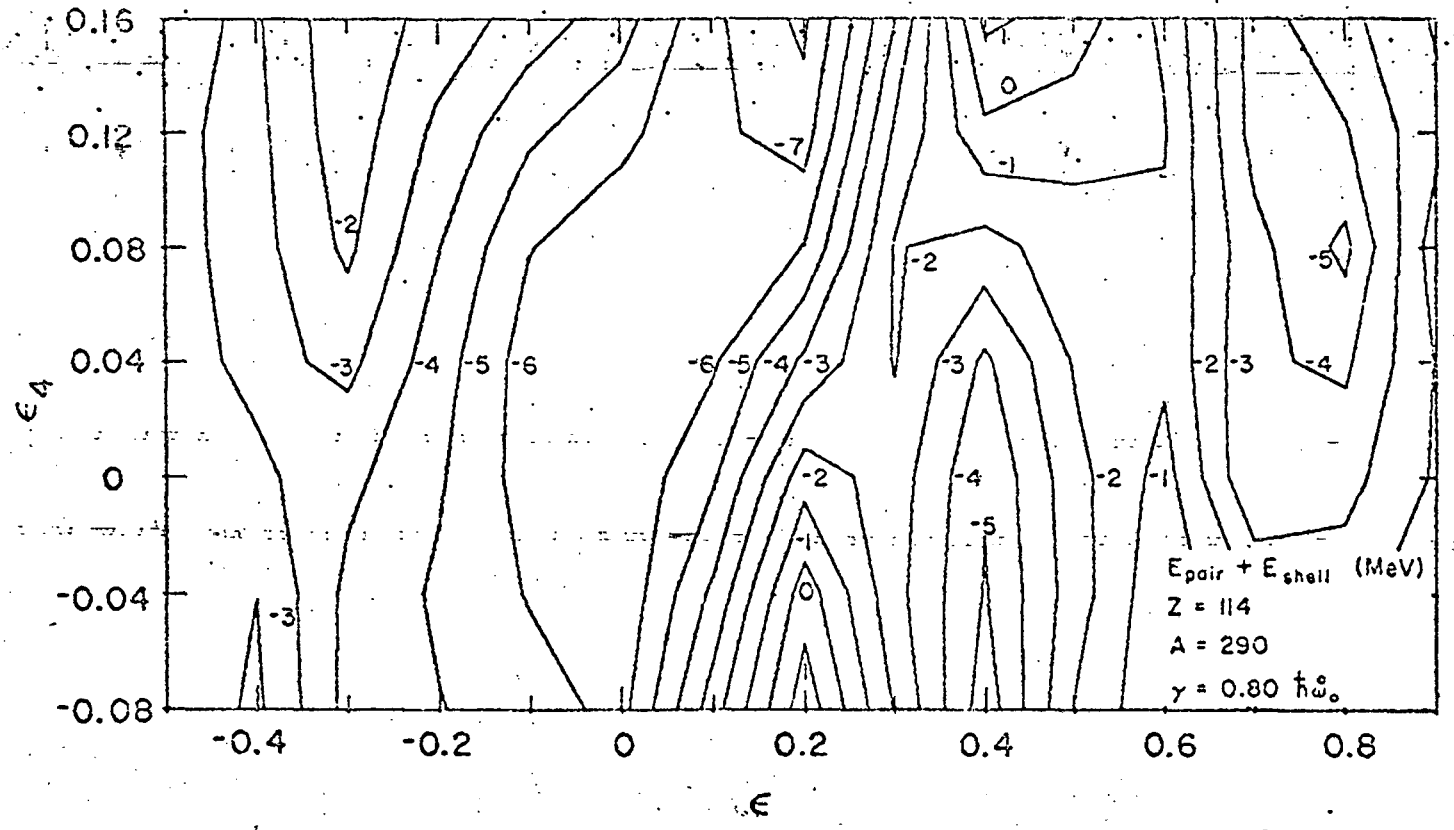
0.16
0.12
0.08
0.04
0
-0.04
-0.08
ϵ_4
-0.4
-0.2
0
0.2
0.4
0.6
0.8
ϵ
$E_{pair} + E_{shell}$ (MeV)
Z = 114
A = 290
γ = 0.80 $\hbar\omega_0$
XBLE83-2118

FIG 19 b

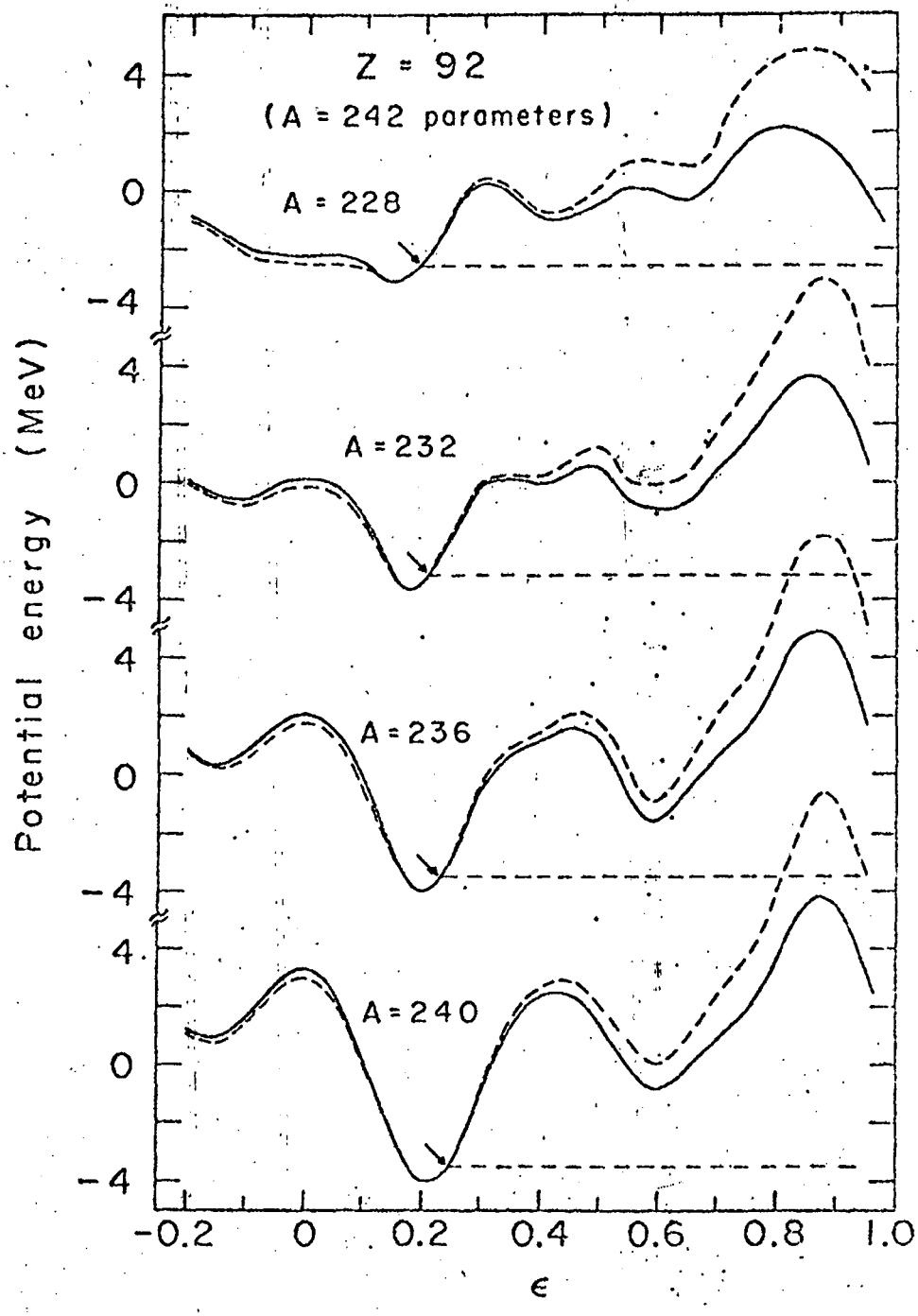
Z = 92
(A = 242 parameters)
A = 228
A = 232
A = 236
A = 240
Potential energy (MeV)
4
0
-4
-0.2
0
0.2
0.4
0.6
0.8
1.0
ϵ
XBL608-3516

FIG 20a

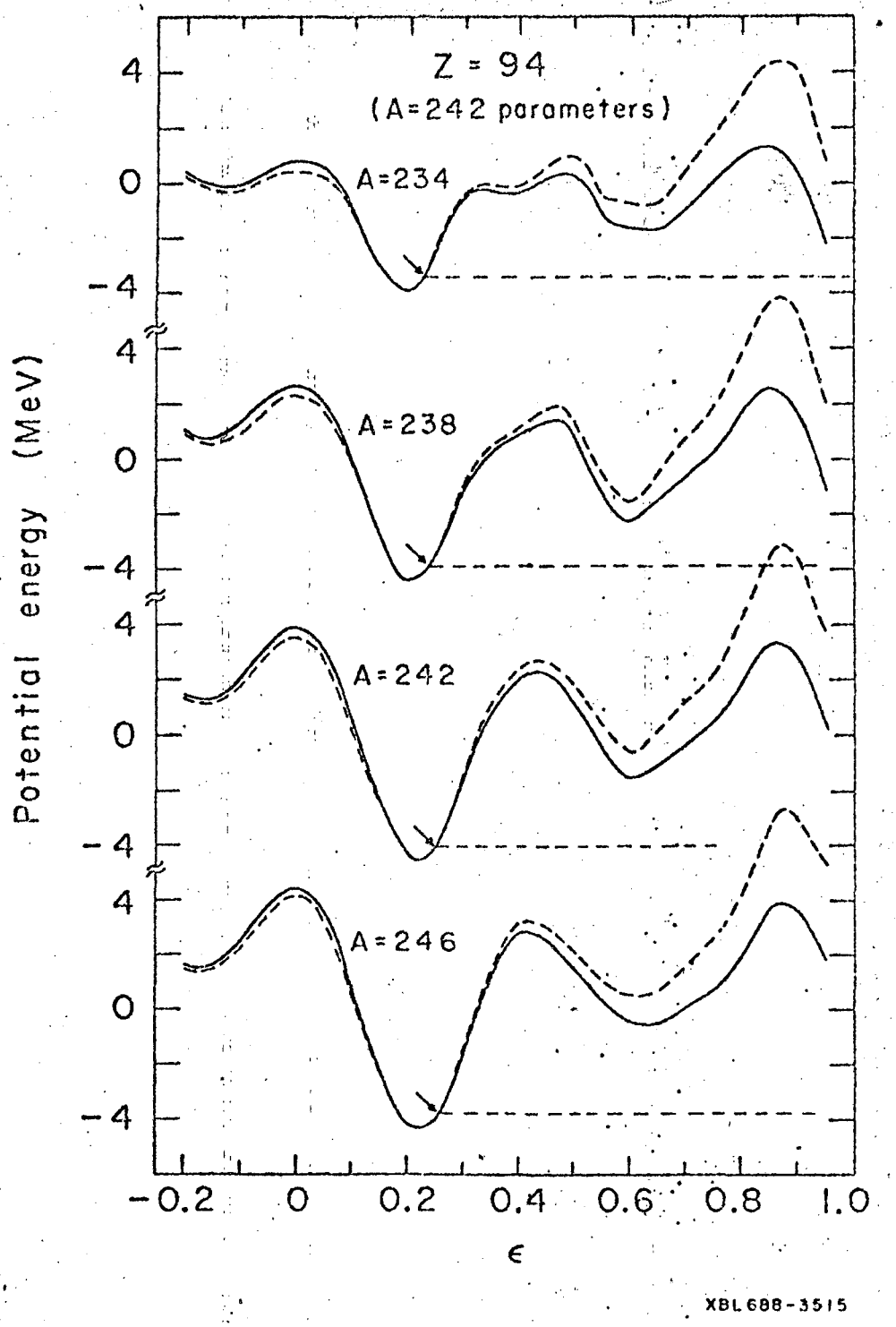
Z = 94
(A=242 parameters)
A=234
A=238
A=242
A=246
Potential energy (MeV)
4
0
-4
-0.2
0
0.2
0.4
0.6
0.8
1.0
ε
XBL688-3515

FIG 30 b

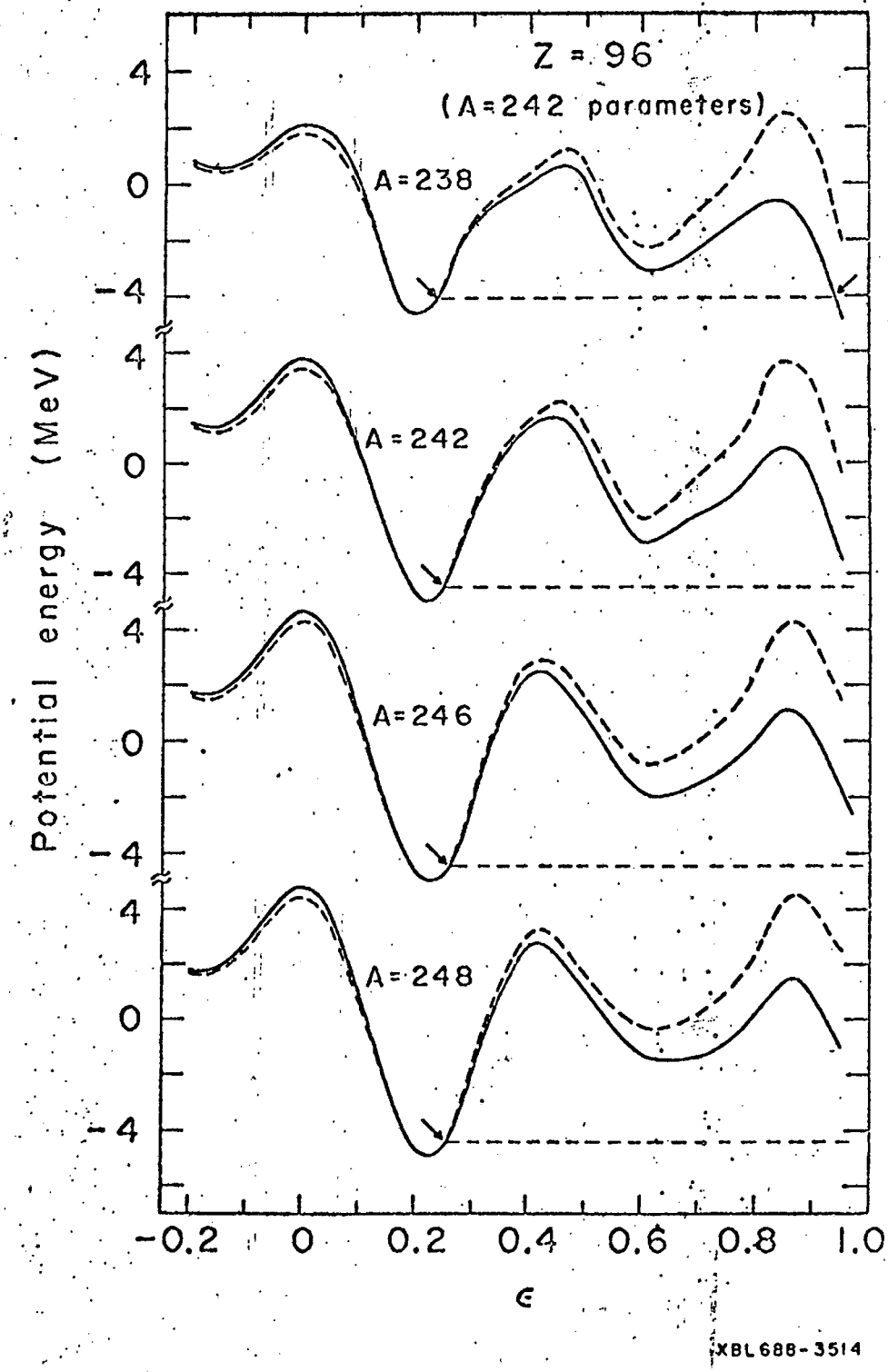
Z = 96
(A=242 parameters)
A=238
A=242
A=246
A=248
Potential energy (MeV)
4
0
-4
-0.2
0
0.2
0.4
0.6
0.8
1.0
ε
XBL688-3514

FIG 20c

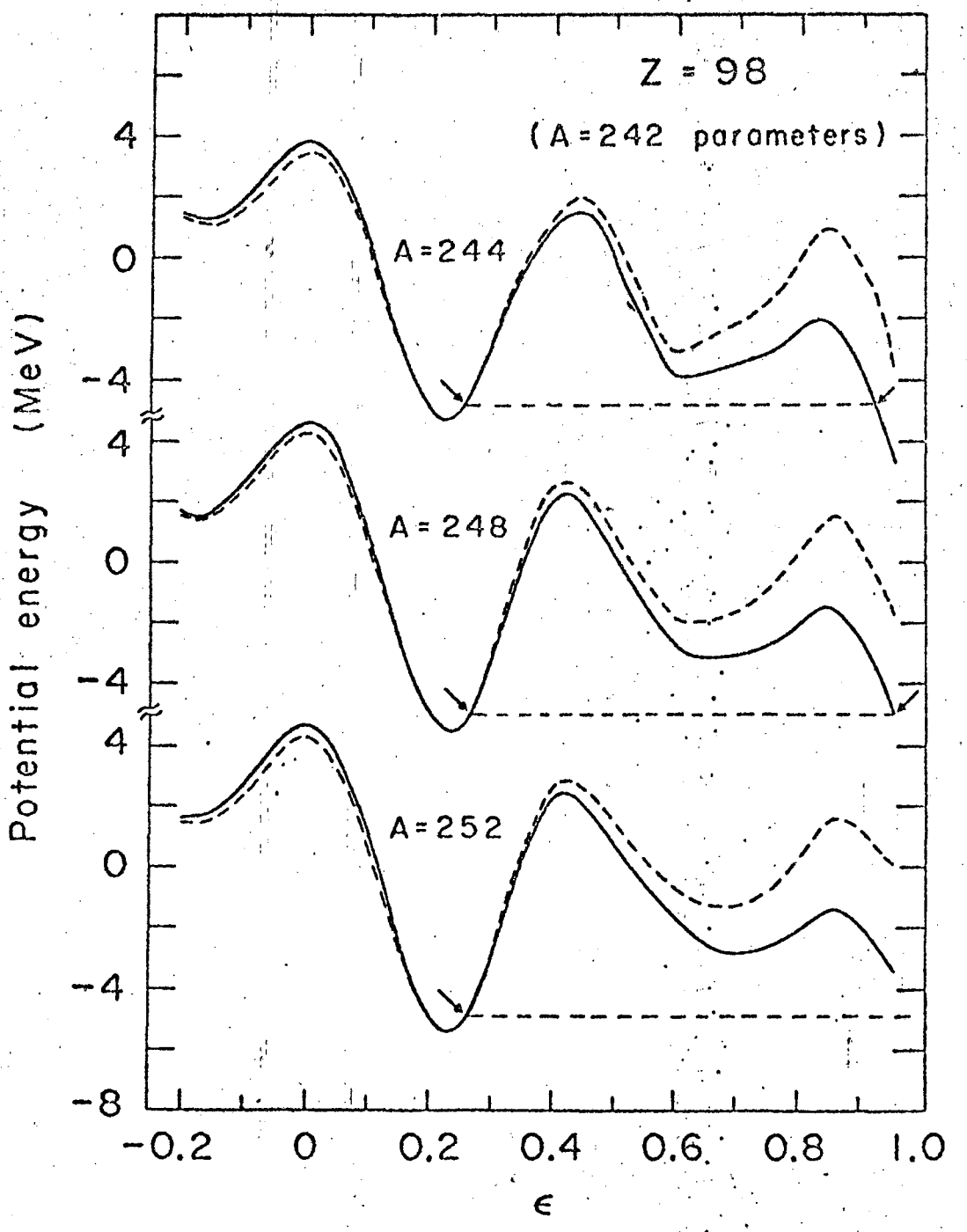

XBL688-3513

FIG 20 d

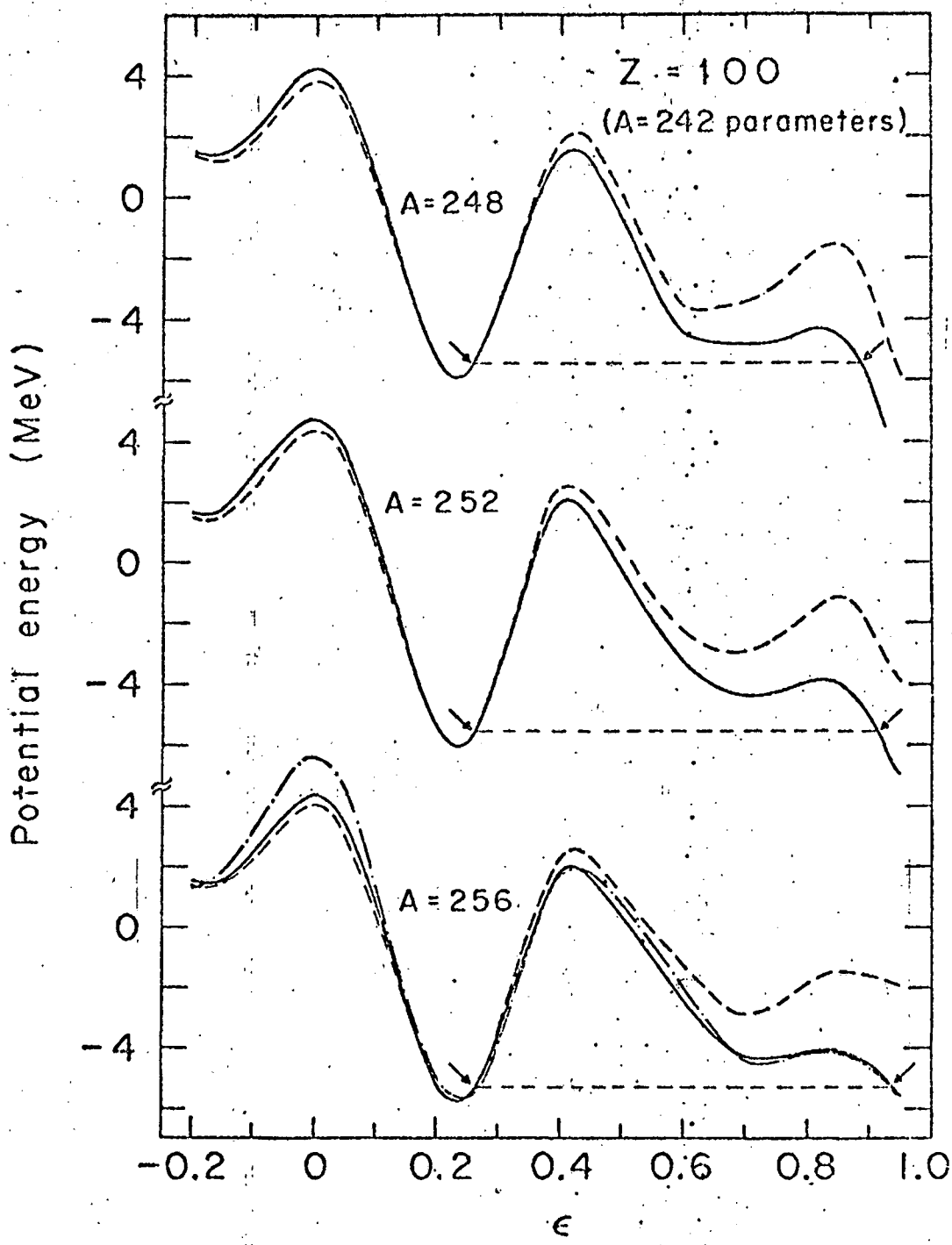
Z = 100
(A=242 parameters)
A=248
A=252
A=256
Potential energy (MeV)
4
0
-4
-0.2
0
0.2
0.4
0.6
0.8
1.0
ε
XBL688-3512

Fig 20 e

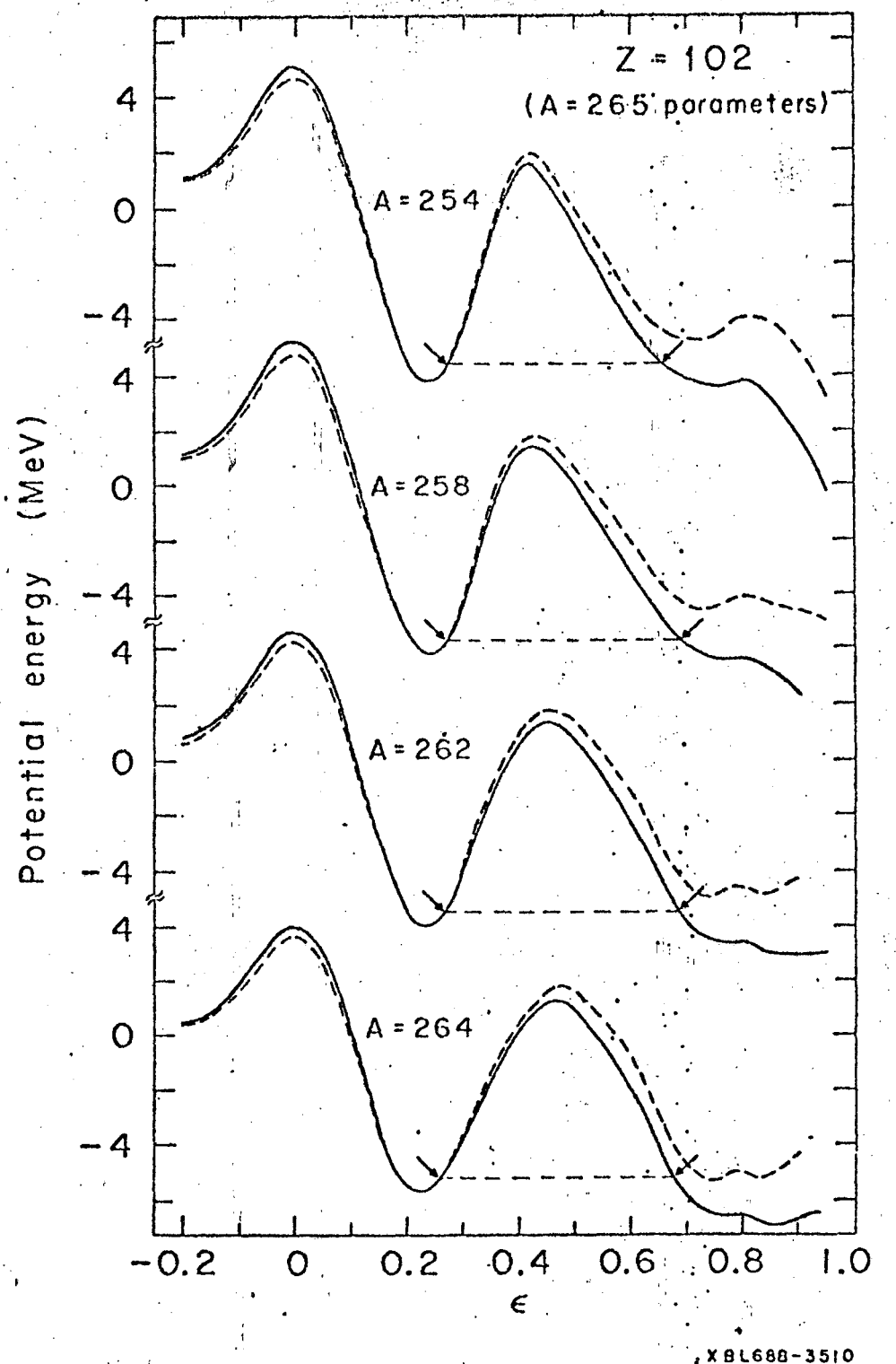
Z = 102
(A = 265 parameters)
A = 254
A = 258
A = 262
A = 264
Potential energy (MeV)
4
0
-4
-0.2
0
0.2
0.4
0.6
0.8
1.0
ε
XBL688-3510

FIG 20 f.

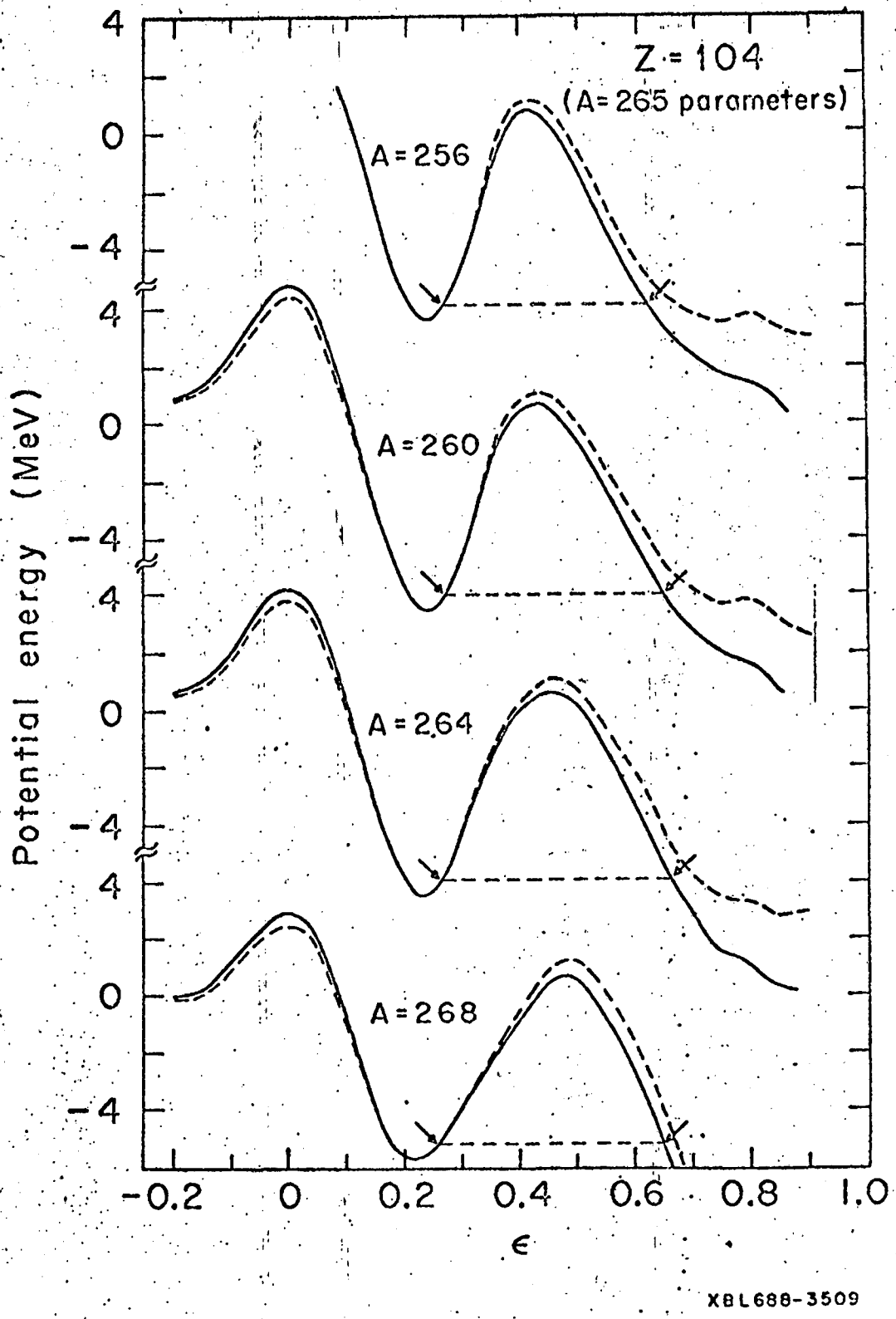
Z = 104
(A = 265 parameters)
A = 256
A = 260
A = 264
A = 268
Potential energy (MeV)
4
0
-4
-0.2
0
0.2
0.4
0.6
0.8
1.0
ε
XBL688-3509

FIG 20 g

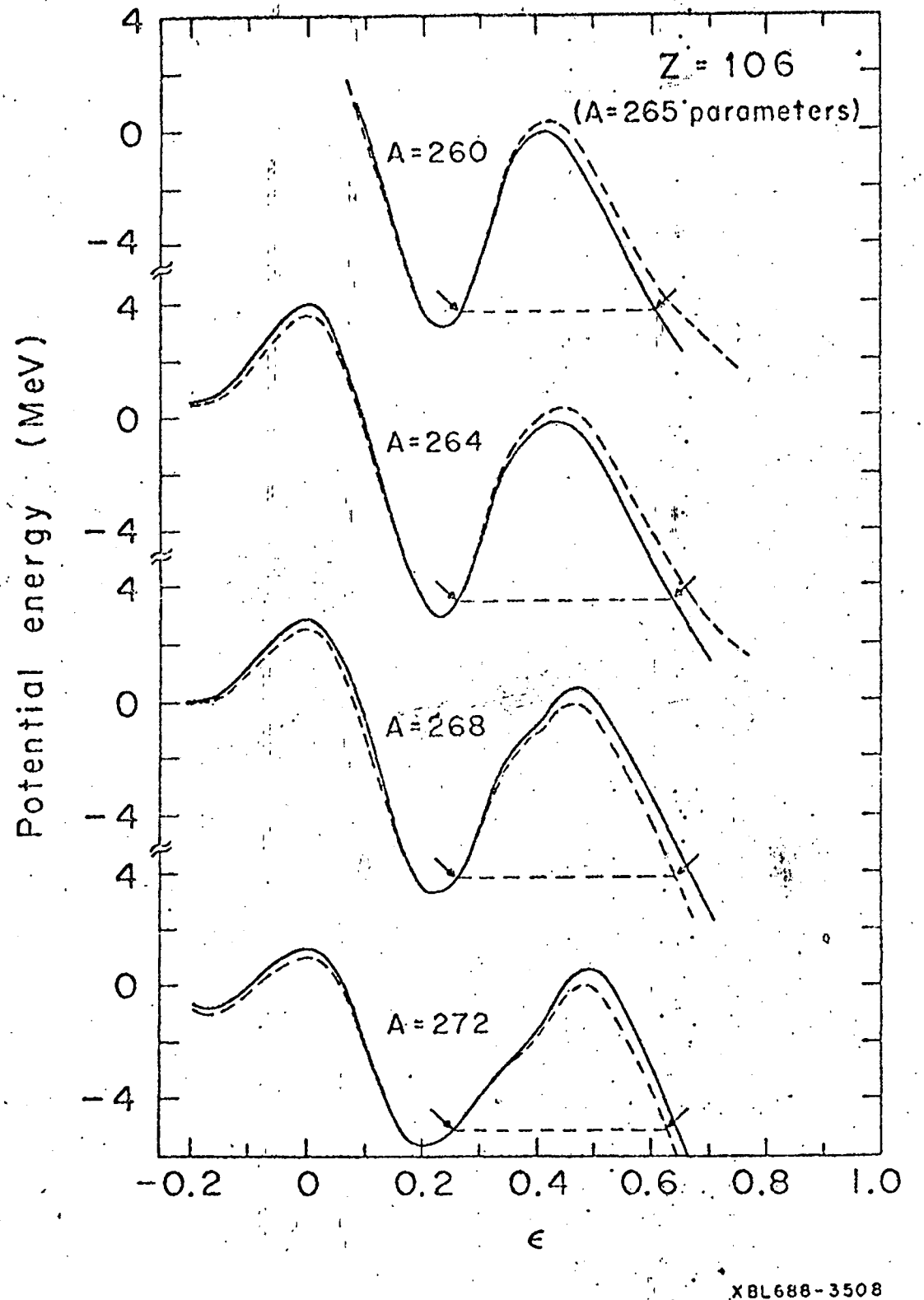
Z = 106
(A=265 parameters)
A=260
A=264
A=268
A=272
Potential energy (MeV)
4
0
-4
-0.2
0
0.2
0.4
0.6
0.8
1.0
ε
XBL688-3508

FIG 20 b...

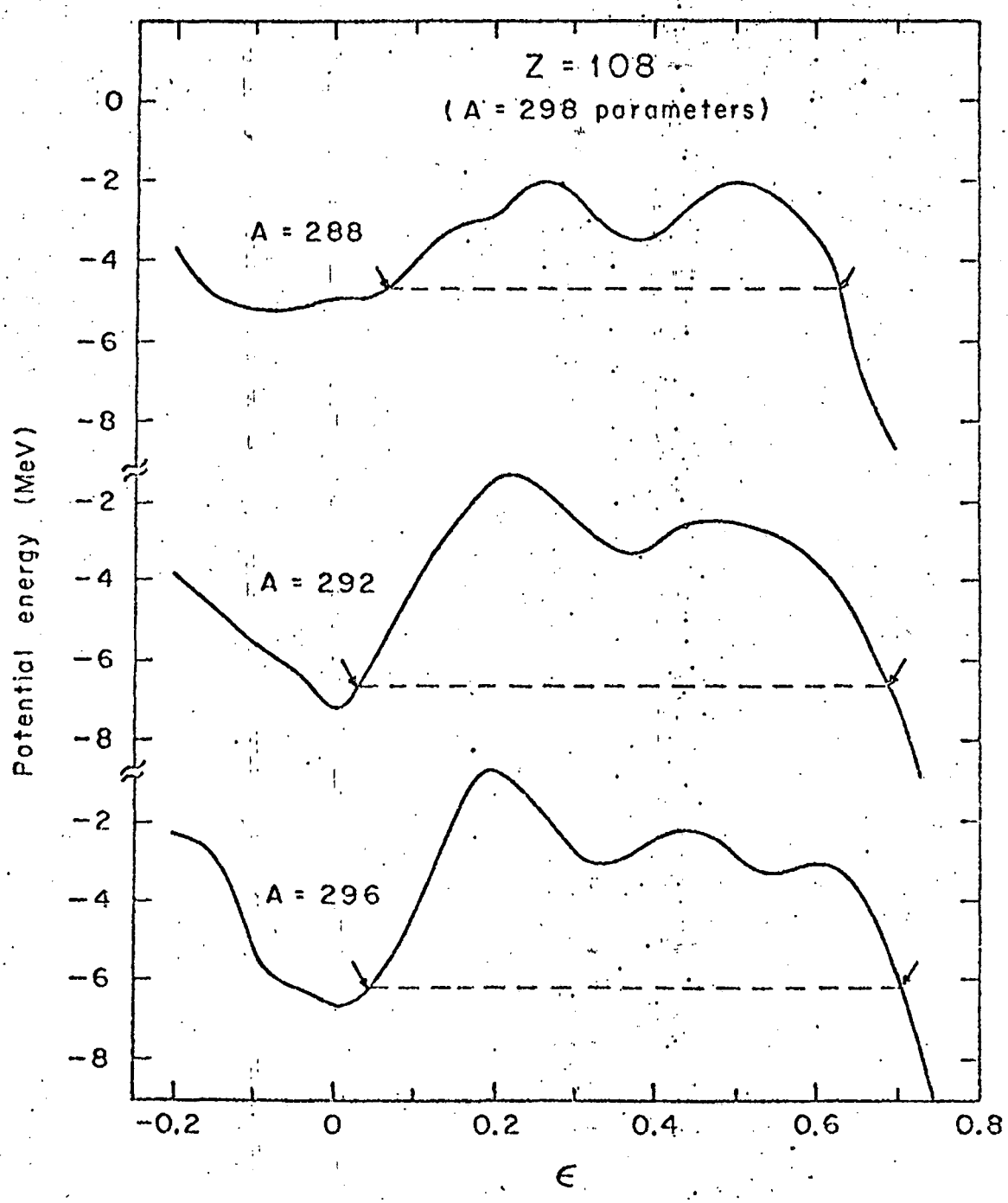
Z = 108
(A = 298 parameters)
A = 288
A = 292
A = 296
Potential energy (MeV)
0
-2
-4
-6
-8
-0.2
0
0.2
0.4
0.6
0.8
ε
XBL688-3532

FIG 20 i

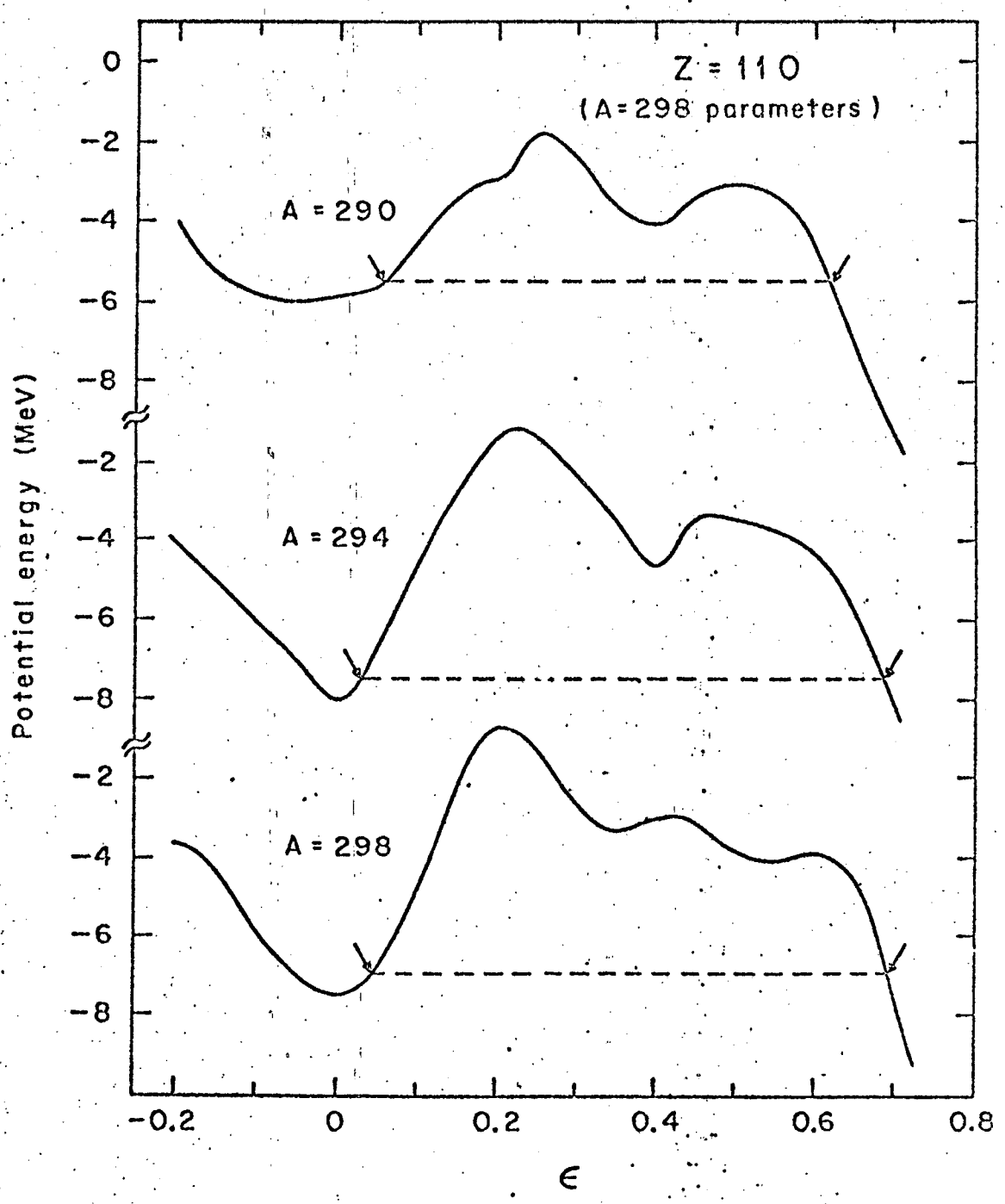
Z = 110
(A=298 parameters)
A = 290
A = 294
A = 298
Potential energy (MeV)
0
-2
-4
-6
-8
-0.2
0
0.2
0.4
0.6
0.8
ε
XBL688-3531

FIG. 20

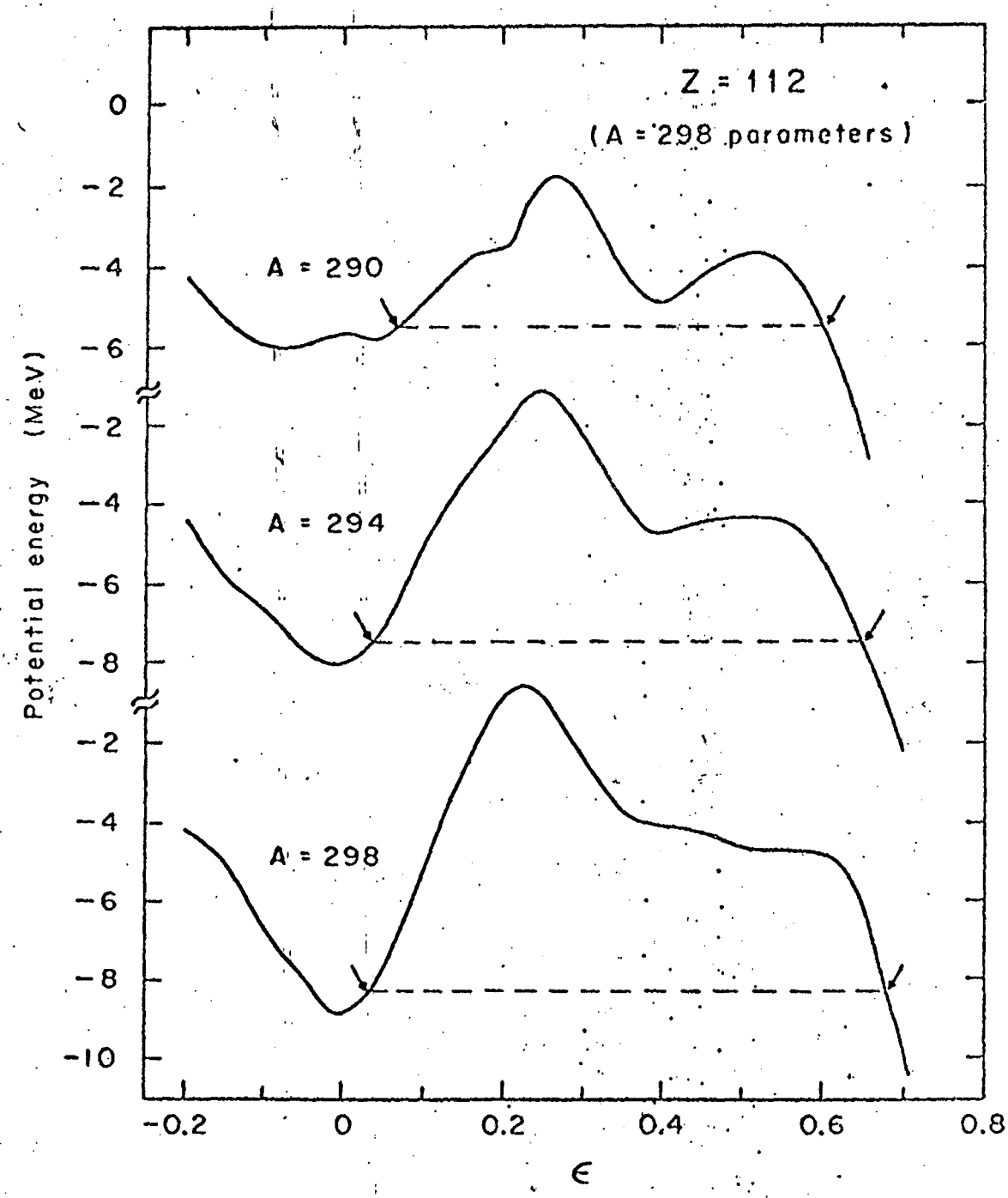

XBL688-3529

FIG. 20 k.

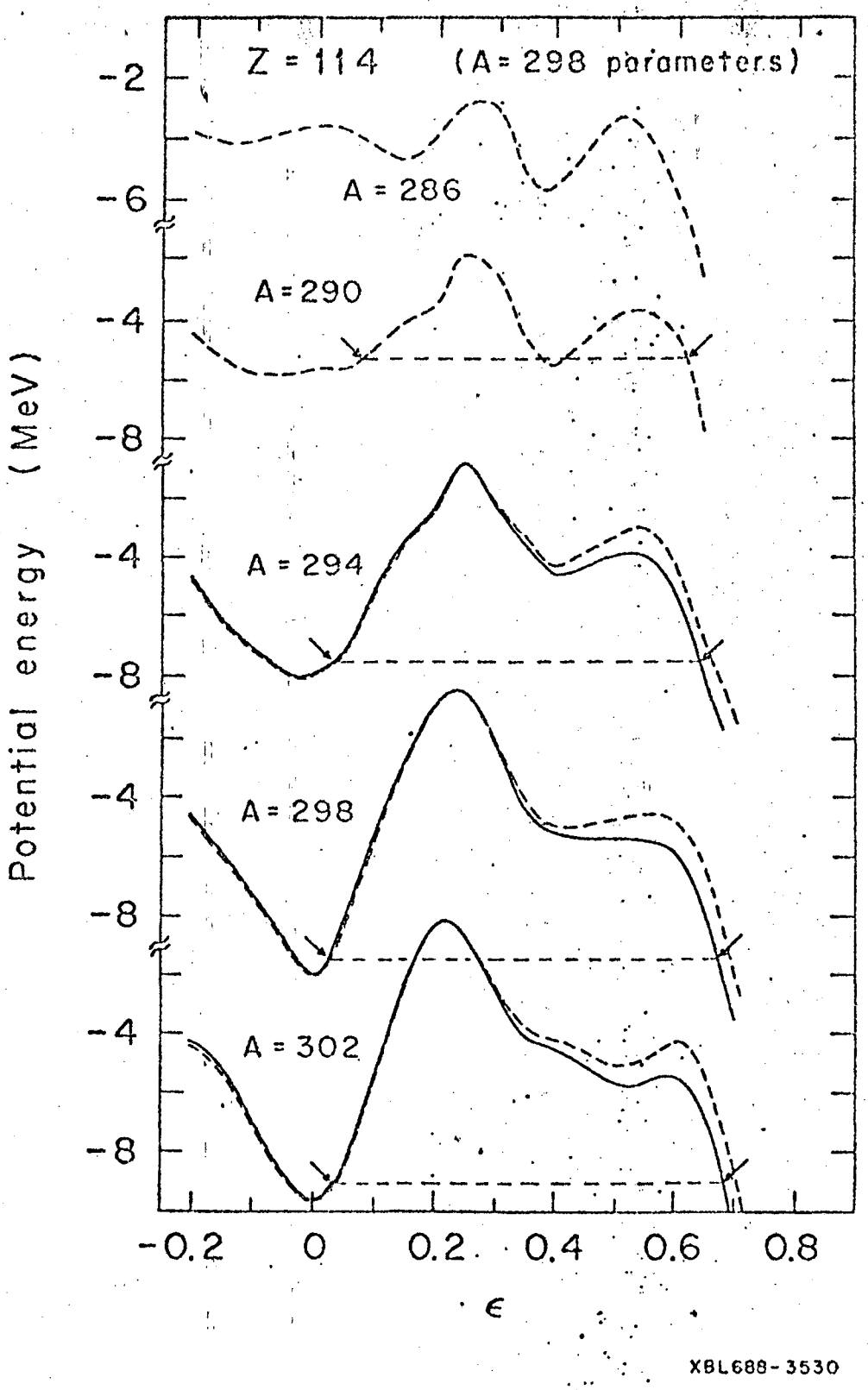
Z = 114 (A = 298 parameters)
A = 286
A = 290
A = 294
A = 298
A = 302
Potential energy (MeV)
-2
-6
-4
-8
-0.2
0
0.2
0.4
0.6
0.8
ε
XBL688-3530

FIG. 20 2

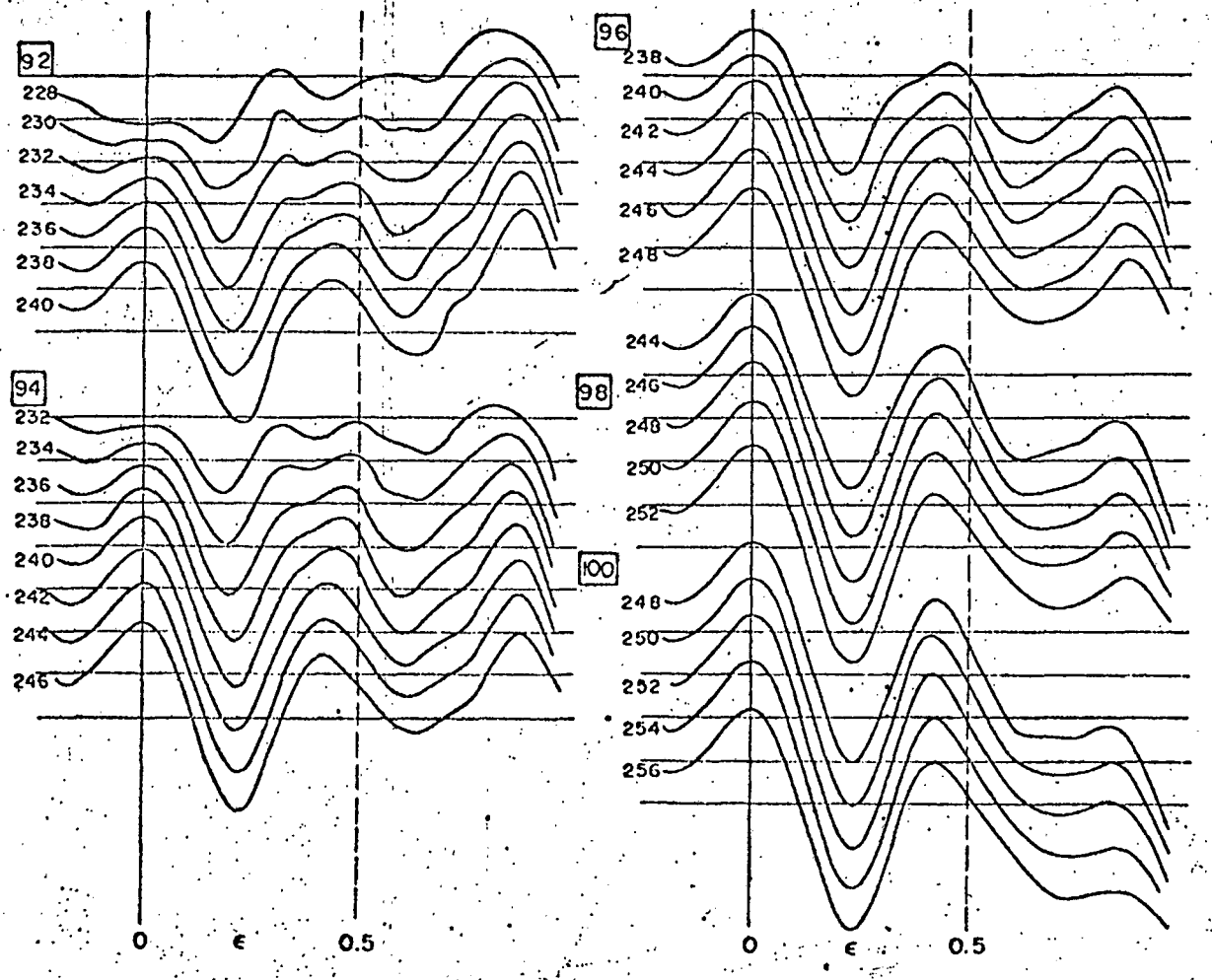

Separation between successive horizontal lines = 2 MeV

XBL691-1638

FIG 20 m

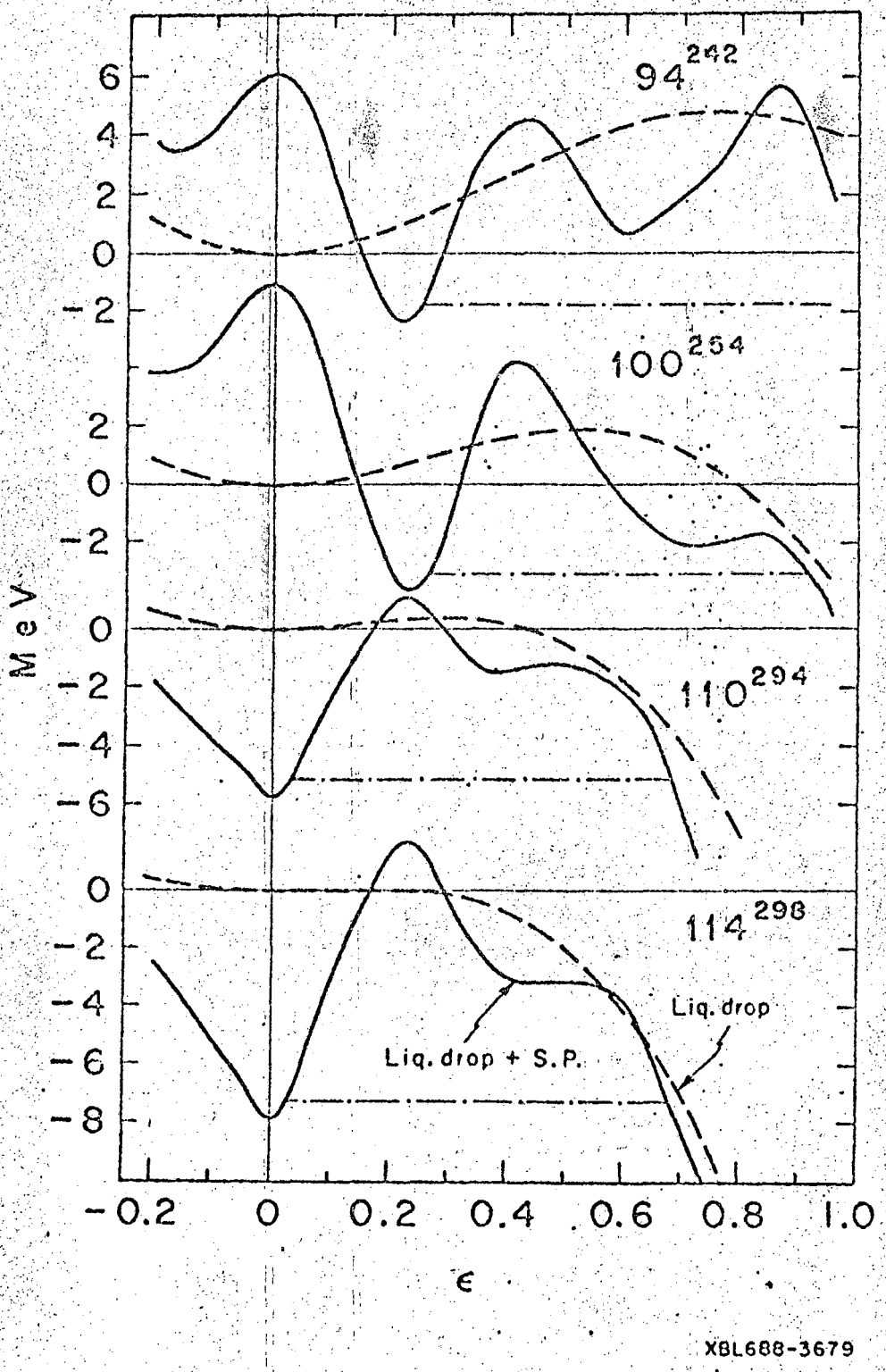
94^{242}
100^{254}
110^{294}
114^{298}
Liq. drop
Liq. drop + S.P.
MeV
ε
6
4
2
0
-2
-4
-6
-8
-0.2
0
0.2
0.4
0.6
0.8
1.0
XBL688-3679

FIG 21

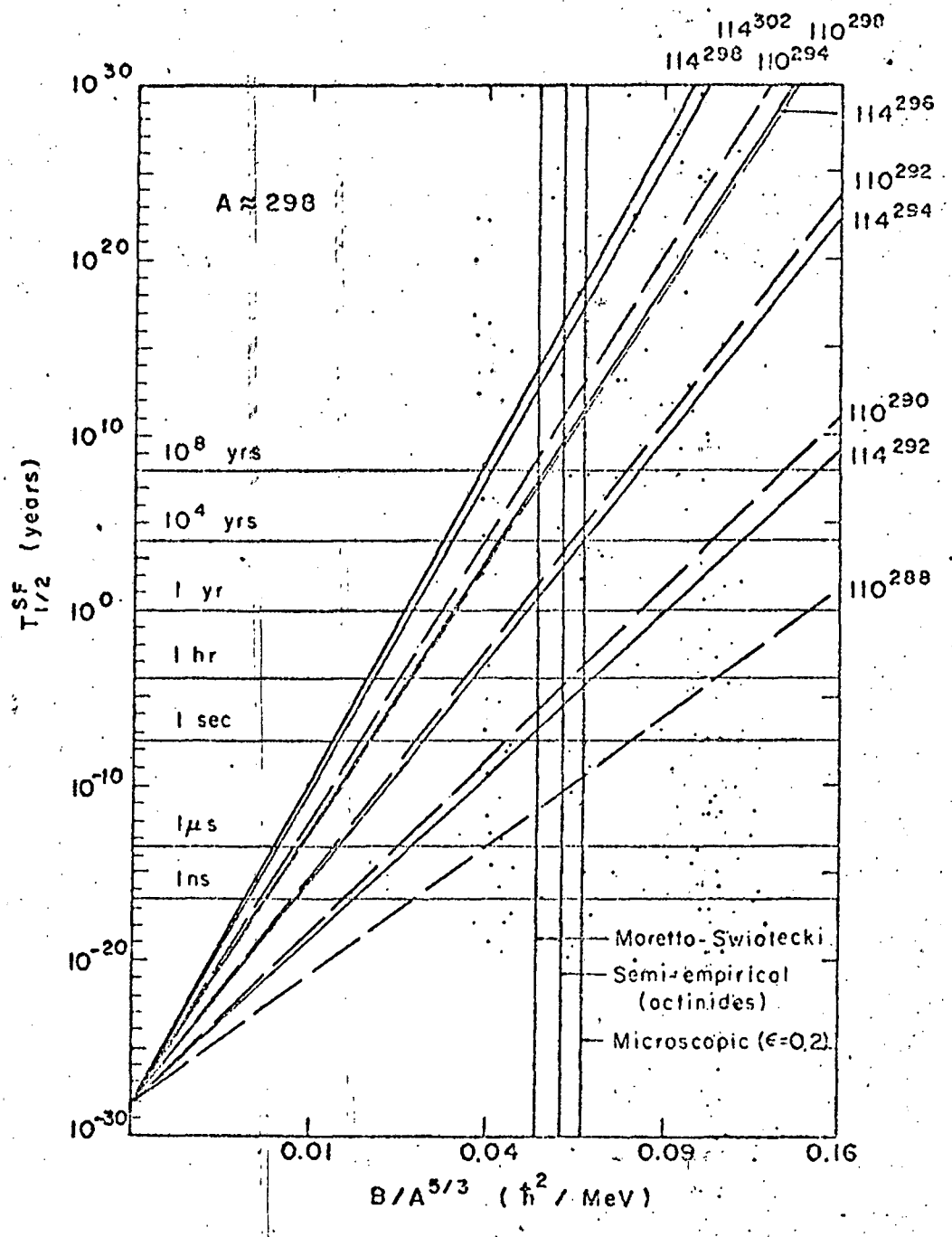

XBL691-1640

FIG. 22

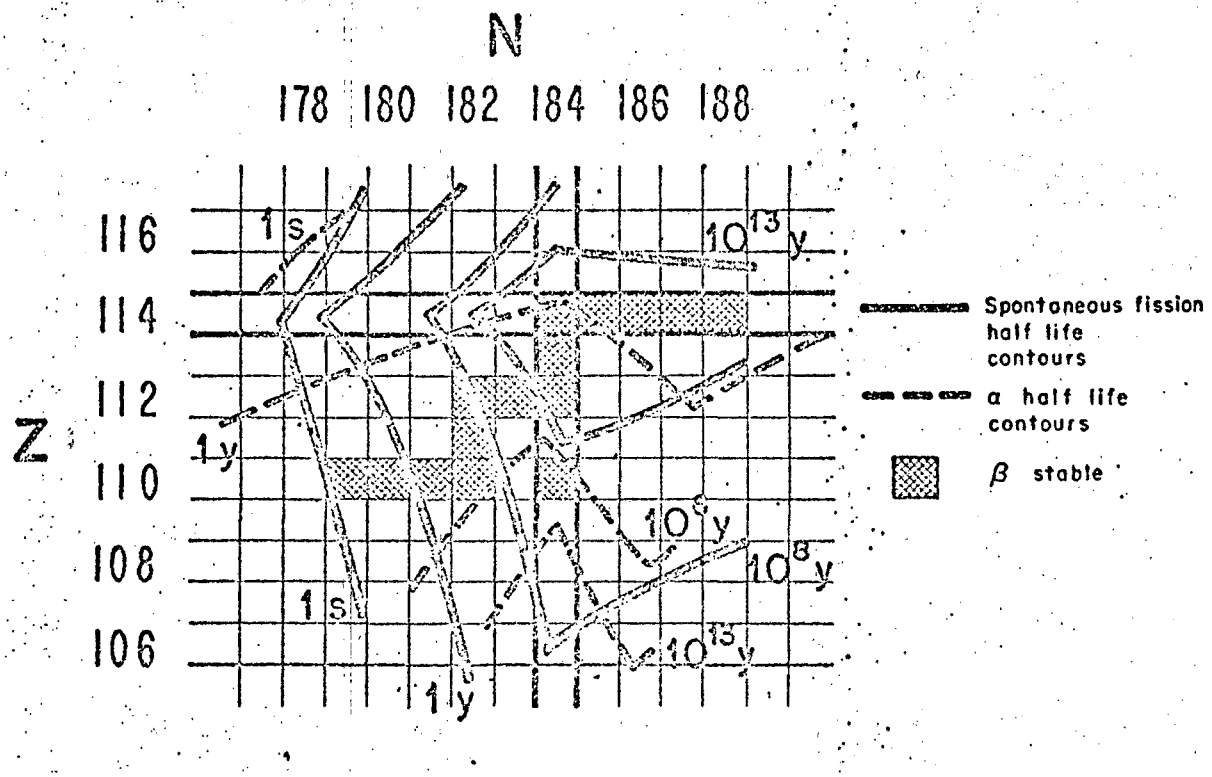
N
178
180
182
184
186
188
Z
116
114
112
110
108
106
1 s
10^13 y
1 y
10^9 y
10^8 y
1 s
10^13 y
1 y
Spontaneous fission half life contours
α half life contours
β stable
XBL688-3557

FIG 23

H 1																	He 2
Li 3	Be 4											B 5	C 6	N 7	O 8	F 9	Ne 10
Na 11	Mg 12											Al 13	Si 14	P 15	S 16	Cl 17	Ar 18
K 19	Ca 20	Sc 21	Ti 22	V 23	Cr 24	Mn 25	Fe 26	Co 27	Ni 28	Cu 29	Zn 30	Ga 31	Ge 32	As 33	Se 34	Br 35	Kr 36
Rb 37	Sr 38	Y 39	Zr 40	Nb 41	Mo 42	Tc 43	Ru 44	Rh 45	Pd 46	Ag 47	Cd 48	In 49	Sn 50	Sb 51	Te 52	I 53	Xe 54
Cs 55	Ba 56	La 57 71	Hf 72	Ta 73	W 74	Re 75	Os 76	Ir 77	Pt 78	Au 79	Hg 80	Tl 81	Pb 82	Bi 83	Po 84	At 85	Rn 86
Fr 87	Ra 88	Ac 89-103	104	105	106	107	108	109	110	111	112	113	114	115	116	117	118
119	120	121															

LANTHANIDE SERIES	La 57	Ce 58	Pr 59	Nd 60	Pm 61	Sm 62	Eu 63	Gd 64	Tb 65	Dy 66	Ho 67	Er 68	Tm 69	Yb 70	Lu 71
ACTINIDE SERIES	Ac 89	Th 90	Pa 91	U 92	Np 93	Pu 94	Am 95	Cm 96	Bk 97	Cf 98	Es 99	Fm 100	Md 101	No 102	Lr 103

121	122	123	124	125	126	

FIG 24

TECHNICAL INFORMATION DIVISION
LAWRENCE RADIATION LABORATORY
UNIVERSITY OF CALIFORNIA
BERKELEY, CALIFORNIA 94720